



ISTITUTO ITALIANO DI TECNOLOGIA



HyQ - Design and Development of a Hydraulically Actuated Quadruped Robot

Claudio Semini

University of Genoa, Italy

and

Italian Institute of Technology (IIT)

A thesis submitted for the degree of

Doctor of Philosophy (Ph.D.)

April 2010

Thesis supervisors:

Prof. Darwin G. Caldwell (Principle Adviser)

Advanced Robotics Department

Italian Institute of Technology (IIT)

Dr. Nikos G. Tsagarakis

Advanced Robotics Department

Italian Institute of Technology (IIT)

Copyright © 2010 by Claudio Semini

All rights reserved

Abstract

Legged machines promise greater mobility in rough and unstructured terrain than wheeled vehicles. In the future, especially quadruped robots are expected to be employed for a variety of dangerous and dirty tasks in fields like search and rescue, humanitarian demining etc. The objective of this dissertation is to make a significant contribution toward the development of a highly dynamic quadruped robot. This versatile platform is intended to serve as a tool to deepen the understanding of terrestrial locomotion, to assess the applicability of different hydraulic actuation systems to legged robots and to facilitate the future construction of useful robots for various tasks. To this end, this dissertation:

1. presents several design studies aimed at the creation of a quadruped robot.
2. describes the design and experimental testing of a hydraulically powered prototype leg with a focus on its actuator units.
3. explains the construction of the quadruped robot platform including all electric and hydraulic system components.

The developed quadruped robot called HyQ features 12 active degrees of freedom and is designed to perform highly dynamic tasks like jumping and running. Therefore, the robot's joints are either powered by hydraulic or electric actuators, depending on their particular performance and property requirements. While hydraulic cylinders have an excellent power to weight ratio and naturally absorb impact force peaks during running and jumping, electric motors have compact overall dimensions and exhibit a constant output torque profile. Therefore, hydraulic cylinders actuate the hip and knee

joints in the flexion/extension plane of the leg, where most impact forces are acting and high speed/torque with minimum weight are required. The hip abduction/adduction joint is actuated by a compact, yet powerful brushless motor fixed to the robot torso via a connector plate. This way, a modular leg design is accomplished that allows easy mounting and dismounting of the entire leg. Passive compliant elements in the leg play a significant role in energy-efficient locomotion. Therefore a passive compliant ankle joint is studied and suitable springs are selected.

Acknowledgements

As I decided to use active voice in my thesis, you will often find *I* and *my* but also *we* and *our* throughout the text. I would like to stress that the work presented here is the fruit of the effort of several people, who assisted me during the last three years. The beginning of the next paragraph lists these people and their contribution to the project.

I would like to thank the following people:

Prof. Darwin Caldwell for his support, freedom for creativity and for sharing the vision to create such a robot.

Dr. Nikos Tsagarakis for his continuous support in all areas from software to electronics and especially mechanical design. Without his help and experience in designing and constructing robots, HyQ would still be in the design phase.

Dr. Emanuele Guglielmino for his support on everything related to hydraulics and for setting up a hydraulic research network.

Dr. Ferdinando Cannella for his work on the structural and modal FEM analyses of the robot torso, legs and other parts.

Dr. Bram Vanderborcht for his valuable feedback about this dissertation and for sharing his knowledge about variable compliance and locomotion.

Dr. Yousheng Yang for his hands-on experience with hydraulic systems and components and their modelling.

Dr. Jonas Buchli for introducing us into the world of *SL* and his expert knowledge on locomotion.

Michele Focchi, Thiago Boaventura Cunha for their help with the hydraulics and experiments.

Gianluca Pane, Giuseppe Sofia, Alexandre Veinguertener, Jody Saglia, Alberto Parmiggiani and Amir Jafari for their advice and support for the

mechanical design.

Carlo Tacchino and Marco Migliorini for their support for anything related to electronics.

Ivar Thorson and Dr. Thierry Hoinville for their advice on hopping robots and locomotion in general.

Alessio Margan and Dr. Irene Sardellitti for their help in software development.

Dr. David Branson for his valuable comments on the dissertation and Alexander Schmitz for proof-reading it.

Prof. Giulio Sandini and Dr. Michele Guarnieri for telling me about the Italian Institute of Technology and my previous mentors: Prof. Shigeo Hirose, Prof. Rolf Pfeifer, and Dr. Nobuto Matsuhira.

Nadia Garcia-Hernandez, Jody Saglia, Andrea Brogni, Matteo Laffranchi, Jamshed Iqbal, Leonardo Mattos and Phong Huynh Pham for being great lab room-mates and friends who supported me in many everyday questions and problems related to robotics research.

I'd like to specially thank my friends in Italy and at my home town in Switzerland for their friendship and for making life more fun.

Last but not least, I'd like to thank my parents for their never-ending love and support; and my brother Marco and his son Antonio-Julian.

At this point, I would like to express my deep gratitude to the above-mentioned people. Without their help this work would not have been possible.

Grazie mille!

Contents

List of Figures	xi
List of Tables	xv
Glossary	xvii
1 Introduction	1
1.1 Motivations	1
1.2 Objectives and Proposed Approach	3
1.3 Contributions	4
1.4 Outline	5
2 State of the Art	7
2.1 Introduction	7
2.2 Conventional Actuator Types	8
2.2.1 Electric Actuation	8
2.2.2 Pneumatic Actuation	11
2.2.3 Hydraulic Actuation	12
2.2.4 Actuator Comparison and Summary	16
2.3 Early Legged Robots	19
2.4 Highly Dynamic Legged Robots	22
2.4.1 Electric Robots	22
2.4.2 Pneumatic Robots	24
2.4.3 Hydraulic Robots	27
2.4.3.1 Raibert's Robots in the 1980's	27
2.4.3.2 Kenken	29

CONTENTS

2.4.3.3	BigDog	30
2.4.3.4	PETMAN	35
2.4.4	Other Interesting Hydraulic Legged Robots	36
2.5	Research on Legged Locomotion	38
2.5.1	Muybridge Picture Sequences	38
2.5.2	Spring-Mass System	39
2.5.3	Variable Stiffness during Running	41
2.5.4	Anatomy's Influence on Running Performance	41
3	Robot Specifications and Design Studies	45
3.1	Robot Specifications	45
3.1.1	Performance Specifications	46
3.1.2	Physical Specifications and Design Rules	47
3.1.3	Main Stages of Robot Development	48
3.2	Robot Structure	49
3.2.1	Number of Legs and Leg Length	49
3.2.2	Number of Active Joints and Kinematic Structure	50
3.2.3	Actuator Type Selection	52
3.2.4	Leg Configuration on Torso	54
3.2.5	Joint Range of Motion	57
3.3	Joint Torque Estimation	60
3.4	Joint Actuation Design and Kinematics	66
3.4.1	Hydraulic Joints	66
3.4.1.1	Torque Profile Selection	66
3.4.1.2	Cylinder Selection	70
3.4.1.3	Cylinder Attachment on Leg	73
3.4.2	Electric Joints	74
3.5	Leg Prototype with 2 DOF	76
3.6	Passive Compliant Ankle Joint	77
3.7	Spring-Mass Model Simulation	82
3.8	Power System and Energy Source Comparison	84
3.9	Conclusions	85

4	Robot Design and Components	87
4.1	System Overview	88
4.2	Mechanical Design	89
4.2.1	Kinematic Structure	89
4.2.2	Construction Materials	91
4.2.3	Robot Torso	92
4.2.4	Robot Leg (V2)	93
4.2.5	Robot Foot and Ankle Joint	98
4.2.6	Assembled HyQ Robot	99
4.3	Actuation Systems	101
4.3.1	Electric System	101
4.3.1.1	Electric System Overview	101
4.3.1.2	Motor Controller	101
4.3.1.3	Brushless Motor and Harmonic Gear	101
4.3.2	Hydraulic System	102
4.3.2.1	Hydraulic System Overview	102
4.3.2.2	Hydraulic Pump Units	102
4.3.2.3	Proportional Valve	105
4.3.2.4	Hydraulic Cylinder	106
4.3.2.5	Accumulator, Filter and Heat Exchanger	107
4.3.2.6	Manifolds, Fittings and Tubing	107
4.4	Sensory System	109
4.4.1	Position	109
4.4.1.1	Relative Encoder	110
4.4.1.2	Absolute Encoder	110
4.4.2	Pressure	111
4.4.3	Force	111
4.4.4	Inertial Measurement Unit	111
4.4.5	Summary	112
4.5	Robot Control System	113
4.5.1	System Overview	113
4.5.2	CPU Box	114
4.5.2.1	Pentium CPU Board	115

CONTENTS

4.5.2.2	Multifunction I/O Board	115
4.5.2.3	PC104-CAN Board and DC-DC Converter Board	118
4.5.3	Valve Driver Board and Motor Controller	118
4.5.4	Sensor Hub Board	118
4.6	Real-Time Control Software	119
4.7	Conclusions	121
5	Experimental Studies	123
5.1	Hydraulic Valve Frequency Response	123
5.2	Hydraulic Valve+Cylinder Frequency Response	125
5.3	Hydraulic Cylinder Speed Test	128
5.4	Leg Prototype Trajectory Following	130
5.5	Leg Impact Studies	132
5.6	Periodic Hopping with Leg Prototype	135
5.7	Conclusions	140
6	Discussion	145
6.1	Leg Prototype (Leg V1) vs. Final Leg (Leg V2)	145
6.2	HyQ's Electric and Hydraulic Actuator Comparison	148
6.3	Comments about Hydraulics for Mobile Robots	150
7	Conclusion and Future Work	153
7.1	Conclusions	153
7.2	Future Work	154
A	Publications and Patents	157
A.1	Publications	157
A.2	Workshop Posters	158
A.3	Patents	158
B	Definition of Joint Angles and Cylinder Attachment Geometry	159
C	Kinematic and Dynamic Model of 2-DOF Robot Leg	163
C.1	Kinematic Model of 2-DOF Leg	163
C.2	Dynamic Model of 2-DOF Leg	165

D Finite Element Model (FEM) Analysis	171
D.1 FEM Analysis of Torso	171
D.2 FEM Analysis of Leg-Motor Connection	172
D.3 FEM Analysis of Leg	173
E Technical Details	175
E.1 Unit Conversions	175
E.2 Modular Foot Attachment Details	175
E.3 Hydraulic Cylinder Dimensions	177
Bibliography	179

CONTENTS

List of Figures

2.1	Working principle of a two-pole brushed DC motor	10
2.2	Schematic of a basic hydraulic system	13
2.3	Sketch of a double-acting asymmetric hydraulic cylinder	14
2.4	Max. Stress vs. Max. Strain graph for different actuators	18
2.5	Picture selection of early legged robots	20
2.6	Pictures of two early quadruped robots developed by Hirose	22
2.7	Picture selection of electrically actuated quadruped robots	23
2.8	Picture selection of pneumatically actuated robots	25
2.9	Picture selection of Raibert's robots of the 1980's	27
2.10	Pictures of the hydraulic hopping robots KenKenI and KenKenII	29
2.11	Picture selection of various BigDog versions	31
2.12	Pictures of BigDog's engines and actuator units	33
2.13	Pictures of <i>Moog</i> valve series 30 and E024	34
2.14	Picture of biped robot PETMAN	35
2.15	Picture selection of hydraulically actuated robots	37
2.16	Picture sequence of galloping horse by Muybridge	38
2.17	Spring-mass system during one vertical hopping cycle	40
3.1	Kinematic Structure of the active leg joints	50
3.2	Picture selection of legged animals	51
3.3	Sketch of robot leg with joint names	54
3.4	Leg configurations of quadruped robots	55
3.5	Kinematic structure and leg configuration according to Witte et al.	56
3.6	Joint range of motion of Labrador-Retrievers	58
3.7	Plots of vertical jump height and lift-off velocity relation	61

LIST OF FIGURES

3.8	Robot postures during vertical jump	62
3.9	Robot sketch in squat posture with definition of variables	63
3.10	Plots of the results of the <i>knee f/e</i> torque estimation	64
3.11	Sketch of robot model for <i>hip a/a</i> torque estimation	65
3.12	Plots of the results of the <i>hip a/a</i> torque estimation	66
3.13	Sketch of a cylinder for effective lever arm calculation	67
3.14	Study of different torque profile shapes	69
3.15	Sketch of hydraulic joint geometry to calculate <i>a</i> and <i>b</i>	70
3.17	Picture and CAD model of the leg prototype (<i>Leg V1</i>)	77
3.18	Kinematic Structure of the leg including a passive ankle joint	78
3.19	Robot sketch with linear springs and spring-mass model	79
3.20	Spring compression vs. stiffness plot for spring selection	80
3.21	Picture of <i>Nuke Proof</i> compression spring	81
3.22	Plot of the hopping robot simulation	83
4.1	3D model of HyQ with empty torso	87
4.2	3D CAD model of HyQ with a description of the components	89
4.3	Kinematic structure of HyQ with joint names	90
4.4	Picture of the empty robot torso	93
4.5	Plots of torque and joint angles of hip f/e and knee f/e	95
4.6	Cross-section of the CAD model of the electric motor unit	96
4.7	CAD models of HyQ robot leg (V2) with parts description	97
4.8	Pictures of the basic HyQ foot	98
4.9	Picture of the mechanical structure of HyQ (side view)	99
4.10	Picture of the mechanical structure of HyQ (front view)	100
4.11	Pictures of the brushless DC motor and harmonic gear	102
4.12	CAD model of robot torso with the hydraulic system components	103
4.13	Schematic of complete hydraulic system	103
4.14	Pictures of the hydraulic pump units	104
4.15	Picture of <i>Wandfluh</i> valve	105
4.16	Picture of <i>Hoerbiger</i> cylinder	106
4.17	Pictures of hydraulic accumulator, filter and heat exchanger	107
4.18	Pictures of hydraulic manifolds	108

LIST OF FIGURES

4.19	Pictures of <i>Faster</i> quick release coupling	109
4.20	Pictures of the relative and absolute encoders	111
4.21	Pictures of pressure sensor, load cell and inertial measurement unit	112
4.22	Control system architecture	113
4.23	Picture of the on-board computer of HyQ	115
4.24	Picture of the three PC104 board types	116
4.25	Picture of the <i>ELMO Whistle Solo</i> motor controller board	119
4.26	Screen shot of SL software environment	120
5.1	Hydraulic schematic of the valve test experiments	124
5.2	Bode plot of valve frequency response	125
5.3	Picture of the hydraulic cylinder test bench	126
5.4	Hydraulic schematic of the valve+cylinder test experiments	127
5.5	Bode plot of valve+cylinder frequency response	127
5.6	Plot of cylinder speed experiments	129
5.7	Pictures of prototype leg on vertical slider	130
5.8	Hydraulic schematic of 2-DOF prototype leg	131
5.9	Plot of angle vs. time for the <i>hip f/e</i> and <i>knee f/e</i> joint	132
5.10	Result plots of the leg impact experiments with active control	134
5.11	Result plots of the leg impact experiments with closed valves	135
5.12	Zoom into cylinder speed test plot	136
5.13	Time plots of position and force during continuous hopping	137
5.14	Phase plot of vertical hopping for different P-gains	138
5.15	Phase plot of vertical hopping for different supply pressures	139
5.16	Phase plot of vertical hopping for different Weights	140
5.17	Picture sequence of hopping leg prototype	141
6.1	Torque output profiles of <i>Leg V1</i> and <i>Leg V2</i>	147
B.1	Definition of joint angles of HyQ	160
B.2	Definition of joint angles and cylinder attachment geometry	161
C.1	Sketch of 2-DOF leg with definition of variables	164
D.1	Result plots of the FEM analysis of the robot torso	172

LIST OF FIGURES

D.2	Result plots of the FEM analysis of the motor connection	173
D.3	Result plots of the FEM analysis of the leg	174
E.1	Simplified drawing of the lower leg including the foot	176
E.2	Drawing of the Hoerbiger hydraulic cylinder LB6	177

List of Tables

2.1	Rotor speeds of synchronous AC motors	11
2.2	Comparison of the three conventional actuator types	17
2.3	Summary of BigDog specifications and performance results	34
2.4	List of estimated locomotion parameters based on body weight	43
3.1	List of importance of actuator requirements for leg joints	54
3.2	Joint range of motion of dog study and HyQ robot	59
3.3	Selection of hydraulic cylinders showing parameter a and b	72
3.4	Selection of hydraulic cylinders showing maximum torque	72
3.5	Selection of hydraulic cylinders showing the weight	72
3.6	Specification of a selection of DC brushless motor <i>emoteg</i>	76
3.7	Specifications of a selection of harmonic gears	76
3.8	Specifications of mountain bike rear suspension springs	81
3.9	List of simulation parameters for the spring mass model	82
3.10	Energy densities of batteries, fossil fuel and mechanical springs	84
4.1	HyQ robot system specifications	88
4.2	List of robot parts/components weights	90
4.3	Comparison of Material Properties	92
4.4	List of hydraulic joint geometric parameters	94
4.5	List of weight and inertia of the 5 main leg parts	97
4.6	List of specifications of the hydraulic pump units	104
4.7	List of specifications of the hydraulic valve	106
4.8	List of specifications of the hydraulic cylinder	107
4.9	Summary of the sensors used on HyQ with specifications	112

LIST OF TABLES

4.10	Specifications of Pentium CPU Board	116
4.11	Specifications of multifunction I/O board	117
4.12	Sensaray board 1-4: connection list	117
6.1	List of geometric design parameters of <i>Leg V1</i> and <i>Leg V2</i>	146
6.2	Comparison of two actuator units	148
E.1	List of unit conversions	175
E.2	List of <i>Hoerbiger</i> cylinder dimensions	177

Glossary

CAD	Computer Aided Design
CAN	Controller Area Network
COM	Centre of Mass
DOF	Degree of Freedom
FEM	Finite Element Model
HyQ	Hydraulic Quadruped
LxWxH	Length x Width x Height
PID	Proportional Integral Derivative
PWM	Pulse Width Modulated
SL	Simulation Laboratory

GLOSSARY

1

Introduction

The construction of walking machines has fascinated mankind ever since. With today's technology we are able to build dynamic legged machines. These machines are superior to wheeled vehicles in terms of mobility on rough terrain. Wheels have great performance on a paved, flat surface, but get easily stuck on rough terrain like sand, snow, rubble, rocks or forest beds. Legs on the other hand do not need a continuous path of support, but only isolated footholds. Furthermore, they allow active suspension of the body and easy adaptation to uneven terrain. In fact, evolution has created a big variety of legged animals from a body size of less than 1mm (insects) to over 10m (dinosaurs). The agility of some of these animals is exceptional. The mountain goat for example has excellent rock climbing and balancing skills, the squirrel runs smoothly on trees and the cheetah is the fastest runner of all animals.

The next section tries to answer the following questions: What are the motivations of constructing a highly dynamic quadruped robot? What are its benefits? And what are possible applications for such a machine?

1.1 Motivations

Most of today's legged robots lack the ability to perform highly dynamic tasks such as jumping and running. The two main reasons for this are the limited actuator performance in terms of speed and torque and the high stiffness of the joints. Actually, most of these robots are actuated by electric motors that lack the necessary power-to-weight

1. INTRODUCTION

ratio and cannot cope with high impact force peaks. Fluidic actuation like hydraulics or pneumatics and mechanical springs in combination with electric motors are promising alternatives due to their intrinsic compliance. In fact, some robots that are powered with these actuators performed very high jumping or fast running with different gaits. However, all of them are specialized for a limited number of very particular tasks and lack versatility. Furthermore, they are often connected to an external power source and therefore less suitable for real applications as described below.

Despite the advantages of legs over wheels, almost none of today's robots actually showed this superiority. Most legged robots need flat terrain to walk and run and have great difficulties to handle disturbances. The reason for this is mainly based on the highly non-linear dynamics of legged systems and the complexity to control many degrees of freedom in real-time.

An exception to all this, however, is the *BigDog* robot. During the last years, this quadruped robot regularly stunned the public with online videos that demonstrated its ability to perform highly dynamic tasks like running or balance recovery after slipping on ice. Besides these abilities, the robot's versatility allows it also to climb a pile of rubble or a steep slope. BigDog shows that today's technology is ready to construct such a versatile and highly dynamic robot; a fact that is a big source of motivation to realize a robot like HyQ¹.

Possible applications of such a machine (other than research) principally include tasks in areas that are dangerous for human beings and not suitable for wheeled vehicles:

- support for search and rescue operations in disaster areas after earthquakes, tsunami, landslides or avalanches.
- transport of emergency supplies (such as food, first aid) to disaster areas that are difficult or impossible to reach by trucks or helicopters.
- support for humanitarian demining of former war zones.
- inspection tasks in dangerous areas.

¹HyQ is the abbreviation for *Hydraulic Quadruped*.

1.2 Objectives and Proposed Approach

- various tasks in contaminated zones.
- support for forestry related tasks such as cutting small bushes for prevention against spreading forest fires.

I mentioned *highly dynamic* legged robots several times so far, but I have not defined its meaning yet. What separates a highly dynamic robot from other robots? For legged robots the general definition includes all dynamically stable robots that are able to accelerate their own body upwards so that all legs lift off the ground; for example during running (e.g. trot, bound, gallop for quadrupeds) or jumping and hopping. Furthermore, the definition includes all robots with the ability to recover balance after sliding on a slippery surface or after a strong external impact. A good example is Raibert's *3D biped* robot that is able to perform a somersault (flip) on a treadmill and keep its balance after landing [Playter and Raibert, 1992]. I added the word *highly* to make a clear separation from passive dynamic walkers as defined in [McGeer, 1990], which are based on limit cycle walking on an inclined plane, driven by gravity.

1.2 Objectives and Proposed Approach

The above mentioned reasons lead to the development of HyQ, a highly dynamic and versatile quadruped robot powered by a combination of electric and hydraulic actuators. The objectives of the robot can be summarized as follows:

- The creation of a versatile robotic platform able to perform highly dynamic tasks such as running and jumping, and able to move autonomously (in terms of energy and control) in difficult terrain, where wheeled robots cannot go.
- To study and test the applicability of hydraulic actuation to power legged robots, evaluating both oil and water as power transmitting media. Furthermore to evaluate low-level control algorithms, new system configurations and to test novel propulsion systems to increase the robot's operating time.
- To study biologically inspired locomotion focusing on dynamic running gaits and the importance of (adjustable) joint compliance, energy-efficiency, gait pattern generation, gait transitions and robot balancing skills.

1. INTRODUCTION

The aim of the present dissertation is to make a significant contribution toward the achievement of the above mentioned objectives. This document describes in details the design and construction of this legged machine. Moreover, it is intended to serve as a base for the construction of future similar robots and as technical and scientific report for people conducting research within the HyQ project and its collaborators.

The proposed approach to reach this aim is structured as follows:

1. define the specifications of the robot.
2. conduct design studies based on research in the field of animal locomotion, legged robotics, my own considerations and simulations.
3. design and construct a leg prototype for experiments to evaluate the mechanical design and the selected hydraulic actuator unit.
4. improve the design of the leg based on the experimental results.
5. design and construct the complete robot including onboard hydraulic actuation system.

1.3 Contributions

The contributions of this dissertation are the following:

- Design and construction of the quadruped robot *HyQ* with hybrid (hydraulic and electric) actuation system.
- Periodic hopping experiments with a 2-DOF¹ prototype leg to examine the overall compliance of the system including proportional controller gain, leg weight and oil pressure.
- Design guidelines for rotational robot joints driven by linear actuators, including the selection of geometric values to find a beneficial relation between joint torque and angle

¹Degrees of Freedom

1.4 Outline

This dissertation is organized as follows: Chapter 2 reports on the state of the art of highly dynamic legged robots with a focus on their actuation systems. Three types of actuation are presented and compared with each other. Chapter 3 presents the specifications of the HyQ robot and a series of studies on the robot design. Chapter 4 explains the robotic platform in details with a description of the mechanical design, the components of the sensor and actuation system and the computational unit. Chapter 5 shows the results of the experiments that were performed with both a prototype leg and the hydraulic actuator unit. Chapter 6 discusses the results and Chapter 7 ends this dissertation with the conclusions and an outlook into the future of the project.

1. INTRODUCTION

2

State of the Art

2.1 Introduction

A robot is per definition a machine with moving parts that accomplish a task. These motions are generated by actuators. Since a robot without moving parts would not be a robot, actuators are one of its most important components. The selection of suitable actuators is therefore a crucial part during the design process of a robot. This selection depends on many factors, such as size, weight, performance specifications, price and availability.

A vast number of actuator types exist with very different properties. The three conventional types of actuators for robot joints are electric, pneumatic and hydraulic actuators. They have been successfully used for all kinds of robots during the last decades. Newer actuators are based on Shape Memory Alloys (SMA), Electro-Rheological Fluids (ERF), Electro-Active Polymers (EAP) and piezoelectric actuators, to name only a few. [Mavroidis et al., 1999] and [Hollerbach et al., 1992] provide good introductions and overviews about these actuators. These newer technologies however do not (yet) meet the requirements of a legged robot as presented in this dissertation. Therefore this chapter will focus on the three conventional types of actuators and their application to legged robots.

First of all, I explain the basic principles of operation of these actuator types, focusing on the different kinds of electric motors and hydraulic cylinders. The robot

2. STATE OF THE ART

presented in this dissertation is actuated by a combination of these two actuator types, according to the specifications and performance requirements defined in section 3.1. A summary and actuator comparison concludes the first part of this chapter.

Since this dissertation describes the design of a highly dynamic legged robot, this chapter continues with the state of the art of these robots separated by type of actuation. Special focus lies on quadruped (four-legged) robots, but includes also monopod (one-legged), biped (two-legged) and hexapod (six-legged) machines if of particular relevance and significance. This overview is limited to the mechanical design of robots and does not include aspects of control. A review of early legged robots dating back to the 1960's precedes that section. The chapter ends with a short review of some aspects of locomotion research on animals.

2.2 Conventional Actuator Types

This section introduces the three conventional types of actuators (electric, pneumatic and hydraulic) that are most commonly found in today's robots. It ends with a summary of actuator comparison studies performed in the last few decades.

These three actuation types are based on two different fundamental principles of power conversion: Electric actuation is based on electric energy that is converted into mechanical energy. Pneumatic and hydraulic actuation are based on a fluid under pressure to generate mechanical motion and are therefore also called *fluid power actuators*.

2.2.1 Electric Actuation

The fundamental principle of all electric actuators is based on the force that is generated by an electric current flowing inside the wire of a coil in the presence of a magnetic field. There are several types of electric actuators mainly distinguished by the number of coils, their configuration, type of synchronization and current profile (DC or AC)¹. The remainder of this section will briefly introduce the most important types.

¹direct current (DC), alternating current (AC)

2.2 Conventional Actuator Types

The simplest electric actuator is a solenoid. The linear solenoid consists of a coil of wire, a fixed iron or steel frame and a movable iron or steel plunger, which is connected to a load. The electromagnetic field created by the current in the coil, exerts a force on the plunger [Kurfess, 2004]. The plunger is accelerated by this force and moves the load.

While there exist also other linear electric actuators, they are far less common than rotary electric actuators. Therefore the subsequent discussion is limited to the latter type. **Brushed DC motors** are constructed with a wound rotor (with coils) and a stator with either permanent magnets or coils. They usually have two or more poles and use direct current and brushes to alternately power the rotor coils. The so-called armature is the rotating part of the motor that contains the coils and the mechanical commutator, which are electric terminals that slide under the brushes. The commutator and brushes conduct the current to the coils and are mounted in a way to create the following effect: Opposite polarities of the energized rotor coils and the stator magnet attract each other and the rotor turns until it is aligned with the stator. Just before the alignment is happening, the brushes move across the commutator terminals and energize the next coil [Mavroidis et al., 1999]. Fig. 2.1 explains the working principle of a rotating two-pole brushed DC motor.

Brushless DC motors do not have brushes to accomplish the switching of the coils. Instead, they need an electronically controlled commutation system. While the rotor contains the permanent magnet, the coils are located on the outside at the stator. This way, the problem of leading current to a moving armature is solved. However, sensors that measure the position of the rotor (and therefore the position relative to the stator coils) become necessary. The sensors are either rotary encoders or hall-effect sensors. The latter sensor type varies its voltage output in response to changes of a magnetic field.

Brushless DC motors are popular in the robotic field because of their higher speed and torque capabilities, higher power density, low maintenance and improved efficiency in comparison with brushed DC motors. They are faster because they do not have brushes that create friction and require less maintenance because no brushes have to be replaced periodically. They are more efficient because the heat created in the

2. STATE OF THE ART

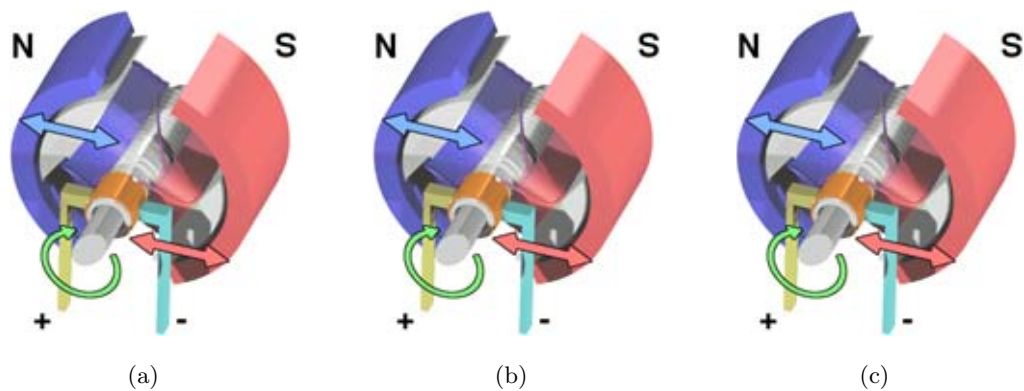


Figure 2.1: Model of a two-pole brushed DC motor shown in three different positions during a rotation, illustrating the working principle. Two permanent magnets with different polarities are located outside on the left (N) and right side (S); the armature contains two coils and the commutator terminals. **(a)** The left coil is repulsed from the left magnet and the rotor starts rotating clockwise; **(b)** the rotor continues to turn; **(c)** when the coil and magnet get aligned, the commutator reverses the direction of current through the coil, which reverses the magnetic field. Then the process starts again. (Images taken from Wikipedia [Wikipedia, 2010])

coils of the stator can dissipate more quickly through the motor housing. Disadvantages include high initial cost and more complicated motor controllers [Kurfess, 2004, Tsagarakis et al., 2007].

AC motors are driven by alternating current (AC). As in the brushless DC motor, the coils are located in the stator of the motor. AC motors can have 2, 4, 6, etc. poles. An alternating current in the coils produces a rotating magnetic field. There are two types of AC motors, depending on the type of rotor used. The first type is the *synchronous motor*, which rotates exactly at the supply frequency or a submultiple of the supply frequency. The rotor is constructed from either permanent magnets or electromagnets energised by direct current supplied through slip rings. The second type is the *induction motor*, which turns slightly slower than the supply frequency. The magnetic field on the rotor is created by an induced current. The rotor must have some 'slip': its speed must be less than, or lag behind, that of the rotating stator flux in order for current to be induced into the rotor [Bose, 2006].

2.2 Conventional Actuator Types

The rotor speed of synchronous AC motors depends on the frequency of the AC supply current f_{AC} (usually 50Hz or 60Hz) and the number of motor poles N_{poles} :

$$\omega_{rpm} = \frac{120f_{AC}}{N_{poles}} \quad (2.1)$$

where ω_{rpm} is the rotor speed in rotations per minute [rpm]. Table 2.1 shows the rotor speed of synchronous AC motors with 2-8 poles supplied by an alternating current of 50Hz or 60Hz.

Number of Poles	2	4	6	8
50Hz Frequency	3000	1500	1000	750
60Hz Frequency	3600	1800	1200	900

Table 2.1: Rotor speeds in [rpm] of synchronous AC motors for electric AC current frequencies of 50Hz and 60Hz.

Electric motors are the most widely used actuators in robotics and many other fields. They are therefore inexpensive and available in a big variety of sizes and specifications. Furthermore, they are popular because of their ease and accuracy of control. Their biggest disadvantage is limited actuator performance. Electric motors produce very small torques relative to their size and weight. Therefore reduction gears are necessary to convert velocity into torque. The gears, however, introduce undesired friction and backlash to the actuator unit and reduce its efficiency and backdrivability. In fact, these gears are increasingly becoming the weakest element of an electric motor unit [Tsagarakis et al., 2007] with the risk of breaking if their maximum permitted torque is exceeded.

For a more thorough discussion of this topic, the reader is invited to consult the following literature: [Mavroidis et al., 1999, Kurfess, 2004, Bose, 2006].

2.2.2 Pneumatic Actuation

The most common pneumatic actuator is the pneumatic cylinder. Pressurized gas pushes a piston inside the cylinder, which is connected to the load through a rod. This

2. STATE OF THE ART

creates a linear motion. The force F created inside the cylinder is the product of the fluid pressure P and the piston area A . More details about the operational principle and an explanation of the terms are presented in section 2.2.3 for hydraulic cylinders, which principally work the same way as pneumatic cylinders. Since the working fluid is a compressible gas (e.g. air), pneumatic cylinders are intrinsically compliant. This gives rise to energy efficiency limitations at pressures in excess of about 1MPa [Huber et al., 1997]. Therefore pneumatic cylinders are considerably weaker and slower than their hydraulic counterpart. Since the working fluid has no self-lubricating properties like oil, friction forces at the piston seals are high. On the positive side, there is no need for return lines of the fluid, because the air can simply be exhausted through the outlet valve through a muffler. Furthermore, pneumatics are cleaner, usually non-flammable and generally lighter due to the lower pressure levels and thus lighter construction [Mavroidis et al., 1999].

Another class of pneumatic actuators is the so-called pneumatic muscle actuator (*PMA*), sometimes also called after its inventor *McKibben*. Their simple construction is composed of a braided nylon fibre shell with an internal rubber tube, closed by two end plugs (one with the air inlet/exhaust port). If pressurized air is entering the muscle, the rubber tube expands in diameter and at the same time contracts in length (like a contracting biological muscle), due to the configuration of the interwoven nylon fibres. These actuators can contract up to 25%-30% of their natural length. They are extremely light-weight, tolerate slight misalignment and commonly operate at pressures ranging from 0-0.8MPa. While cylinders are generally controlled by a flow, PMAs are controlled by a pressure. Drawbacks of these actuators are their highly non-linear output force to contraction relation and the fact that they can only create a force in one direction [Caldwell et al., 1993].

2.2.3 Hydraulic Actuation

Hydraulic actuators are driven by a pressurized fluid such as mineral or synthetic oil or water. Other than in pneumatics, common operating pressures are usually around 20-30MPa and can reach up to 70MPa. The difficulty of high-pressure containment begins to outweigh high pressure advantages at about 40-45MPa [Huber et al., 1997].

2.2 Conventional Actuator Types

A basic hydraulic system consists of a pump, tank, filter, valves, tubing and an actuator (e.g. a cylinder), as shown in Fig. 2.2.

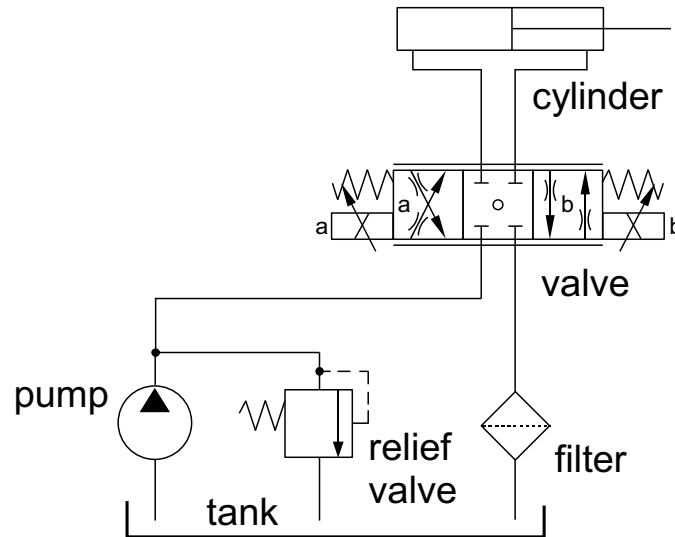


Figure 2.2: Schematic of a basic hydraulic system including a unidirectional fixed-displacement pump, a pressure relief valve, an oil tank, a solenoid operated proportional valve and a double-acting cylinder.

The pump creates hydraulic flow, the pressure relief valve keeps the maximum pressure at an adjustable preset level, the proportional valve controls the flow direction and magnitude and the hydraulic cylinder generates force to move a load. The efficiency η of a hydraulic pump is usually around 80-90%. The hydraulic power is the product pressure P and flow Q :

$$\text{Power} = P \cdot Q \quad (2.2)$$

More details about the proportional valve are provided in Section 4.3.2.3. The most important characteristics of hydraulic cylinders are provided next.

Fig. 2.3 shows a simple sketch of a double-acting asymmetric¹ cylinder with the most important geometric parameters and terms. It is double-acting since it can both push and pull. Its asymmetry is due to fact that the rod is present only on one side of the piston, which is the separation between the two cylinder chambers. Chamber A and B have therefore different cross-sections:

¹sometimes also called *unequal area cylinder*

2. STATE OF THE ART

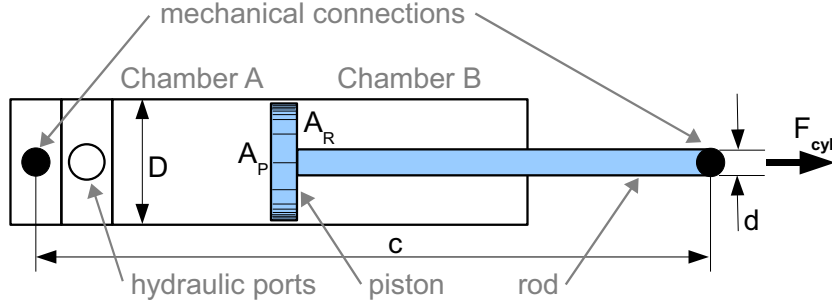


Figure 2.3: Sketch of a double-acting asymmetric hydraulic cylinder with most important geometric parameters and terms.

$$A_P = \left(\frac{D}{2}\right)^2 \pi \quad (2.3)$$

$$A_R = \left(\left(\frac{D}{2}\right)^2 - \left(\frac{d}{2}\right)^2\right) \pi = \frac{\pi}{4}(D^2 - d^2) \quad (2.4)$$

where A_P is the piston area, A_R the piston ring area, D the bore diameter and d the rod diameter. The variable total length of the cylinder is c , which is smallest for a completely retracted rod (c_{min}) and largest for a fully extended rod (c_{max}). The difference between c_{max} and c_{min} is called the stroke or stroke length of the cylinder l_{cs} :

$$l_{cs} = (c_{max} - c_{min}) \quad (2.5)$$

The total length of a hydraulic cylinder is composed of the cylinder body (which includes the hydraulic ports, the two chambers, the piston, seals and end stop cushions), the mechanical connections (cylinder bottom and rod end) and the current extension of the rod. Fig. E.2 shows a drawing of a hydraulic cylinder with its total length L_3 from one mechanical connection to the other. The ratio between the stroke length l_{cs} to the total cylinder length (with completely retracted rod) c_{min} is a number smaller than 1:

$$\frac{l_{cs}}{c_{min}} < 1 \quad (2.6)$$

The longer the stroke, the larger this number, because the relative contribution of the *dead* (or *overhead*) cylinder length to the total length is decreasing. Real-

istic numbers are from around 0.1 for short strokes up to 0.8 for very long strokes [Hoerbiger, 2008].

The output force of the cylinder F_{cyl} depends on the oil pressure inside the two chambers and on the piston area A_P and piston ring area A_R :

$$F_{cyl} = P_A A_P - P_B A_R - F_{friction} \quad (2.7)$$

where P_A and P_B are the hydraulic oil pressures of cylinder chamber A and B, respectively and $F_{friction}$ the friction force inside the cylinder.

Since the hydraulic fluid has a low compressibility and allows high pressures, hydraulic actuators have a relatively fast response and can provide a high force at the same time. High power can be transported through thin and flexible hoses with the power supply at a remote location. Additionally, they are reliable, mechanically simple, usually with low noise and relatively safe during operation [Mavroidis et al., 1999]. On one hand long transmission lines add a lag in the control of the system, but on the other hand they introduce a certain degree of compliance, which is related to the bulk modulus of the fluid (the reciprocal of compressibility). The bulk modulus β :

$$\beta = V_0 \frac{\partial V}{\partial P} \quad (2.8)$$

is a physical property of a fluid, which dominates the dynamic phenomena and depends not only on the oil compressibility but also on the free air presence in the oil as well as on the hose elasticity [Cunha et al., 2009]. This compliance prevents damage to the mechanical structure of a machine, for example if the shovel of an excavator hits a rock or if the leg of a running robot hits the ground or an obstacle.

The drawbacks of hydraulics are mainly related to the hydraulic oil itself and leakages. Low pressure leaking oil poses a threat of contaminating the surrounding environment. Pressurized oil can be harmful to human because it can pierce skin and damage the eyes. However, with proper design, leakage can be virtually eliminated [Hollerbach et al., 1992]. Another disadvantage is the highly non-linear characteristics of a hydraulic system due to non-linear properties of valves, cylinders, bulk modulus, change of oil viscosity with temperature, volumetric changes, etc. [Cundiff, 2001].

2. STATE OF THE ART

These characteristics may complicate the control, modelling and simulation of hydraulic systems. However, today's knowledge of the field and the increasing processing power of computers and micro-controllers help to reduce these difficulties. Another drawback is the fire hazard of oil for high temperatures. A heat exchanger (or cooler) that keeps the oil at a desired temperature, generally solves this problem and additionally keeps oil viscosity constant.

2.2.4 Actuator Comparison and Summary

This section will compare the properties of the three actuation types that have been discussed above and give a summary. Table 2.2 lists the most important properties and performance measures of electric, pneumatic and hydraulic actuation.

Linear actuators, including pneumatic and hydraulic cylinders but also newer types of actuators, are often compared with their maximum *stress* and *strain*. The actuation stress σ is defined as the applied force per unit cross-sectional area of an actuator. Like pressure it has the unit of Pascal [Pa]. σ_{max} is the maximum value of actuation stress in a single stroke which produces maximum work output. The actuation strain ϵ is defined as the nominal strain produced by an actuator: an actuator of initial length L extends to a total length of $(1 + \epsilon)L$. It is a ratio and therefore unitless. ϵ_{max} is the maximum value of actuation strain in a single stroke which produces maximum work output [Huber et al., 1997]. These two values are especially useful to compare a variety of different actuator types with each other.

Fig. 2.4 shows a chart with the classification of a selection of linear actuators including hydraulic, pneumatic and some of the newer type actuators mentioned above in the introduction of this chapter (section 2.1). The graph was originally published in [Huber et al., 1997] and was re-drawn in [Gomis-Bellmunt and Campanile, 2010]. The graph shows that both pneumatic and hydraulic actuation have a very high maximum strain. In terms of maximum stress, hydraulics (20-70MPa) is almost two orders of magnitudes stronger than pneumatics (0.5-0.9MPa).

2.2 Conventional Actuator Types

Property	Electrical	Pneumatic	Hydraulic
basic system	solid state logic, power amplifiers, DC or AC motors, gear boxes, coolers	compressor, interstage coolers, pressure controls, filter, dryers, mufflers, valves, actuators	pump, pressure regulators, filters, heat exchangers, servo valves, actuators, accumulators
working principle	electricity	air, nitrogen, combustion products	high quality oil, water based solutions, synthetic liquids
power supply	a few Volts to 460V	0.04-0.9MPa	0.4-70MPa
efficiency	over 90% for large systems	seldom over 30%	seldom over 60%
max. stress	low	fair	excellent
force to weight ratio	<i>poor</i> : Motor and gearing must be carried by each sub-system	<i>fair</i> : Light weight, but low pressures	<i>excellent</i> : Very high pressures
temp. sensitivity	low in the operating range	very high, since volume and pressure are directly related to temperature	low, except for viscosity changes
heat removal	poor, relative to hydraulic	heat removal normally no problem	excellent, at remote heat exchangers
safety of operation	safest system electrical shock hazard and grounding must be considered	flying debris from ruptures can be dangerous, explosions possible when volatile oils are present	leakage of flammable fluids and fire hazards high, velocity jets of fluid can pierce skin, damage eyes
costs	relatively low	low	high

Table 2.2: Comparison of the three conventional actuator types: electric, pneumatic and hydraulic. (Adapted from [Mavroidis et al., 1999] with additional information from [Hollerbach et al., 1992, Caldwell et al., 1995, Huber et al., 1997])

2. STATE OF THE ART

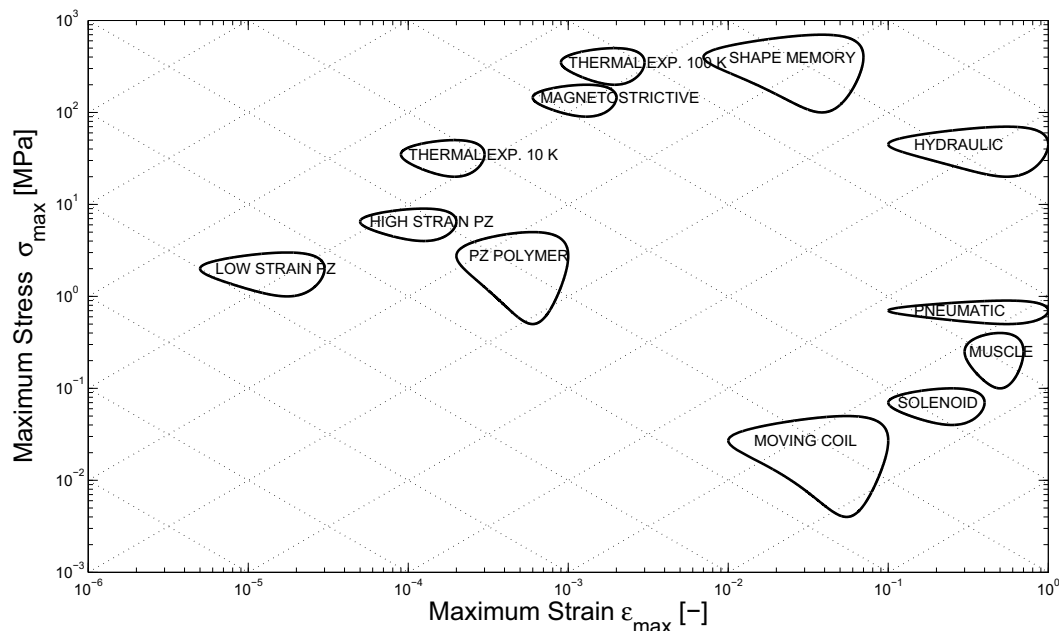


Figure 2.4: Maximum Stress vs. Maximum Strain graph for different actuator types such as pneumatic, hydraulic, Piezo (PZ), SMA and muscles. (Image taken from [Gomis-Bellmunt and Campanile, 2010], which is based on [Huber et al., 1997])

In the field of robotics, nowadays electric motors are the most common actuators. During the beginning of robotics research in the 1960's and 1970's however, hydraulic actuation was the first choice (see section 2.3). Later, due to the technological advances in the field of electric motors and microcontrollers, electric actuation became more and more popular and hydraulic actuation has only been used by few robotic researchers. Electric motors became more compact, available in a big range of sizes and performances, easier to control and inexpensive. However, their limitations due to low power to weight ratio and gears are increasingly problematic in the construction of robots designed for dynamic motions. Pneumatics and hydraulics are therefore gaining renewed interest in the robotics community. The main obstacles that keeps researchers of robotics from using hydraulics are the following:

- Compact hydraulic system components are not yet available on the market and most of the few existing components are still very expensive.
- Construction of prototype machines with changing configurations can be messy because of the hydraulic oil in the tubes and components.

2.3 Early Legged Robots

This section will give a historical review of the earliest legged robots with a particular focus on quadrupeds. The major part of the following information was copied from [Song and Waldron, 1989], [Raibert, 1986] and [González-de Santos et al., 2006] and is marked accordingly at the end of the paragraphs. The reader is invited to consult these books to get a more detailed review.

In 1960, an extensive study of linkage mechanisms for legged locomotion was undertaken by Shigley. In that paper, he proposed several mechanisms which could be used as legs for walking machines. These mechanisms included four-bar linkages, cam linkages, pantograph mechanisms, etc. He also built a vehicle with four rectangular frames. Each frame served as a leg and was nearly as long as the body. The legs were moved in pairs and the stroke was short enough to ensure static stability. The motion of the legs was controlled by a set of double-rocker linkages. Although it did function, it required non-circular gears for uniform velocity of foot motion and was found to be not practical [Song and Waldron, 1989].

In the early 1960's, the Space General Corporation developed two walking machines in order to explore the concept of legged locomotion for a lunar rover. One of these was an externally powered, six-legged machine, while the other was a self-contained, eight-legged machine. The leg motions of both machines were coordinated by cams and transmitted by linkages. These vehicles were quite effective within their design goals. The eight-legged machine could turn on its own length using a form of skid steering. The terrain adaptability was poor, however, due to lack of the necessary degrees of freedom [Song and Waldron, 1989].

In the mid 1960's, Mosher and Liston built a four-legged walking truck at General Electric (Fig. 2.5(a)). The project was part of a decade-long campaign to build better teleoperators, capable of providing better dexterity through high-fidelity force feedback. The machine Mosher built stood 3.3m tall, weighed 1400kg, and was powered hydraulically. Each of the driver's limbs was connected to a handle or pedal that controlled one of the truck's four legs. Whenever the driver caused a truck leg to push

2. STATE OF THE ART

on an obstacle, force feedback let the driver feel the obstacle as though it were his or her own arm or leg doing the pushing. Despite its dependence on a well-trained human for control, this walking machine was a landmark in legged technology, and it continues to be a significant advance over many of its successors [Raibert, 1986].

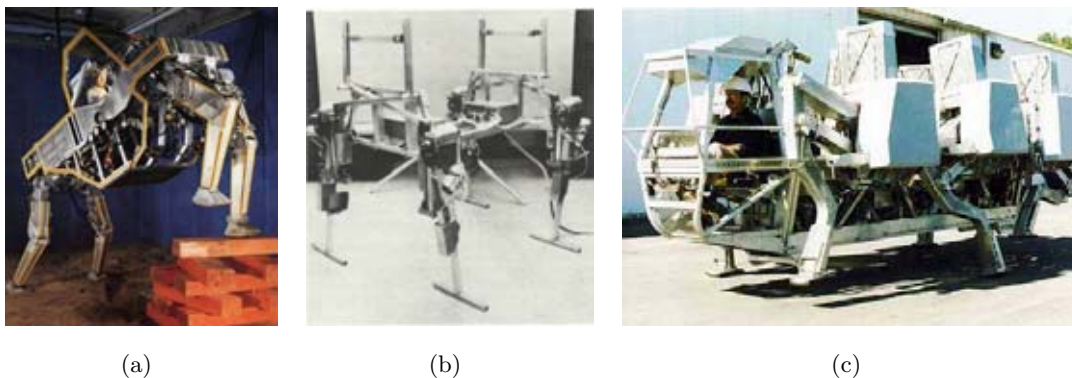


Figure 2.5: Picture selection of early legged robots: (a) GE Walking Truck; (b) Phony Pony and (c) ASV hexapod [González-de Santos et al., 2006, Song and Waldron, 1989].

In 1966, McGhee and Frank built a medium-sized (50kg) quadruped called *Phony Pony* (Fig. 2.5(b)). Each leg was based on a two DOF system with rotary joints actuated by electric motors. The feet were based on an inverted T-shape structure that provided stability in the frontal plane. Each joint had a number of sensors for detecting whether the joint was locked, in forward motion or in backward motion. With these three different states, and using electronic logic based on flip-flops, they created a state machine with six synchronized states. The robot performed the quadruped crawl and the diagonal trot depending on the selected state diagram. The Phony Pony was a milestone of paramount significance because it inspired McGhee, then at the Ohio State University (OSU), to build new machines that also became important milestones in the history of walking robots: the OSU hexapod and the Adaptive Suspension Vehicle (ASV) [González-de Santos et al., 2006].

The OSU hexapod, built in 1977, was the first computer-controlled walking robot. Its legs were based on an insect leg type with three rotary joints driven by electric

motors. This robot became the experimental test bed for a large number of scientific results related to gait generation, robot control, and force distribution algorithms. In 1986, McGhee along with Waldron, who was still at OSU, built and tested the 2700kg *ASV hexapod* (Fig. 2.5(c)), possibly the largest and most extraordinary terrain-adapted walking machine ever built [González-de Santos et al., 2006].

In 1976, Hirose started the development of a large series of quadruped robots at the Tokyo Institute of Technology. In a recent article [Hirose et al., 2009] he gives an overview of his first robots: *KUMO-I* was the first prototype model of his walking robot inspired by a daddy long-legs¹ in 1976 (Fig. 2.6(a)). The leg length is 1.5m and the weight of the robot 14kg. The robot had 8 DOF to perform walking in the sagittal plane. However, each leg has only one actuator and uses a clutch mechanism to reduce the total weight of the robot. The locomotion ability is insufficient because of the limited power of the actuators. The results suggest that straightforward mimicking of animals is not effective to develop a walking robot. *PV-II* is the second prototype with the so-called gravitationally decoupled actuation, a solution to make walking robots more energy-efficient. The leg length was 0.9m and the weight of the robot 10kg. The originally proposed *3D pantographic mechanism (PANTOMECH)* was adopted to increase the leg's workspace and reduce the weight of the leg. This mechanism expanded the prismatic motion of the three orthogonal axes provided on the torso part and simplifies their control. In 1979, the *PV-II* was the world's first success in sensor-based stair climbing using leg-end tactile sensors and posture sensors [Hirose et al., 2009].

TITAN III (Fig. 2.6(b)) has improved on the *PANTOMECH* legs with an increased mobility range and reduced weight by using carbon fibre composite plastic. The length of the legs is 1.2m, and the weight of the robot 80kg. The feet of *TITAN III* are equipped with whisker sensors and a signal processing system that is made up of wires with shape memory alloy properties that have hyperelastic characteristics and measure the status of ground contact. Moreover, the robot is equipped with a posture sensor, and is loaded with an intelligent gait control system called perspective gait supervisory system (*PEGASUS*) for the purpose of making decisions regarding the sensor information in an integrated manner and realizing terrain-adaptive static walking [Hirose et al., 2009].

¹a family of spiders (cellar spider)

2. STATE OF THE ART



Figure 2.6: Pictures of two early quadruped robots developed by Hirose at Tokyo Institute of Technology: (a) *KUMO-I* and (b) *TITAN III* [Hirose et al., 2009].

During the subsequent three decades until today, the robotic research community has created hundreds of legged robots with a variety of sizes, number of legs, configurations, materials, actuator types and power systems. A big part of them are listed in the *Walking Machine Catalogue*, which can be found online following the link provided here: [Berns, 2010]. The interested reader is invited to consult this website or refer to the article of Machado et Silva that gives a good overview of legged robots [Machado and Silva, 2006].

2.4 Highly Dynamic Legged Robots

This section presents the state-of-the-art of highly dynamic legged robots. (Refer to section 1.1 for a definition of the term *highly dynamic*.) This review presents a selection of the most significant robots, separated by type of actuation. Special focus lies on quadruped (four-legged) robots, but includes also monopod (one-legged), biped (two-legged) and hexapod (six-legged) machines if of particular relevance and significance.

2.4.1 Electric Robots

As stated in above section about the actuator comparison (section 2.2), electric motors are not optimal to directly actuate highly dynamic legged robots, mainly because of

2.4 Highly Dynamic Legged Robots

their low output torque and necessity of reduction gears. However by adding springs to the joints (either in series with the motor or on a passive joint) dynamic motions have been achieved in several robots. This section will provide an overview of the most relevant of these robots.

In the end of the 1990's, Martin Buehler started the development of the *Scout* robot series at the Ambulatory Robotics Lab (ARL) of McGill University. In 1999 he presented *Scout II* (Fig. 2.7(a)), a dynamically stable running quadruped robot with a very simple mechanical design: it only has one active rotational joint per leg located at the hip, which rotates the leg in the sagittal plane. The leg itself consists of an upper and lower leg that are connected via a spring to form a compliant prismatic joint [Buehler et al., 1999]. *Scout II* weighs 27kg and has the following dimensions: 0.55m x 0.48m x 0.27m (LxWxH)¹. Some years later, *Scout II* was able to perform a stable bounding gait with a forward velocity of up to 1.3 m/s [Poulakakis et al., 2005].

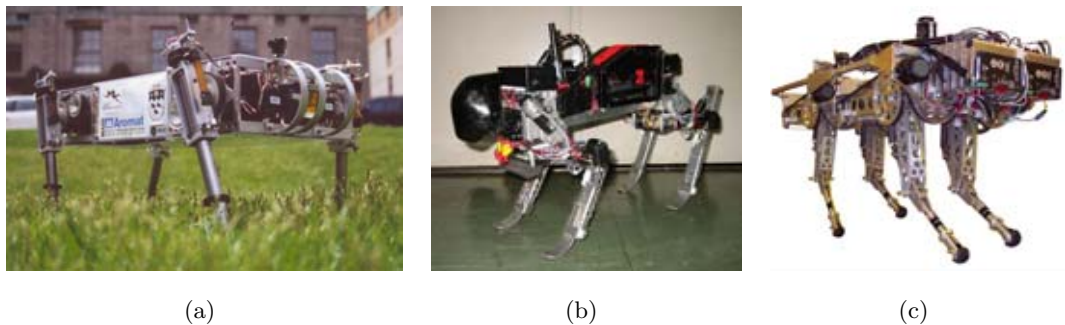


Figure 2.7: Picture selection of electrically actuated quadruped robots: (a) *Scout II* [Poulakakis et al., 2005]; (b) *Tekken II* [Kimura et al., 2007] and (c) *KOLT* [Estremera and Waldron, 2008].

The quadruped robot *Patrush* and later the *Tekken* series are developed by Hiroshi Kimura and colleagues. *Tekken II* shown in Fig. 2.7(b) is a small quadruped robot of 0.3m length and 4.3kg weight. It is actuated by electric motors. Mechanical springs add compliance to the joints. The robots are mainly used to study biologically inspired controllers based on central pattern generators (CPG) and joint reflexes. Kimura also

¹LxWxH: Length x Width x Height

2. STATE OF THE ART

conducted studies on quadruped bounding by utilizing the natural dynamics of the mechanical system [Kimura et al., 1999, Zhang et al., 2006].

The *KOLT* robot shown in Fig. 2.7(c) was developed by Kenneth Waldron and his group at Stanford University in collaboration with Ohio State University. The quadruped robot has electric actuation with mechanical springs for added compliance. The robot weighs 80kg and has the following dimensions: 1.75m x 0.6m x 0.8m (LxWxH). For the running experiments, the robot was attached to a boom that permitted free motion in the plane. The robot successfully performed stable trotting with 1.1m/s on a treadmill [Palmer and Orin, 2007, Estremera and Waldron, 2008].

Some interesting electrically actuated monopods have been developed: In the mid 1990's Buehler presented the *ARL Monopod*, a planar one-legged robot with a prismatic leg. It was able to hop at a top speed of 1.2m/s, which made it the fastest electrically actuated legged robot at that time. Thanks to its mechanical coil-spring in the leg and the exploitation of the natural dynamics, it had a very low average power consumption [Gregorio et al., 1997]. Other more recent monopods are *Thumper*, based on the Electric Cable Differential (ECD) leg of Jonathan Hurst that is able to perform planar hopping. A combination of pulleys and steel cables, allow the separate control of leg length, leg stiffness and hip angle. This 38kg robot is able to perform energy efficient hopping by temporarily storing energy in leaf springs [Hurst and Rizzi, 2008].

The common feature of all these robots is the compliant element in the legs, realized either with coil or leaf springs. These springs accomplish two functions: they allow energy-efficient locomotion based on the natural dynamics of the robot mechanics and they protect the gears of the electric motors from excessive force/torque peaks.

2.4.2 Pneumatic Robots

There exist a number of pneumatically actuated robots that are able to perform highly dynamic tasks. Some of them are constructed with pneumatic cylinders and others with McKibben muscles. This section presents the most relevant of these robots.

2.4 Highly Dynamic Legged Robots

Airhopper is a quadruped robot developed at the Hirose laboratory of the Tokyo Institute of Technology (Fig. 2.8(a)) that is designed to carry supplies over uneven terrain to disaster areas or isolated districts [Tanaka and Hirose, 2008]. It is a leg-wheel hybrid robot with dimensions of 1.29m x 1.2m x 0.6m (LxWxH) and a mass of 34.6kg. Each robot leg is constructed with a four-bar linkage actuated by three custom single-acting pneumatic cylinders and has an electrically driven wheel at its end. The robot's light-weight construction allows it to perform a powerful vertical jump that lifts up its feet 0.85m from the ground. The pressure in the cylinders is 0.6MPa during the acceleration phase of the jump. The robot actively dampens the impact at touch-down, by extending the decelerating phase of the robot.

Both the electric and pneumatic power supplies are external. An internal air tank is installed to provide temporary air supply. The robot is designed to use its wheels to move on flat surfaces and take steps or jumps if rough terrain and obstacles are in the way. Due to its four-bar linkage design, the foot can only be moved on a specific surface relative to the leg attachment to the body. It has therefore a limited choice in foot-hold selection, which makes walking over rough terrain a more difficult task.

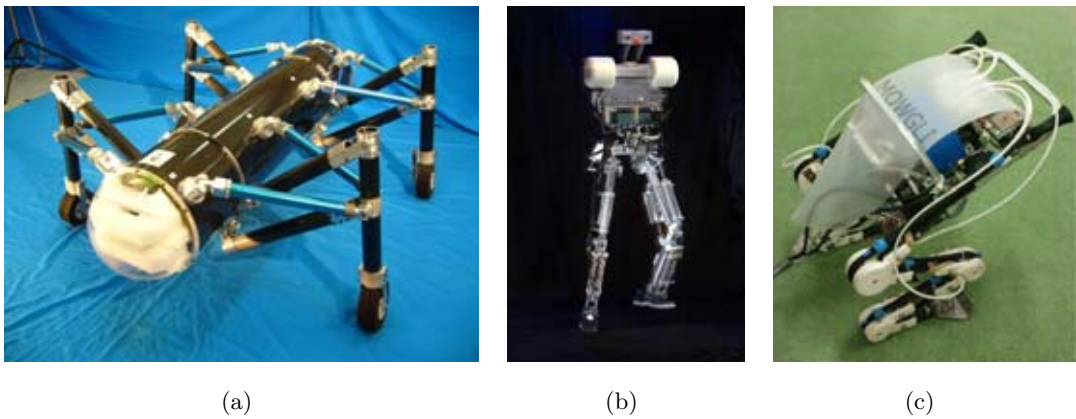


Figure 2.8: Picture selection of pneumatically actuated robots: (a) quadruped robot *Airhopper* of Tokyo Institute of Technology (Japan) actuated by pneumatic cylinders [Tanaka and Hirose, 2008]; (b) biped robot *Dexter* of Anybots Inc. actuated by pneumatic cylinders [Anybots Inc., 2010] and (c) jumping robot *Mowgli* of University of Tokyo (Japan) actuated by pneumatic muscles [Niiyama et al., 2007].

2. STATE OF THE ART

Dexter is a biped robot developed by Anybots Inc., a private company founded in 2001 and based in California (USA). According to their website [Anybots Inc., 2010] (no scientific publication is available), Dexter is 1.78m tall (Fig. 2.8(b)), weighs 61kg and is able to balance dynamically on two legs, walk, jump, and will be able to run. The website further explains that there are no stable postures that it can be put in where it can balance without active feedback, so it has to constantly adjust based on its sense of balance. The joints of Dexter are powered by pneumatic cylinder actuators. The power supply of the robot is off-board.

Some videos on the website show Dexter’s balancing and walking abilities. Anybots Inc. states that Dexter learned how to walk with its *learning software*. One of the videos shows the robot perform a powerful vertical jump from a squat posture, reaching a maximum jumping height of around 0.2m and land on the feet again without losing balance.

Mowgli is a biped robot developed at the Intelligent Systems and Informatics Laboratory of University of Tokyo (Japan) [Niiyama et al., 2007]. The robot has the shape of a frog with large, strong hind legs (Fig. 2.8(c)). Each leg features three DOF and is actuated by three pneumatic McKibben muscles of different sizes. The largest muscle is the one closest to the body and actuates the hip joint. The remaining two muscles are smaller and are bi-articular, which means that they work on two joints rather than just one. The lower bi-articular muscle allows a fast ankle rotation. The robot weighs 3kg and is 0.9m long with extended legs. The power supply of the robot is off-board.

Mowgli has successfully performed several highly dynamic motions: during a vertical jump it reached a maximum toe to ground distance of 0.26m. In another experiment, it was able to execute a jump of 0.4m onto a chair using a dynamic whole body motion.

To the current date, none of these robots is versatile to perform all three locomotion modes: walk, run and jump. Neither locomotion on rough terrain has been shown. Furthermore, we believe that pneumatic actuators are not the optimal choice for versatile, highly dynamic legged robots, mainly due to the lower power-to-weight ratio and response time compared to hydraulic actuators.

2.4.3 Hydraulic Robots

A special focus of this review is given to hydraulically actuated robots, since the main actuation system of the robot presented in this dissertation is also hydraulic.

2.4.3.1 Raibert's Robots in the 1980's

Marc Raibert and his colleagues at the Leg Labs at Carnegie Mellon University (CMU) and later Massachusetts Institute of Technology (MIT) set many milestones in dynamic legged locomotion. They constructed several hopping and running robots.

In 1979, Marc Raibert started to build his first hopping robot: A computer controlled pogo stick. It was intended to serve as a model for learning about control and active balance that eventually would lead to a fundamental understanding of legged locomotion. This first planar monopod robot was improved and resulted in the monopod *3D hopper* shown in Fig. 2.9(a). This robot was able to hop in place, travel from point to point on a plane under velocity or position control and maintain its balance when pushed [Raibert, 1986].

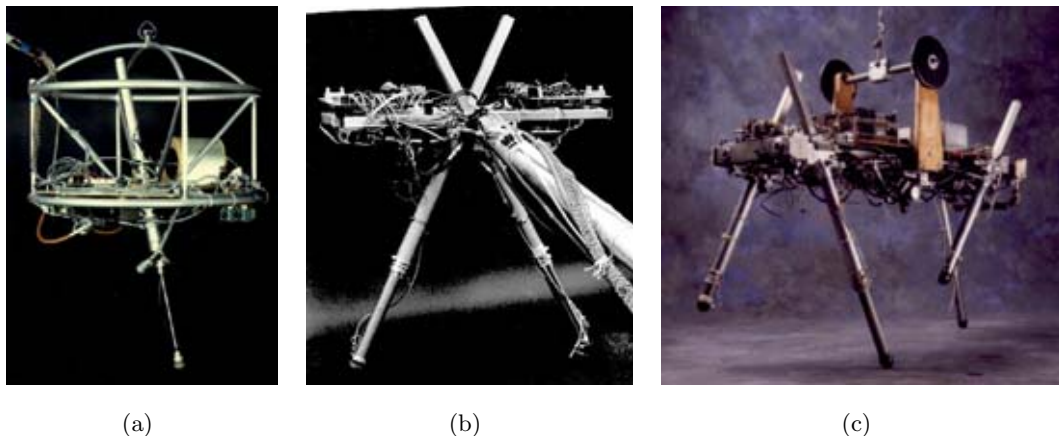


Figure 2.9: Pictures of three robots built by Raibert in the 1980's: (a) monopod 3D-hopper; (b) 2D-biped and (c) quadruped robot [Raibert, 1986, MIT Leg Lab, 2010].

The underlying control principle treats hopping height, forward speed and body at-

2. STATE OF THE ART

titude as three separate control problems. Hopping height was adjusted by the amount of thrust given for each hop. Forward speed was regulated by extending the foot forward to a position that will provide the necessary acceleration during the stance phase. Body attitude was controlled during the stance phase by moving the hip. A state machine switched between the states to synchronize the control. The couplings between these activities were treated as disturbances by the three separate controllers. This control principle is often referred to as *Raibert's three-part control* and is a milestone in legged locomotion research [Raibert, 1986].

Raibert later built biped and quadruped robots with prismatic legs that were able to run and hop (Fig. 2.9(b) and Fig. 2.9(c)). He proved that his control method can be extended to biped and quadruped running. Since there is only one foot on the ground at any time during biped running, the same three-part control as for a monopod can be used. For quadrupeds, the concept of the *virtual leg* was used. If two legs act in unison (touching and leaving the ground at the same time) they can be considered as a functionally equivalent virtual leg located at the centre of the leg pair. The quadruped is therefore reduced to a biped for which the three-part control is working. Depending on the grouping of the legs (either diagonal, front/hind or left/right pairs) this resulted in different quadruped running gaits: trot, pace and bound, respectively [Raibert et al., 1986].

Raibert's quadruped robot had the following dimensions: 1.05m x 0.35m x 0.95m (LxWxH) and weighed around 25kg. The four prismatic 3-DOF legs were hydraulically actuated (2 DOF in the hip and 1 DOF to change the leg length) and had a pneumatic spring that provided compliance and temporary energy storage. The computational unit and the hydraulic power supply were not carried onboard. The robot achieved trotting, pacing and bounding on the laboratory floors [Raibert, 1990].

While Raibert's first robot was actuated by three pneumatic cylinders, the 3D hopper was driven by two hydraulic cylinders for hip positioning and a pneumatic cylinder with air spring as leg. All subsequent robots were driven by hydraulic cylinders in the hip and a combination of a hydraulic cylinder with air spring for the leg itself. The leg length of multilegged robots needs to be controlled rapidly, since the legs have to be

moved in symmetry and have to be retracted quickly during the flight phase to avoid hitting the ground. All described robots had prismatic legs.

2.4.3.2 Kenken

Sang-Ho Hyon and his colleagues at Tohoku University (Japan) started the development of a hydraulic quadruped robot in 1998. They first built the monopod robot *KenKenI* (Fig. 2.10(a)) and later a biped version *KenKenII* (Fig. 2.10(b)), but never actually constructed a quadruped robot. Nevertheless, they achieved impressive results [Hyon et al., 2003b, Hyon et al., 2003a].

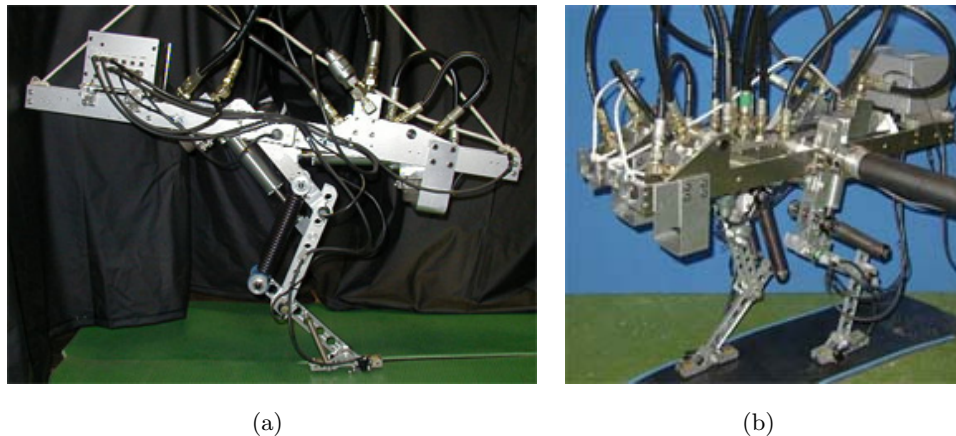


Figure 2.10: Pictures of the hydraulic hopping robots: (a) KenKenI and (b) KenKenII [Hyon et al., 2003b, Hyon et al., 2003a].

KenkenI is the one-legged version with two active and two passive DOF with springs. The leg consists of four segments including a foot (or toes). While the upper two joints (hip and knee) are actuated by hydraulic cylinders, the ankle joint is passively moved by a pantograph structure with springs, as shown in Fig. 2.10(a). The toes contain a ground contact sensor and are connected to the leg with a passive rotational joint with spring. KenKenII was the extended version with two identical of those legs. All valves and control electronics were on-board, but the electric and hydraulic power supplies were off-board. The robots were connected to a boom, which was rotating around a

2. STATE OF THE ART

central pole and permitted the robots to freely move in a 2D plane.

2.4.3.3 BigDog

Marc Raibert and some of his colleagues founded Boston Dynamics Corporation in the year 1992 as a spin-off from the MIT. The company's initial focus was on software for human simulations, such as *DI-Guy*, which was mainly used for military applications [Boston Dynamics Corp., 2010]. In 2005 however they presented a first version of their quadruped robot called *BigDog* (Fig. 2.11(a)) the preliminary result of a project funded by the Defence Advanced Research Projects Agency (DARPA) of the US American military. According to [Buehler et al., 2005], the project's main goal is the development of a mechanical mule with the following properties:

- power autonomous
- capable of carrying significant payloads
- operating outdoors
- with static and dynamic mobility
- fully integrated sensing for mobility
- able to jump over a 1m ditch, climb 45° (100%) slopes, run at 5m/s, and carry over 50kg payload.

The robot presented in 2005 (let us call it *BigDog 2005*) was 1m tall, 1m long and 0.3m wide, and weighed about 90kg. It had four legs with four DOF each: three active rotational joints powered by hydraulic cylinders and one passive linear joint in the foot based on a pneumatic spring. In two other publications in the year 2006, [Playter et al., 2006, Buehler et al., 2006] and a stunning video published on internet, Boston Dynamics presented BigDog with a new leg configuration. While initially the knees of all four legs were pointing to the front, the newer version (let us call it *BigDog 2006*) featured an *X configuration*, where the front and hind knees pointed to each other, to the centre of the robot (Fig. 2.11(b)). Unfortunately, none of the publications explains the reason for this change, but it was likely due to stability reasons. The robot

was able to walk up and down 25° inclines, trot at speeds up to 1.8m/s, walk over loose rock beds at 0.7m/s and carry over 50kg of payload.

Boston Dynamics regularly stuns with amazing videos of BigDog published on their website [Boston Dynamics Corp., 2010] and recently on their youtube channel [Youtube, 2009]. The first one in February 2006 showed the robot trotting slowly over grass, loose rock beds, snow and on slopes, turning on the spot and keeping balance after kicks from the side. In March 2008 the second video was released, showing a new version of BigDog (Fig. 2.11(c)), able to walk through forest, snow, up and down slippery slopes, recover balance after sliding on ice and after kicks from the side, carry over 150kg of payload, cross a pile of scattered concrete blocks and run in the laboratory with a bounding gait. The major difference is a new kinematic structure of the robot leg: an additional active rotational joint was added in the flexion/extension plane.

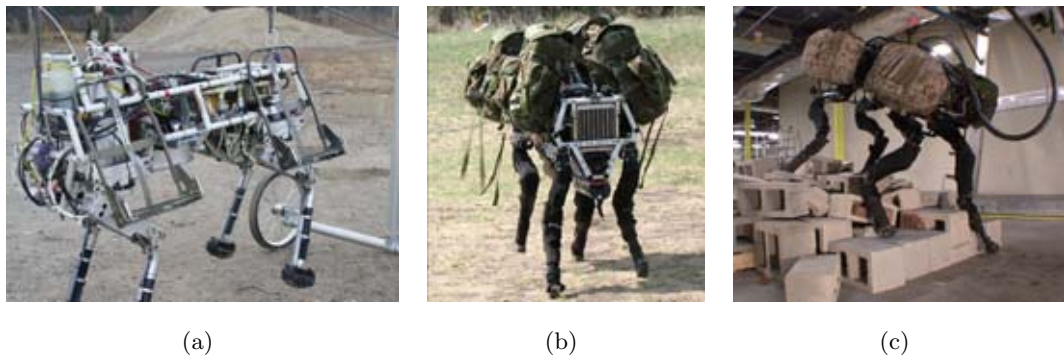


Figure 2.11: Picture selection of various versions of BigDog: **(a)** *BigDog 2005* [Buehler et al., 2005]; **(b)** *BigDog 2006* [Playter et al., 2006] and **(c)** *BigDog 2008* [Raibert et al., 2008].

This new version (let us call it *BigDog 2008*) was presented in a short paper by Raibert [Raibert et al., 2008], unfortunately with little details and not mentioning the reasons for the additional leg DOF. We can only speculate and guess that the third active rotational joint in the plane allows to choose from a bigger selection of footholds (better traction) and to choose the angle between the ground plane and the lowest leg segment. The latter is important to select the direction of the force vector created by

2. STATE OF THE ART

the spring in the lowest leg segment.

In 2009 Boston Dynamics released a few new videos on their youtube channel [Youtube, 2009] showing BigDog at the beach walking on sand and in shallow water, walking on mud, following a human operator in the forest and showing its reflexes in different situations. To the authors best knowledge, no other scientific article than the four mentioned above has been published about BigDog until the time of writing of this dissertation, except [Howard, 2008], which is a paper about visual odometry for autonomous ground vehicles with BigDog as one of the applications.

Since the BigDog project is mainly sponsored by the American military, very little information regarding the details of the design, components, and specifications of the robot are known. Not much has been officially published about its control, balance and foot-hold planning algorithms either. But it is certain that the control is based on Raibert's previous research in the 1980's. Some more details have been recently published on the Boston Dynamics website in a presentation-style overview containing 22 slides [Boston Dynamics Corp., 2008]. It provides some details about its architecture, engine, actuators units, hydraulic circuit, sensors, on-board computer and software, processes and control principles.

Fig. 2.12 shows some pictures of the engine and actuator unit of the previous (*BigDog 2006*) and new (*BigDog 2008*) version of the robot. The new engine is a two-stroke, single cylinder *Leopard* go-kart engine with around 11kW power and up to 9000rpm. It is water-cooled and features an electric starter. The hydraulic actuator units consists of a custom made cylinder with integrated 2-stage electro-hydraulic valve and position and force sensor. The pictures show that BigDog is equipped with *MOOG* valves of series 30 (or type 50, the equivalent version for industrial use).

The MOOG valve series 30 (Fig. 2.13(a)) is a two-stage electro-hydraulic servo valve with compact dimensions (40mm x 38 mm x 39mm) and low weight (190g). The first stage is actuated by a torque motor that controls the position of a flapper inside a nozzle. This way the hydraulic flow of stage one moves the valve spool, which controls the main flow of stage two. It is basically a hydraulic amplifier circuit. The valve

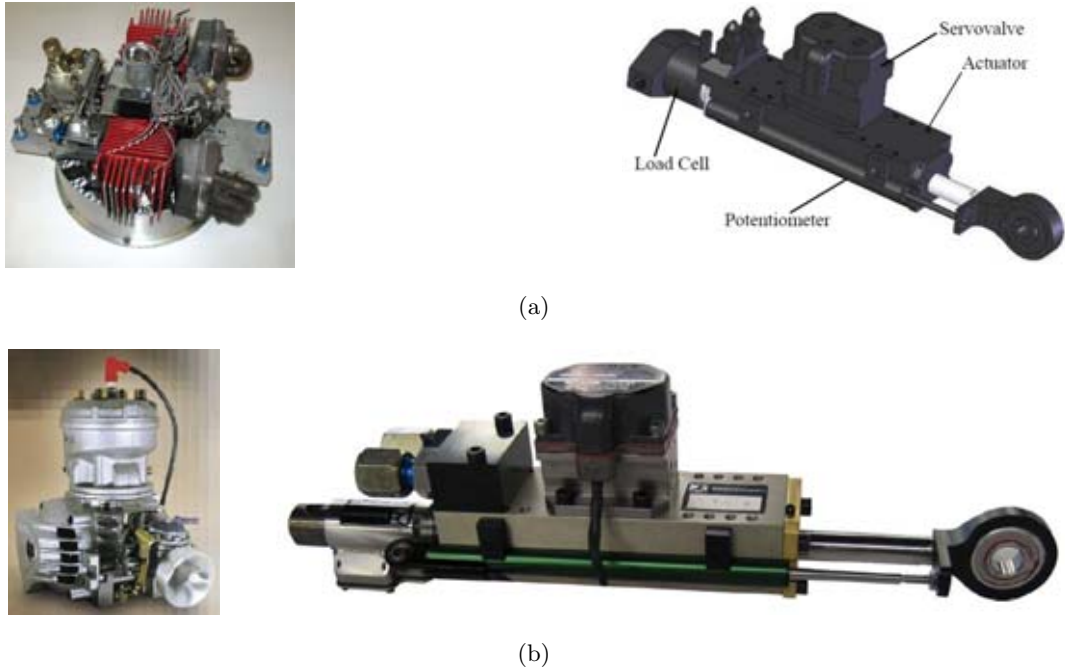


Figure 2.12: Pictures of BigDog’s actuation system components: engine on the left and hydraulic cylinder with integrated valve and sensors on the right: **(a)** components of *BigDog 2006* [Buehler et al., 2006] and **(b)** components of *BigDog 2008* [Boston Dynamics Corp., 2008].

has a high bandwidth of $>200\text{Hz}$ (frequency response: relationship of no-load spool position to input current) for peak sinusoidal inputs of $\pm 25\%$ of rated current with a supply pressure of 20.7MPa (3000psi). The clear advantages of this valve are the small dimensions and weight and fast response. On the other hand, it has a very high cost of $>2000\text{Euro}$ and a big leakage flow of up to 0.47lpm (litres per minute) with spool at null position at 20.7MPa supply pressure. A leakage of up to 0.35lpm is always present at 20.7MPa independent from the spool position [MOOG Inc., 2007].

The MOOG valve series E024 (Fig. 2.13(b)) has comparable performance specifications, but has only half the weight (92g). Its price is roughly 1.2 times higher than the one of the series 30. The valve is designed for motorsport applications like racing cars [MOOG Inc., 2003].

2. STATE OF THE ART



Figure 2.13: Pictures of *Moog* valves: (a) series 30 and (b) series E024.

Table 2.3 contains a summary of the most significant specifications and performance results of *BigDog 2008*, based on Raibert’s paper of 2008 [Raibert et al., 2008] and the above mentioned overview slides [Boston Dynamics Corp., 2008].

Description	Value
weight	about 109kg
dimensions	1.1m x 0.3m x 1m (LxWxH)
DOF per leg	4 active (rotational) + 1 passive (linear)
hydraulic pressure	20.7MPa (3000psi)
engine power	11kW (15hp)
engine max. speed	9000rpm
joint control rate	1000Hz
main control rate	200Hz
cylinder diameter/stroke	not known
max. payload on flat terrain	154kg
longest continuous operation	10km hike (2.5hours)
performed locomotion gaits	walk, trot, running trot, bound
max. forward speeds	walk 0.2m/s, trot 2m/s, bound 3.1m/s

Table 2.3: Summary of the most significant specifications and performance results of *BigDog 2008* based on [Raibert et al., 2008, Boston Dynamics Corp., 2008].

2.4 Highly Dynamic Legged Robots

Based on (2.2) and the hydraulic pressure and engine power listed in Table 2.3, we can estimate the maximum flow rate of the hydraulic system. Assuming a pump efficiency of 80-90%, this leads to a flow rate of 25.5-28.7lpm. (See section E.1 for unit conversions.) Part of the flow is leaked back to the tank due to the internal leakage of the 16 valves. Assuming that each DOF is controlled by a MOOG series 30 valve, this results in a total leakage flow up to 5.6lpm for a supply pressure of 20.7MPa.

The most recent development in this project was a press release in the beginning of February 2010. It stated that DARPA has awarded Boston Dynamics a contract of 32 million US dollars for a project called *Legged Squad Support System (LS3)* that will last 30 months. LS3 is a dynamic robot that will manoeuvre in difficult terrain, carrying up to 180kg of load and having enough fuel for missions covering 32km and lasting 24 hours. The first walk out is scheduled for 2012 [Boston Dynamics Corp., 2010].

2.4.3.4 PETMAN

Another impressive robot created by Boston Dynamics is called *PETMAN*, Fig. 2.14.

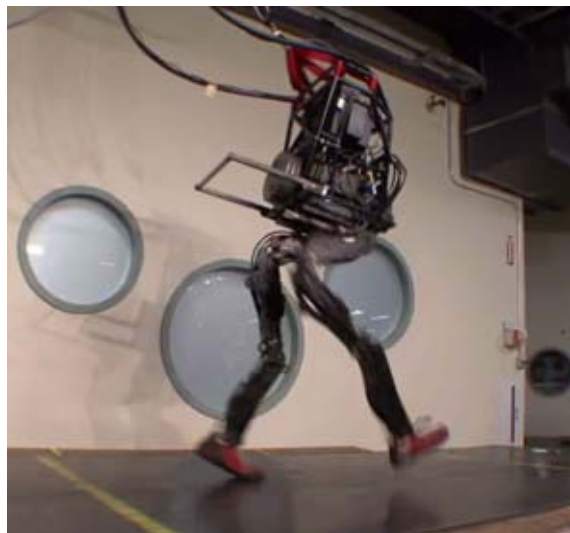


Figure 2.14: Picture of biped robot PETMAN developed by Boston Dynamics [Boston Dynamics Corp., 2010].

It has been presented on their website and on their youtube channel in the end of October 2009 [Boston Dynamics Corp., 2010]. To the author's best knowledge, no

2. STATE OF THE ART

scientific publication is available so far. The popularity of the youtube video however was huge: in less than three days it reached half a million views. PETMAN is designed for testing chemical protection clothing used by the US army. It is a biped robot with hydraulically actuated legs, similar to the ones of BigDog. It is equipped with real shoes at the feet and is able to perform a smooth human-like walking gait on a treadmill. If pushed from the side, it can recover the disturbance and keeps on walking.

2.4.4 Other Interesting Hydraulic Legged Robots

Besides the above mentioned highly dynamic hydraulic robots, there exists a number of other interesting hydraulic legged robots:

Roboshift (Fig. 2.15(a)) is a power-autonomous, industrial-scale biped robot with a weight of 550kg and a height of 2.4m. Its development at the University of New South Wales in Australia started in the end of the 1990's, but had to be stopped after 2005 due to safety reasons [Cronin, 2005]. *Sarcos Ltd.* is the producer of several hydraulically actuated humanoid robots (e.g. *DB*, *CB*, *Primus*), Fig. 2.15(b). These robots are used to study human behaviour, including active balance and dynamic full body motions [Atkeson et al., 2000, Cheng et al., 2007, Hyon, 2009]. In 2009, *Raytheon Sarcos* presented an impressive hydraulic exoskeleton (Fig. 2.15(c)) [Raytheon Sarcos, 2010]. *BLEEX* (Fig. 2.15(d)) is another hydraulic exoskeleton developed by Kazerooni et al. at UC Berkeley since 2000 [Kazerooni and Steger, 2006]. Fig. 2.15(e) shows the hip prototype of the humanoid robot *HYDROÏD* that is currently being developed by Alfayad et al. at the Laboratoire d'Ingénierie des Systèmes de Versailles (LISV) in France [Alfayad et al., 2009].

Titan XI (Fig. 2.15(f)) is a large size hydraulically actuated quadruped robot developed at the Hirose Lab of the Tokyo Institute of Technology, Japan. The 7000kg robot is designed for construction work on slopes. [Hodoshima et al., 2007]. *Comet III* (Fig. 2.15(g)) is a 900kg hydraulic hexapod robot developed for humanitarian demining [Barai and Nonami, 2008]. Both robots are able to perform statically stable walking. Another hexapod robot developed in Finland is the *Walking Forest Machine* (Fig. 2.15(h)) from *Plustech Oy* (a *John Deere* subsidiary), which is designed for harvesting

2.4 Highly Dynamic Legged Robots

work in forests. The company claims that the six legs spread the weight of the machine evenly minimizing soil erosion and damage to tree roots [John Deere Corp., 2010].

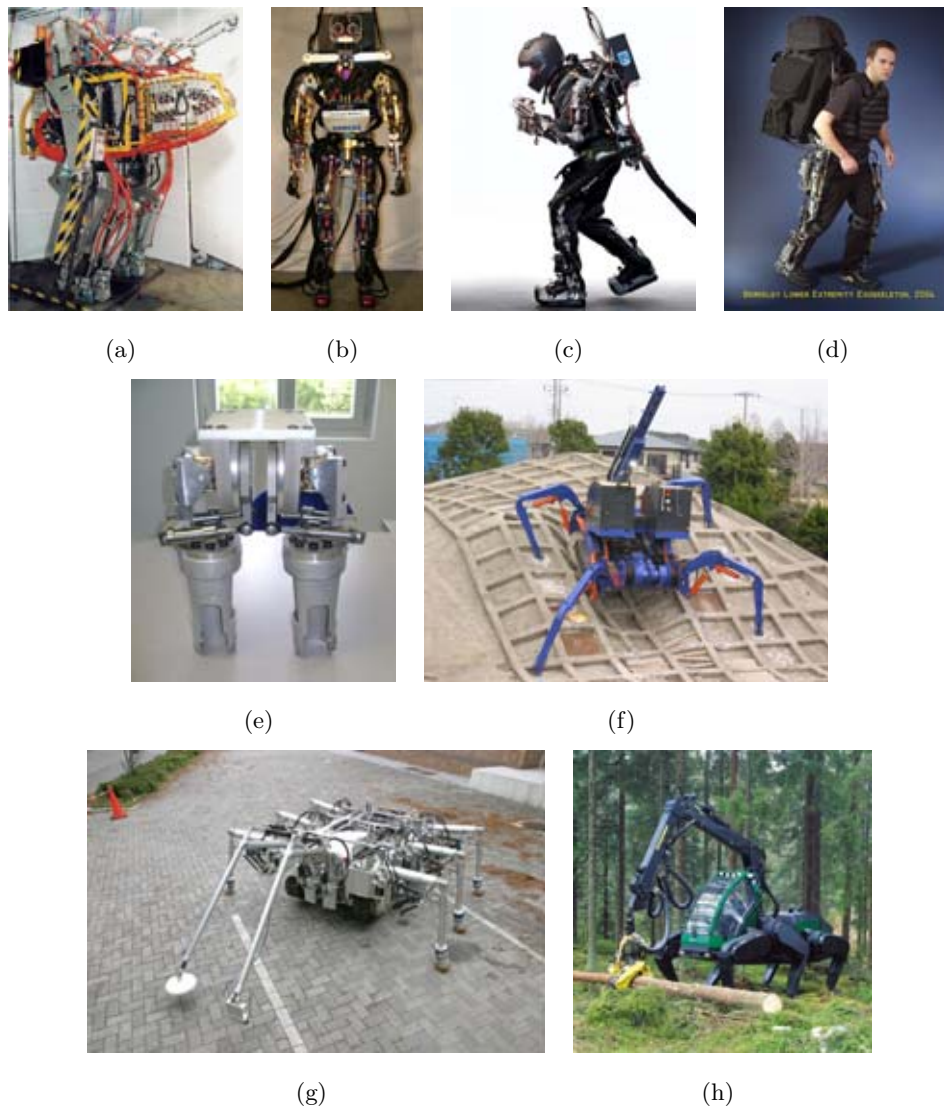


Figure 2.15: Picture of (a) RoboShift [Cronin, 2005]; (b) Sarcos Primus [Stephens and Atkeson, 2009]; (c) Sarcos exoskeleton [Raytheon Sarcos, 2010]; (d) BLEEX exoskeleton [Kazerooni and Steger, 2006]; (e) hip prototype of *HYDROÏD* [Alfayad et al., 2009]; (f) TITAN XI [Hodoshima et al., 2007]; (g) COMET 3 [Barai and Nonami, 2008] and (h) Walking Forest Machine [John Deere Corp., 2010].

2. STATE OF THE ART

2.5 Research on Legged Locomotion

Many researchers studied animal and human locomotion and the related bio-mechanical properties of the legs. These results are a fundamental base for the design, dimensioning and control of legged machines. This section will therefore report the most relevant results.

2.5.1 Muybridge Picture Sequences

In the 19th century, the English photographer Eadweard Muybridge achieved one of the first milestones in understanding animal running. He used several cameras to capture the single phases during running and proofed for the first time that all four of a horse's hooves left the ground at the same time during a gallop. Fig. 2.16 shows a picture sequence of a galloping horse.

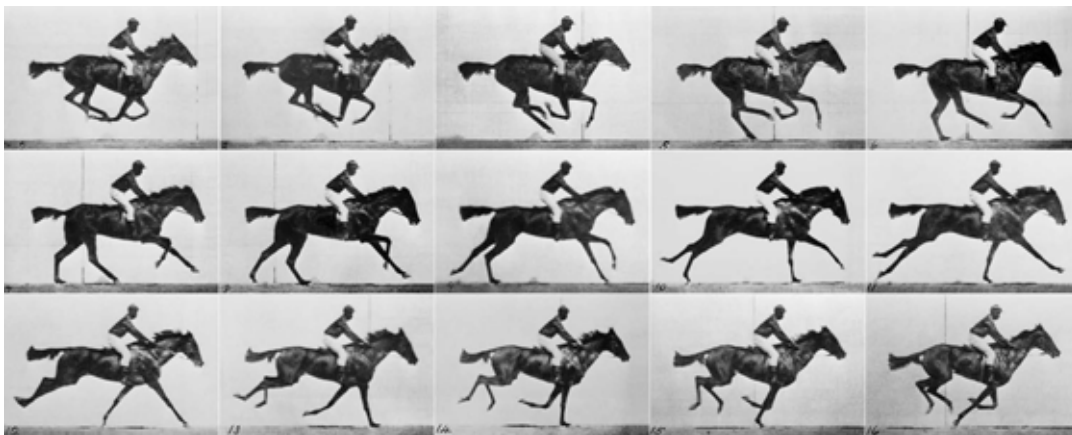


Figure 2.16: Picture sequence of galloping horse, photographed in the 19th century by Eadweard Muybridge.

He took a big collection of picture sequences of fast motions of humans and animals, ranging from dogs and horses to elephants. His main interest lied in dynamic motions that are too fast for the human eye to analyse in detail, such as running, jumping, athletics and wrestling.

2.5.2 Spring-Mass System

Research on the mechanical behaviour of walking and running resulted in two widely accepted conclusions:

The tendon muscle system of the leg, especially the *gastrocnemius* tendon located in the tibia, acts like a spring and stores energy from one step to the next. This is especially important for energy efficient running. There is biological evidence that all kinds of running animals and humans have a spring-like behaviour. The compliance of this spring does not only absorb impact shocks but also allows the recycling of up to 40-50% of the energy during running [Cavagna et al., 1964, Alexander, 1992, Alexander, 2003].

Another important conclusion related to this compliance is that the centre of mass is performing a motion similar to a bouncing ball during running and hopping. Running is therefore frequently referred to as a bouncing gait [Raibert, 1986]. Therefore spring-mass models are used to describe the motion of the centre of mass [Blickhan, 1989, McMahon and Cheng, 1990]. They are also known as Spring Loaded Inverted Pendulum (SLIP) models [Schwind and Koditschek, 1997]. While the mass is concentrated in the COM¹ above the spring, the leg, foot and spring are considered massless.

Fig. 2.17 shows a simplified spring-mass system during a vertical hopping cycle. During the stance phase² the spring gets compressed until the COM reaches its lowest position. Subsequently the COM accelerates until the leg lifts off the ground. During the flight phase³ the COM performs a ballistic air phase. When the leg touches down on the ground again, the cycle repeats.

The equations of motion of the system are different for the stance and flight phase. During the stance phase we have to consider a spring-mass system connected to the ground as follows:

¹Centre Of Mass

²the phase between leg touch-down and leg lift-off, the robot foot is always on the ground

³the phase between leg lift-off and leg touch-down, the robot foot is always in the air

2. STATE OF THE ART

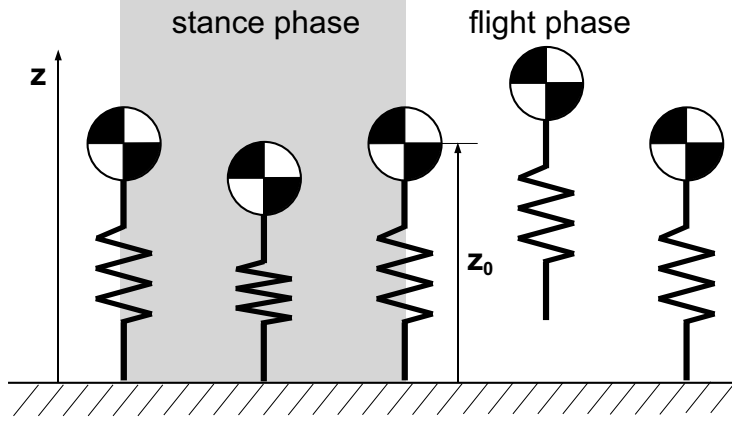


Figure 2.17: Spring-mass system during one vertical hopping cycle. The stance phase is marked with a grey background. (Adapted from [Blickhan, 1989]).

$$\ddot{z} = \frac{1}{m}(F - c\dot{z} + k(z_0 - z)) - g \quad (2.9)$$

where m is the mass, \ddot{z} , \dot{z} and z the acceleration, velocity and position of the mass (positive direction opposite to gravity), z_0 the uncompressed leg length, c the damping coefficient, k the spring stiffness, F an external force (positive direction opposite to gravity) and g the gravitational acceleration.

During the flight phase only the gravitational acceleration g is acting on the COM:

$$\ddot{z} = -g \quad (2.10)$$

These two differential equations can be written in the state space notation:

$$\dot{\mathbf{Z}} = \mathbf{A}\mathbf{Z} + \mathbf{B} \quad (2.11)$$

with the state vector \mathbf{Z} defined as follows:

$$\mathbf{Z} = \begin{pmatrix} z \\ v \end{pmatrix} \quad (2.12)$$

where $v = \dot{z}$ is the velocity of the COM.

During the stance phase ($z \leq z_0$), based on (2.9) we obtain:

$$\mathbf{A} = \begin{pmatrix} 0 & 1 \\ -\frac{k}{m} & -\frac{c}{m} \end{pmatrix} \quad \mathbf{B} = \begin{pmatrix} 0 \\ \frac{F}{m} + kz_0 - g \end{pmatrix} \quad (2.13)$$

During the flight phase ($z > z_0$), based on (2.10) we obtain:

$$\mathbf{A} = \begin{pmatrix} 0 & 1 \\ 0 & 0 \end{pmatrix} \quad \mathbf{B} = \begin{pmatrix} 0 \\ -g \end{pmatrix} \quad (2.14)$$

2.5.3 Variable Stiffness during Running

Researchers of bio-mechanics investigated the influence of leg stiffness on the control of running gaits. They concluded that many animals adjust leg stiffness to control their running gait and change their centre of mass motion. They tune their leg stiffness to the running frequency, stride length, hopping height and ground stiffness in a way that the natural dynamics (see spring-mass model of section 2.5.2) lead to an energy-efficient locomotion.

Hurst presents a summary of these studies in his dissertation [Hurst, 2008]. He concludes that: *In general, lower speeds and slower stride frequencies result from lower leg stiffness, while higher speeds and stride frequencies result from higher leg stiffness.*

2.5.4 Anatomy's Influence on Running Performance

Hoyt and Taylor measured the oxygen consumption of horses on a treadmill running at different speeds [Hoyt and Taylor, 1981]. They used the amount of oxygen to estimate the consumed energy. They concluded that freely running horses choose the gait and speed that minimize energy consumption. Fig. 2.18 shows a graph taken from their paper that illustrates the energy vs. running speed relation for horses. A newer study by Farley and Taylor measured the trot-gallop transition speeds of horses. They observed that horses do this transition at lower speeds if they added weight to the back of the horse. They concluded that horses switch from trot to gallop when musculoskeletal forces reach a critical limit at foot touch-down, presumably to reduce the chance of injury [Farley and Taylor, 1991].

Heglund and Taylor studied how speed and stride frequency change with body size [Heglund and Taylor, 1988]. They observed animals from 0.030kg mice to 200kg horses on a treadmill. They measured their speed and stride frequencies at so-called *equivalent*

2. STATE OF THE ART

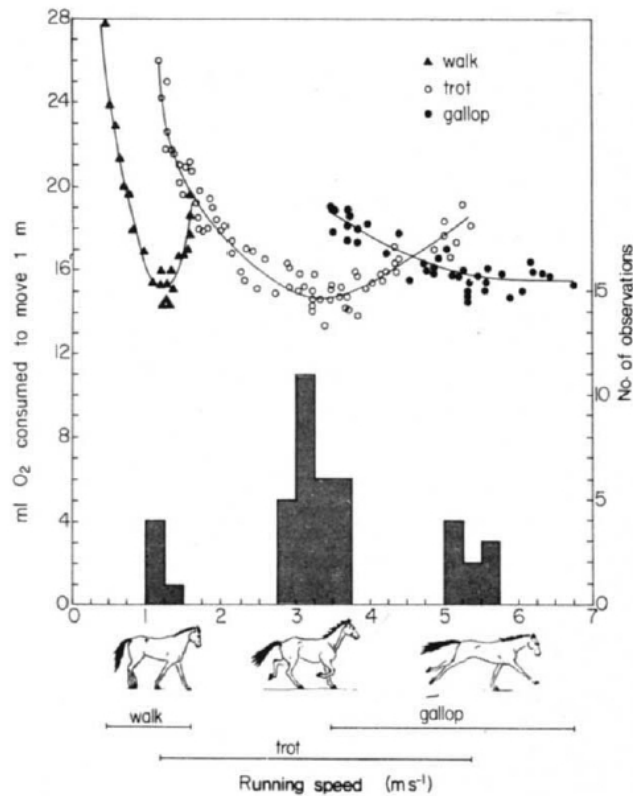


Figure 2.18: Plot of oxygen cost (energy) to move a unit distance vs. walking/running speed of different horse gaits. There is an energy minimum for the walk and trot gait. No minimum was found for the gallop gait due to the speed restriction given by the treadmill. If allowed to select their own speed, horses chose three speeds which coincide with the energetically optimal speed for each gait (see black histogram in the bottom of the graph). (Image taken from [Hoyt and Taylor, 1981])

speeds for trotting, trot-gallop transition and gallop and concluded that they are related to body weight M by the following expression:

$$aM^b \tag{2.15}$$

where a and b are coefficients that are different for each equivalent speed. Table 2.4 lists the estimated forward speeds and stride frequencies for different body weights according to the estimation of [Heglund and Taylor, 1988]. These results are useful to define robot specifications and design parameters.

2.5 Research on Legged Locomotion

Equivalent Speed	50kg	60kg	70kg	80kg	90kg	Unit
Minimum trotting speed	1.57	1.64	1.71	1.77	1.82	$\frac{m}{s}$
	1.70	1.67	1.64	1.62	1.61	$\frac{1}{s}$
Preferred trotting speed	2.60	2.70	2.80	2.88	2.96	$\frac{m}{s}$
	2.01	1.97	1.93	1.90	1.87	$\frac{1}{s}$
Trot-gallop transition speed	3.56	3.73	3.86	3.97	4.07	$\frac{m}{s}$
	2.33	2.27	2.26	2.17	2.13	$\frac{1}{s}$
Preferred galloping speed	5.53	5.71	5.87	6.01	6.13	$\frac{m}{s}$
	2.41	2.34	2.29	2.24	2.20	$\frac{1}{s}$
Maximum sustained galloping speed	7.39	7.63	7.84	8.02	8.19	$\frac{m}{s}$
	2.49	2.42	2.36	2.31	2.27	$\frac{1}{s}$

Table 2.4: List of estimated locomotion parameters for equivalent speeds based on body weight, according to [Heglund and Taylor, 1988].

2. STATE OF THE ART

3

Robot Specifications and Design Studies

This chapter presents the specifications of the *HyQ* robot and a series of studies that I conducted to determine the robot's design: After defining the specifications we have to decide about the general structure of the robot, including the number of legs, the number of joints per leg, joint ranges of motion and the kinematic structure of the legs and torso. In a next step, we have to estimate the required torques of each joint and select the actuator type based on the above mentioned specifications. Furthermore, this chapter presents studies on the hydraulic and electric joint actuation design and kinematics, introduces the leg prototype and ends in studies about leg compliance, spring-mass systems and a power system comparison.

3.1 Robot Specifications

Before starting the design of any kind of machine or device, it is important to define its objectives and specifications. For a first prototype of a machine, initial specifications are usually rather vague. During the design process, they are gradually adjusted and finally determined.

In the case of a legged robot, not only its performance specifications but also physical and design specifications have to be defined. Performance specifications describe

3. ROBOT SPECIFICATIONS AND DESIGN STUDIES

everything related to the desired tasks and motions of the robot, terrains, its velocity, its time of operation etc. Physical specifications describe the robot's size and weight. Design specifications give general design guidelines.

However, it is not trivial to determine reasonable specifications for high-performance legged machines, because only few of them have been constructed up to now and most of them for specific applications. Nevertheless their achievements constitute a useful base for specifying new robots. Another very important source of inspiration is nature. Evolution has come up with a variety of very high-performance legged animals, whose kinematics and performance are extensively studied by biologists. Their reports build another solid base of inspiration for the construction of machines.

The remainder of this section will define performance, physical and design specifications of the robot (numbered with a tag like **SP1.1** for easy referencing) and end with a brief description of the different robot development stages. The objectives and possible future applications of the robot are described in chapter 1.

3.1.1 Performance Specifications

In terms of performance we defined the following specifications:

- Ability to walk with different gaits: static walk (always a minimum of three feet on the floor) and trot (diagonal leg pairs move together, always a minimum of two feet on the ground) [**SP1.1**]
- Ability to run with different gaits: flying trot (diagonal leg pairs move together, with robot in the air between the steps (*flight phase*)) and bound (front leg pairs and hind leg pairs move together, with flight phase); eventually pace (left leg pairs and right leg pairs move together, with flight phase) and gallop (several foot fall sequences possible, with flight phase). A maximum trotting speed of $3 - 4 \frac{m}{s}$ is targeted¹. [**SP1.2**]
- Ability to walk over rough terrain, such as uneven roads, rubble, forest beds, grass, pebbles [**SP1.3**]

¹based on Table 2.4 and a robot mass of 90kg

- Ability to keep balance after unexpected disturbances such as rough or slippery terrain or external forces acting on robot [SP1.4]
- Ability to perform a vertical jump from squat posture with a jump height of 0.15m (vertically travelled distance of robot COM after all feet left the ground) [SP1.5]
- Ability to perform a safe and stable landing after dropping the robot from 0.15m, with initial impact on either all four feet or a pair of diagonal legs [SP1.6]
- Ability to carry a payload of 5-10kg [SP1.7]
- Power autonomy for 8 hours without recharging or refuelling [SP1.8]

3.1.2 Physical Specifications and Design Rules

Physical specifications (targeted robot size and weight) are difficult to specify in the beginning of the design process. However, they are important values for dimensioning the components and designing the mechanical structure. The size of the robot for example is strongly influenced by the size of the commercially available components. Especially hydraulic system components are still rather bulky and only few compact solutions are on the market. Therefore we conducted preliminary research in catalogues and with components suppliers to get a rough idea of the size of a compact hydraulic pump unit with motor and tank, oil cooler, accumulator, filters and valves. To fit everything on board of the robot (including robot electronics), we estimated a robot torso length of roughly 1 meter. The estimated weight of the hydraulic system alone is around 30-40kg. Adding the mechanical structure of the robot (including robot torso and legs) and all onboard electronics, the total weight of the robot reaches 70-90kg. With external hydraulic power supply, the weight drops to about 50-60kg.

We defined the following general **design rules** for the robot:

- Keep it simple [SP2.1]
- Use off-the-shelf components if possible (they are generally cheaper, have better documentation and lower delivery times) [SP2.2]

3. ROBOT SPECIFICATIONS AND DESIGN STUDIES

- Construct a versatile platform that is not specialized on a particular task e.g. only running or only jumping [SP2.3]
- Build a modular design with the possibility to easily replace parts of the robot, e.g. the robot leg with all its actuators as a unit, cables with connectors on both ends (facilitates debugging, maintenance and component updates) [SP2.4]
- Keep robot parts and components as light as possible; especially the leg segments far from the torso to keep the leg inertia as low as possible [SP2.5]
- Keep total construction costs of robot low [SP2.6]

3.1.3 Main Stages of Robot Development

One of HyQ's goals is the energy-autonomous operation for several hours. Since today's battery technology is not ready yet to provide energy for extended operation times of mobile robots, combustion engines (with energy stored in fuel) are a better choice than electric motors (with energy stored in batteries). The energy density of fuel is more than one order of magnitude higher compared to batteries (see section 3.8). The disadvantages of combustion engines are the noise and exhaust emissions, which however are acceptable for outdoor machines.

We therefore decided to divide HyQ's development process into 3 stages:

- Stage 1 has external electric and hydraulic power supply and therefore does not carry a pump unit and batteries on board.
- Stage 2 has an onboard hydraulic system with a pump actuated by an electric AC motor with external electric power supply.
- Stage 3 has an onboard hydraulic system with a pump powered by an onboard internal combustion engine with a generator that supplies the electric energy for onboard electronics and electrically actuated joints.

Stage 1 will be the lightest version of the robot and used for initial system testing and for indoor research of quadruped locomotion with the robot on a treadmill.

3.2 Robot Structure

This section and the remainder of the chapter present a series of design studies that will build the foundation of the robot design (Chapter 4) and components selection.

3.2.1 Number of Legs and Leg Length

The decision to build a quadruped robot rather than a biped or hexapod was mainly based on the inspiration by nature and other robots like the ones presented in chapter 2. Nature has come up with a vast range of different quadruped animals with impressive abilities: The cheetah for example is the fastest land animal with velocities up to 120 km/h. Mountain goats have great climbing and balancing skills, cats are very agile and horses are able to carry heavy loads.

A quadruped also seems to be a good choice from the point of view of a system and controller designer. Four legs are less complicated to construct and maintain than six. The robot costs less and its weight is lower. Furthermore, the computational unit is simpler since less sensors have to be sampled and less actuators controlled. The power system can also be smaller. In terms of controller design, obviously it is less demanding to coordinate and control four than six legs.

With above reasoning a biped would be better than a quadruped. The control of bipeds, however, is considered to be difficult due to their small support base. An active balancing control is necessary and therefore a much more complex control system. A quadruped on the other hand, is stable as soon as three or four feet are on the ground and the COM of the robot is inside the support polygon [González-de Santos et al., 2006].

Next, we have to select a suitable leg length. Based on the initial investigation mentioned above in section 3.1.2, we know that the robot will have an approximate length of about 1m. On one hand, over-proportionally long legs are more likely to collide with each other; on the other hand, an over-proportionally long body needs a stronger structure and is less agile. Horse and dog breeders talk about a *rectangular shape* when comparing body length with leg length of their breeds [McDowell, 1950]. Depending on origin and intent of the dog breed (e.g. a fox hunter, sprinter or pack-running hound),

3. ROBOT SPECIFICATIONS AND DESIGN STUDIES

dogs feature a big range of different conformations. A square shape seems to be a good compromise between agility, endurance and strength to carry loads.

To allow enough space for the actuators, the legs will not be fixed at the very front or end of the robot torso, but rather shifted towards the centre of the robot. Following above considerations, we can therefore assume that the leg should be about 0.7m-0.8m long.

3.2.2 Number of Active Joints and Kinematic Structure

Once defined the number of legs we have to determine the number of active joints for each leg. Similar to above mentioned reasons, the less actuated joints, the less complex and expensive the robot. Furthermore, a crucial design criterion for the legs is low inertia and mass (see design rule **SP2.5**). Each actuator adds weight to the leg (except for a pantograph leg, see Hirose's robots in section 2.3). However, a minimum of three active DOF is required to place the foot in a three dimensional space.

A common design structure has two active DOF in the leg-sagittal plane ¹ of the robot and a third DOF in the vertical plane perpendicular to it. Fig. 3.1 shows this kinematic structure. This design has been previously used in several quadruped robots, e.g. TekkenII, KOLT and BigDog 2006 (refer to chapter 2 for descriptions of these robots).

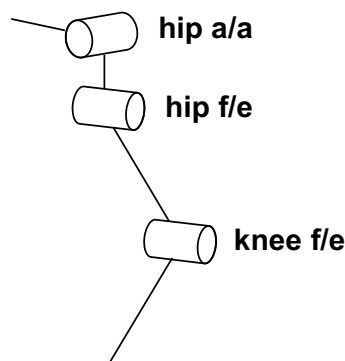


Figure 3.1: Kinematic Structure of the active leg joints.

¹the leg plane parallel to the plane that cuts the body into two halves of equal portions

Additionally, Fig. 3.1 contains the definition of the joint names. According to the biological terms we decided to name the two joint in the leg-sagittal plane *hip flexion/extension (hip f/e)* and *knee flexion/extension (knee f/e)*. The third joint is called *hip abduction/adduction (hip a/a)*. This nomenclature is valid for both the front and hind legs. Appendix B contains a detailed definition of all joint angles and names.

This structure is simple and allows the robot to perform a wide range of tasks. We decided to construct the legs of the first version of HyQ with this kinematic structure. However, a leg with this structure does not permit to choose the ground contact angle and select the foot location at the same time. The ground contact angle determines the direction of the force vector created by the linear spring in the lowest leg segment of a compliant ankle joint (see section 3.6). This angle is also directly related to the amount of traction between the foot and the ground. This is especially important for walking on slopes and slippery surfaces. A third active joint in the leg-sagittal plane could solve these issue. Experiments with the first version of HyQ will show if this is a serious problem or not.

If we look at nature and compare several leg kinematics, we can see two basic types: The *insect type* with legs horizontally sticking out of the body and the *cursorial mammal type* with legs with strong joints in the leg-sagittal plane, Fig. 3.2. The kinematic structure of HyQ is therefore similar to the cursorial mammal type.



Figure 3.2: Picture selection of legged animals with different types of leg kinematics: (a) stick insect (*insect type*) and (b) cheetah (*cursorial mammal type*).

3. ROBOT SPECIFICATIONS AND DESIGN STUDIES

Such a leg kinematic structure is usually referred to as *articulated* or *segmented* leg type, because of the presence of a rotational knee joint and a minimum of two leg segments [Rummel and Seyfarth, 2008]. *Prismatic legs* are the alternative solution and do not feature a rotational knee joint. Instead, a prismatic leg has a linear (prismatic) joint in the knee to adjust the length of the leg and one or two DOF in the hip. Chapter 2 reviewed several types of quadruped robots with prismatic legs, e.g. Scout II 2.7(a) or Raibert’s quadruped of the 1980’s (Fig. 2.9(c)).

3.2.3 Actuator Type Selection

After defining the number of legs and number of actuated joint, we now have to choose the most appropriate actuator type for each joint. Most legged robots are actuated with a single type of actuator, mostly electrically, some pneumatically or hydraulically, as mentioned in the section 2.4 and 2.3. For HyQ we decided to use a hybrid actuation system, with partly electrical and partly hydraulic actuators.

As explained in section 2.2 each actuator technology has its advantages and disadvantages. To choose the most appropriate actuator type for each joint of the robot, we first have to summarize the joint’s main function and requirements.

The joints in the leg-sagittal plane (*hip f/e* and *knee f/e*) are responsible for generating the main forward and upward motion of the robot. During straight walking and running on flat terrain, most work is accomplished by those actuators. Running speed, jump height and most dynamic action performance is directly related to the maximum torque and velocity of these actuators. Additionally, they have to resist high torque peaks during the impact of the foot on the ground. Furthermore, they should have a high power/weight ratio as they are mounted on the leg and thus directly add to the inertia of the leg.

Comparing these requirements with the properties of the conventional actuator types discussed in section 2.2, we decided to use hydraulic cylinder actuators to drive these two joints; especially due to the velocity, torque and impact resistance properties. One disadvantage of cylinders is their shape, which is generally several times

longer than wide. A cylinder needs to be fixed between the upper and lower segment of the joint, so that the force can act on a lever arm and create a torque. One of these segments needs to be long enough to house the cylinder. This is not a problem for the *hip f/e* and *knee f/e* joints, since the leg segments have similar dimension relations as the cylinder and are therefore long enough to host a cylinder. The selection of cylinder dimensions and lever arm is explained in more details in section 3.4.

The *hip a/a* joints are less involved in the creation of forward propulsion, but rather responsible for the balance of the robot. Examples are if the robot is exposed to external disturbances or if moving on rough terrain, inclinations or on slippery surfaces, but also for a suitable weight distribution during normal walking on flat surfaces or running gaits like gallop. To support the robots weight and react quickly to keep balance, both a reasonable joint torque and velocity are required. To reduce leg inertia, the actuator is fixed to the torso; a high power/weight ratio is therefore less important than for the other joints. Cylinder actuators are not suitable for this joint because their long dimension would require an attachment inside the robot torso. This however makes the leg less modular and its replacement for maintenance becomes more difficult (see design rule **SP2.4**). Therefore an actuator with compact overall dimensions is required.

We therefore selected an electric motor as the actuator for the *hip a/a* joints. The selection of motor type, dimension and gear ratio is explained in details in section 3.4.2. An alternative solution is a hydraulic rotary actuator with similar compact dimensions. However, since they are not off-the-shelf components, expensive and hard to find on the market, we decided to use a commercial electric actuator for the first version of HyQ. As described in section 7.2, we are currently testing the applicability of rotary actuators for HyQ.

Table 3.1 shows the summary of above mentioned actuator requirements for the three active joints in the leg and the selected actuator type.

Now that we know the rough kinematic structure of the leg and the actuator types of the joints, we are able to draw a sketch of the robot leg, Fig. 3.3. Note that the cylinders are directly mounted between the leg segments without transmission belts or

3. ROBOT SPECIFICATIONS AND DESIGN STUDIES

	Hip a/a	Hip f/e and Knee f/e
joint velocity	medium	high
joint torque	medium-high	high
torque peak robustness	medium	high
power/weight ratio	medium	high
compact dimensions	high	medium
selected actuator type	electric motor	hydraulic cylinder

Table 3.1: List of importance of actuator requirements for different joints of the legs.

gears. This allows the cylinder force to act directly on the lever arm to generate the joint torque.

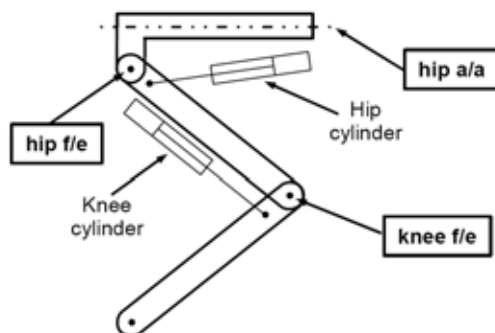


Figure 3.3: Sketch of robot leg with joint names.

3.2.4 Leg Configuration on Torso

Following the design rule *SP2.1* to keep the robot simple, we decided to use the same leg design for both the front and the hind legs. Nichol writes in his PhD thesis [Nichol, 2005] about the way the front and hind legs apply forces during quadrupedal locomotion. He writes that in force plate measurements of quadrupedal locomotion, front legs tend to apply vertical forces, while contributing little thrust, if not adding drag. The hind legs contribute the majority of the thrust. Although the directions of the forces are different, the forces are not very different in magnitude. He concludes that despite these differences in the roles front and hind legs play, it is not clear that a separate leg needs to be designed for each role [Nichol, 2005]. Furthermore, Witte et

al. suggest that front and hind limbs may have the same construction in their paper about the transfer of biological principles into the construction of quadruped walking machines [Witte et al., 2001].

There are different possibilities of attaching the four legs to the torso. The two hind and the two front legs always build pairs and can either be mounted in a *forward* configuration (where the knee joint points to the front of the robot) or in a *backward* configuration (where the knee joint points to the back of the robot). This results in four combinations as shown in Fig. 3.4. These drawings are based on the preliminary leg sketch of Fig. 3.3.

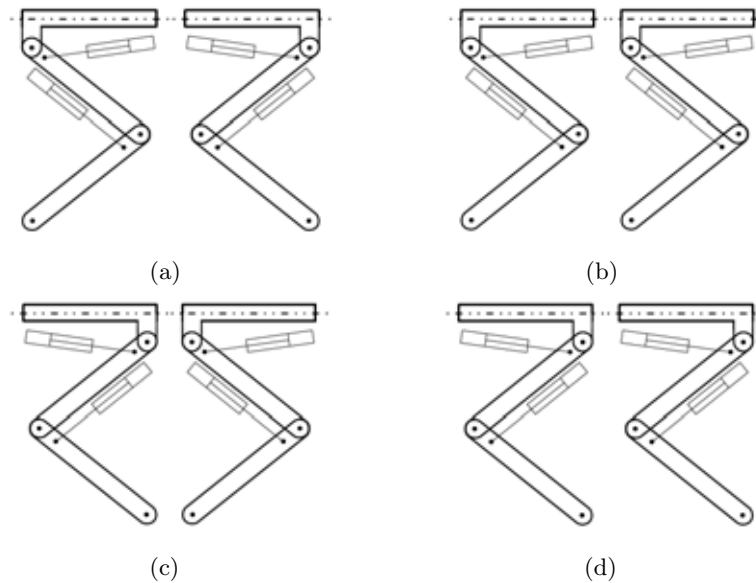


Figure 3.4: Leg configurations of quadruped robots with forward walking direction to the right: **(a)** forward/backward; **(b)** forward/forward; **(c)** backward/forward; **(d)** backward/backward.

Several research groups have investigated, which leg configuration was the most suitable for their quadruped robot. Zhang et al. conducted both simulation and experimental studies with their electric quadruped robot *BiosBot* and concluded that the forward/backward configuration is the most suitable. They found that this configuration reduces slippage between the feet and the ground and that it improves motion performance in general [Zhang et al., 2005]. Meek et al. conducted simulation studies

3. ROBOT SPECIFICATIONS AND DESIGN STUDIES

to find the best configuration to increase the stability of a passive quadruped robot with compliant leg joints. They defined increased stability as decreased pitching motion of the robot. The obtained simulation results also proofed the forward/backward configuration to be most suitable [Meek et al., 2008] to decrease the robot's pitching motion.

Witte et al. on the other hand propose a different configuration based on studies of quadruped animals. They suggest that the scapula and the thigh are to be considered as the two top segments of front and hind legs, respectively [Witte et al., 2001]. They argue that the scapula of cursorial mammals have a large range of motion, since these animals have reduced clavicles (collarbones) compared to other mammals (e.g. human) and therefore considerably contribute to the stride length during locomotion [Fischer et al., 2002]. They suggest a leg kinematic structure with three DOF in the leg-sagittal plane as shown in Fig. 3.5, which is closer to the biological model than our simple structure without ankle joint. Their suggested configuration type fits best into the category of the forward/forward type.

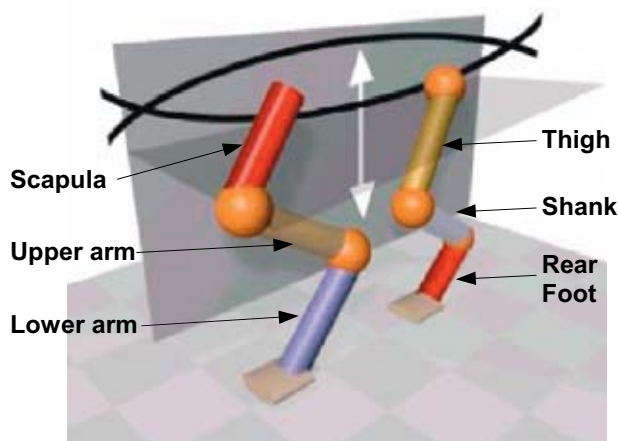


Figure 3.5: Kinematic structure and leg configuration of quadruped cursorial mammals according to Witte et al., where the scapula is considered as the top segment of the front leg, corresponding to the thigh of the hind leg (Adapted from [Witte et al., 2001]).

A survey of existing quadruped robots with cursorial mammal type legs showed indeed no uniform leg configuration:

- **forward/backward:** Biosbot [Zhang et al., 2005], AiDIN [Koo et al., 2007], BigDog2008 [Raibert et al., 2008], Little Dog [Buchli et al., 2009] and AIBO [Fujita and Kitano, 1998]
- **forward/forward:** Bisam [Ilg et al., 1998], BigDog2005 [Buehler et al., 2005] and Warp [Ingvast, 2006]
- **backward/backward:** TekkenII [Kimura et al., 2007], Puppy [Iida et al., 2005] and KOLT [Estremera and Waldron, 2008].

For HyQ we decided to use the forward/backward configuration based on the following reasons:

- Improve the static stability of the robot: Increase the size of the support triangle by moving the robot's hip joints (and therefore feet) far from the COM of the robot (and therefore the feet far from the COM's projection onto the ground).
- Create a versatile platform that is not optimised for a particular task (e.g. only running).
- Based on above mentioned studies and survey of existing quadruped robots.

3.2.5 Joint Range of Motion

The definition of a suitable range of motion of each robot joint is not a simple task. On one hand, a large range of motion is advantageous, because it increases the workspace of the leg and therefore the number of reachable footholds while walking, especially in rough terrain. Furthermore, a large range increases the ability to recover balance and stay up-right after external disturbances or slipping feet and contributes to increase the maximum forward velocity.

On the other hand, the larger the range, the higher the risk of self collisions, for example between the leg and the torso in case of the hip abduction/adduction joint. In case of linear actuators, like for the hip and knee flexion/extension, the joint range of motion in combination with the maximum stroke directly relates to the joint torque output profile. For a fixed actuator stroke length, the larger the joint range, the lower

3. ROBOT SPECIFICATIONS AND DESIGN STUDIES

the peak torque output. This relation is explained in more detail in section 3.4.

For the hip and knee flexion/extension joint, I therefore took a look at nature. I decided that dogs were a good source of inspiration to get a rough idea of possible joint ranges. Jaegger et al. studied and measured the minimum and maximum joint range of 16 Labrador-Retriever dogs [Jaegger et al., 2002]. The angles for the hip and knee flexion/extension joint limits are shown in Fig. 3.6. Since the hip angles are relative to the inclination of the pelvis, the average pelvis angle to the horizontal plane has to be considered too. According to [McDowell, 1950] a standing dog has an average pelvis angle of 30° , as shown in Fig. 3.6(c).

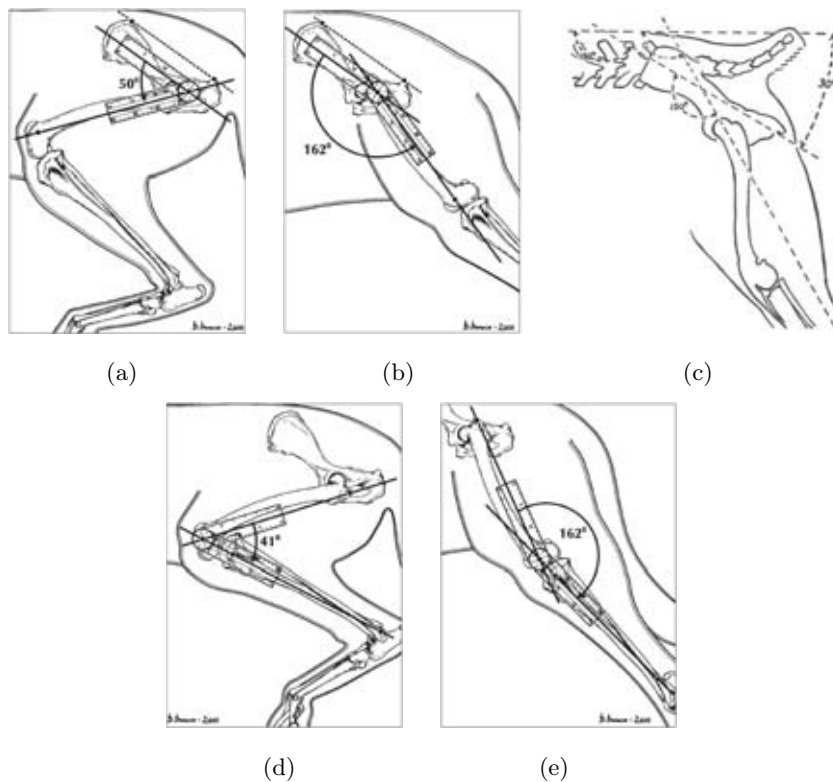


Figure 3.6: Joint range of motion of Labrador-Retrievers [Jaegger et al., 2002] for minimum and maximum angle of hip joint (a),(b) and knee joint (d),(e). The average angle of the pelvis to the horizontal plane of standing dogs is shown in (c) [McDowell, 1950].

These values obviously can only be used to get a rough idea, since the kinematic structure of the robot and the dog legs are quite different; the dog leg for example has an additional rotational joint at the ankle. Furthermore, both the spinal cord of a mammal and its scapula contribute largely to efficient, fast and agile locomotion. The robot does not have either of them.

Nevertheless, I selected the hip and knee flexion/extension joint ranges according to above mentioned study. Table 3.2 summarizes the results of the dog study and the selected joint ranges for the robot. The second column contains the dog angles with the angle definition of the study and the third column the same angles with the angle definition of HyQ according to Fig. B.1. The last column shows the selected angles for HyQ with its angle definition.

	Dog Study	Dog Study (HyQ-AD)	HyQ (HyQ-AD)	Unit
Hip max. flexion	51	-69	-70	<i>degrees</i>
Hip max. extension	162	42	50	<i>degrees</i>
Knee max. flexion	41	139	140	<i>degrees</i>
Knee max. extension	162	18	20	<i>degrees</i>

Table 3.2: Minimum and maximum angles of hip and knee flexion/extension joints of Labrador-Retriever dog study in both angles definition (the one of the study and the *HyQ-Angles Definition* (HyQ-AD)) and the corresponding angle range of HyQ in HyQ-AD.

The joint range of motion of the hip abduction/adduction joint is 120° and therefore the same as the other joints. It ranges from -90° to 30° with the angle definition according to Fig. B.1. 30° is the inclination of the side walls of the torso as mentioned in section 4.2.3. Therefore the leg is able to rotate below the torso until parallel to the side wall. The outside angle of -90° allows the robot to lift the leg high up laterally, which is especially beneficial in rough terrain with large obstacles. A bigger range would make the routing of the hydraulic tubes increasingly more difficult and we believe that it would not improve the robot's performance.

3.3 Joint Torque Estimation

To select, dimension and design the actuation system of a robot it is necessary to estimate the joint torques that are required for different kind of tasks. This obviously strongly relates to the performance specifications defined earlier. Estimating an upper limit of torque is therefore an important part of the design process of a robot.

We will first estimate the peak torque of the knee joints actuated by hydraulic cylinders. We believe that a strong and *explosive* vertical jump of the robot from a crouched posture is a simple and reasonable example of what kind of torque levels are required not only for jumping but also for running. The trot gait for example is a series of jumps with diagonal leg pairs.

To get an estimation of the upper limit of required torque, we calculate the knee torque profile for a vertical jump with a height of 0.15m. This height represents the maximum vertical distance between the robot's COM and the ground during the parabolic flight period measured from the moment of lift-off¹ of all four feet. Furthermore, we assume that all torque has to be generated in the *knee f/e* joint and that the *hip f/e* joint is merely following the motion to keep the robot upright. This provides us with a worst case estimation. Since the robot is left-right symmetric, it is sufficient to consider the motion of only two legs of one side for this simulation and assume that the *hip a/a* joints are fixed to 0° (vertical legs). We will only consider the acceleration and flight phase here; the landing is investigated in section 3.6.

First of all we need to calculate the vertical velocity of the robot at foot lift-off v_{lo} that is necessary to achieve the specified maximum jump height h_{max} . Let us assume that in an ideal situation (no energy loss at lift-off and due to air resistance) the potential energy E_{pot} at the point of maximum height has to be equal to the kinetic energy E_{kin} at the point of lift-off:

$$E_{kin} = \frac{1}{2}mv_{lo}^2 = mgh_{max} = E_{pot} \quad (3.1)$$

¹lift-off is the moment in which the foot leaves the ground

3.3 Joint Torque Estimation

where m is the robot mass and g the earth gravity of 9.81m/s^2 .

This leads to (3.2) and (3.3) that are independent from the robot mass

$$h_{max} = \frac{v_{lo}^2}{2g} \quad (3.2)$$

$$v_{lo} = \sqrt{2gh_{max}} \quad (3.3)$$

With (3.3) we can now calculate the required lift-off velocity to achieve a jump height of 0.15m:

$$v_{lo} = \sqrt{2g \cdot 0.15\text{m}} \approx 1.72 \frac{\text{m}}{\text{s}} \quad (3.4)$$

Fig. 3.7(a) shows the plot of (3.2) for a velocity range from 0 to 2 m/s with a red circle for 0.15m and Fig. 3.7(b) shows the plot of the robot COM height during the ballistic air phase vs. time for different lift-off velocities. The latter plot is obtained by subtracting the distance travelled due to gravity acceleration from the distance travelled due to the initial velocity at lift-off:

$$h(t) = v_{lo}t - \frac{1}{2}gt^2 \quad (3.5)$$

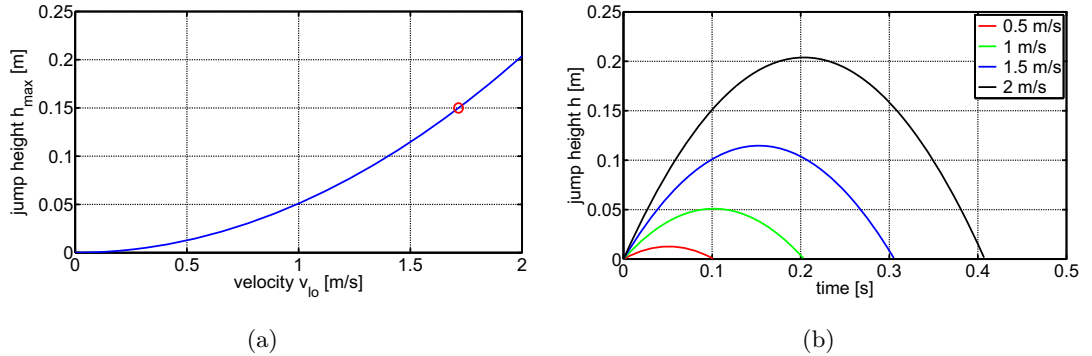


Figure 3.7: Ballistic air phase: The lift-off velocity at the end of the acceleration phase (pushing up) determines the maximum jump height, independent of the mass: (a) plot of vertical jump height vs. lift-off velocity and (b) vertical jump height vs. time plot for different lift-off velocities.

Now that we know the required velocity at lift-off, the next step is to calculate the vertical acceleration a_z necessary to reach the velocity v_{lo} . To simplify the estimation, we consider a constant vertical acceleration during the whole pushing phase. The more

3. ROBOT SPECIFICATIONS AND DESIGN STUDIES

time and distance the robot torso can travel before lift-off, the smaller the required acceleration and force. It is therefore crucial to start the robot from a squat posture close to the corresponding mechanical limits and accelerate until almost stretched legs. To avoid damage to the robot, the acceleration phase of the joints has to finish early enough to slow them down and stop them before hitting the mechanical limits (in case of the *knee f/e* joint). Fig. 3.8 shows a sketch of the described motion.

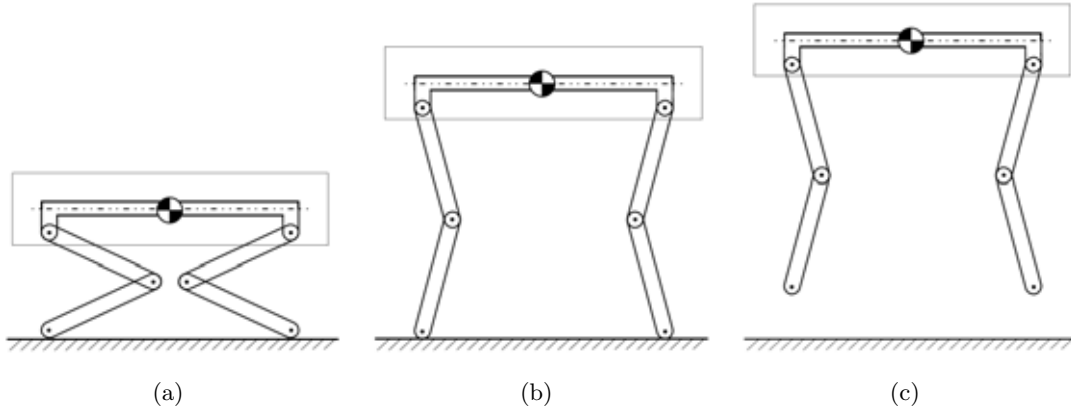


Figure 3.8: Sketch of the robot during a vertical jump motion: (a) the robot in a squat posture at the start of the motion; (b) in a posture with almost fully stretched legs at foot lift-off and (c) during the parabolic flight phase.

To calculate the vertical distance that the robot COM is travelling during the acceleration phase, we need to take into consideration both the joint's range of motion and estimated length of the upper and lower leg segment. While the joint range of motion has been defined in the last section 3.2.5, we can approximate the length of both leg segments to $l_s = 0.35m$ in order to meet the expected leg length of $0.7m$ to $0.8m$, estimated in section 3.2.1. If we assume that during the acceleration phase the *hip f/e* joint of front and hind legs and the two feet form a rectangular shape, the joint angles are related as follows:

$$\theta_1 = \frac{-\theta_2}{2} \quad (3.6)$$

where θ_1 is the angle of the *hip f/e* and θ_2 the angle of the *knee f/e* joint, as defined in Appendix B and shown in Fig. 3.9.

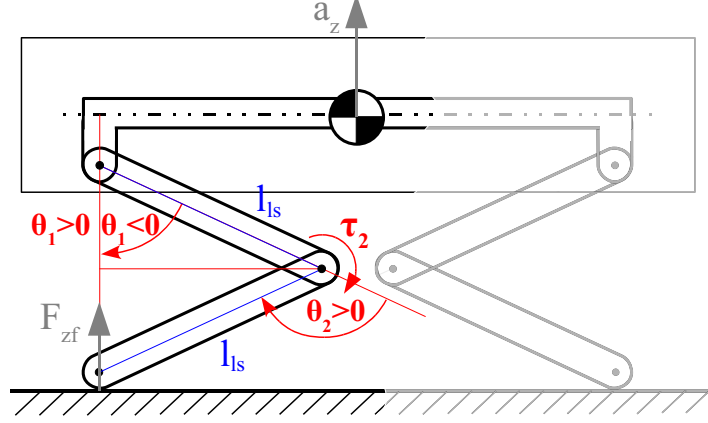


Figure 3.9: Robot sketch in squat posture with definition of variables for the torque estimation of a vertical jump.

Let us assume a start angle of the *knee f/e* joint of $\theta_{2_start} = 125^\circ$, which is close to its mechanical limit of 140° . A reasonable knee angle for the end of the acceleration phase is $\theta_{2_end} = 50^\circ$, this allows to stop the joint motion before hitting the mechanical limits at 20° . Equation (3.6) leads to the corresponding *hip f/e* angles of $\theta_{1_start} = -62.5^\circ$ and $\theta_{1_end} = -25^\circ$. The vertical distance z_{ap} of the COM between the beginning and the end of the acceleration phase can now be obtained as follows:

$$z_{ap} = 2l_{ls}(\cos(\theta_{1_end}) - \cos(\theta_{1_start})) \approx 0.31m \quad (3.7)$$

The results of (3.4) and (3.7) and the following two equations:

$$z_{ap} = \frac{1}{2}a_z t^2 \quad (3.8)$$

$$v_{lo} = a_z t \quad (3.9)$$

finally lead to the vertical acceleration a_z :

$$a_z = \frac{1}{2} \frac{v_{lo}^2}{z_{ap}} = \frac{1}{2} \frac{2g \cdot 0.15m}{2l_{ls}(\cos(\theta_{1_end}) - \cos(\theta_{1_start}))} \approx 4.7 \frac{m}{s^2} \quad (3.10)$$

Before calculating the required vertical force, we have to estimate the robot mass. Based on the preliminary estimation of section 3.1.2, we can assume a worst-case maximum mass of $m_{robot} = 90kg$. To simplify this calculation we neglect the mass of the

3. ROBOT SPECIFICATIONS AND DESIGN STUDIES

foot and lower leg segment and add it to the mass that has to be accelerated. We are now ready to calculate the vertical force F_{ap} during the acceleration phase:

$$F_{ap} = (a_z + g)m_{robot} \approx 1310N \quad (3.11)$$

This force should be equally spread over the four legs and therefore results in a vertical ground reaction force of $F_{zf} = \frac{1}{4}F_{ap} \approx 330N$ at each foot. The required torque in the knee joint depends on the momentary joint angles during the motion and is obtained as follows:

$$\tau_2 = \frac{1}{4}F_{ap}l_s \sin(-\theta_1(t)) = \frac{1}{4}F_{ap}l_s \sin\left(\frac{\theta_2(t)}{2}\right) \quad (3.12)$$

Fig. 3.10 shows the hip and knee angle vs. time and the knee torque vs. knee angle plot during the vertical jump motion. It shows that the lower the robot torso, the higher the torque needed to generate the same force on the ground. This is a realistic result, since we experience the same if we lower our body into squat posture. Note, however, that many simplifications have been made for this simulation. Therefore, the results provide not more than a rough estimation.

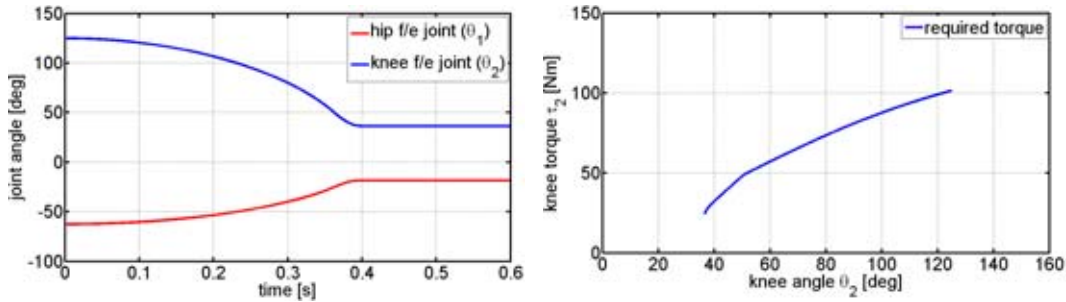


Figure 3.10: Plots with the results of the *knee f/e* torque estimation: Hip and knee joint angles vs. time (left) and knee torque vs. knee angle (right).

To estimate the required torque in the *hip a/a* joint, a static torque analysis has been done: Let us assume that the robot's mass $m_{robot} = 90kg$ is evenly spread on its four legs and that the feet experience no friction on the ground (e.g. on a flat ice surface), as shown in Fig. 3.11. Moreover, all four *hip a/a* joints always have the same

angle θ_0 . The vertical ground contact force at the feet F_{zf} can therefore be expressed as

$$F_{zf} = \frac{1}{4}m_{robot}g \approx 220N \quad (3.13)$$

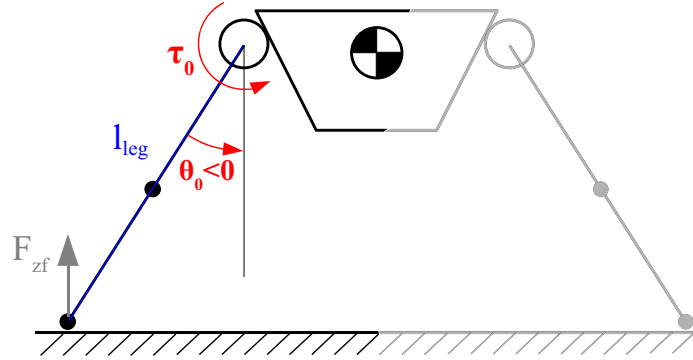


Figure 3.11: Sketch of front view of simplified robot model with definition of variables used for *hip a/a* torque estimation.

For vertical legs ($\theta_0 = 0^\circ$) the torque in the *hip a/a* joint $\tau_0 = 0Nm$. The more the legs spread outside (decreasing $\theta_0 < 0^\circ$), the more torque is required to keep the robot in this posture. This obviously depends also on the length of the leg l_{leg} and can be expressed as follows:

$$\tau_0(\theta_0, l_{leg}) = F_{zf}l_{leg} \sin(-\theta_0) \quad (3.14)$$

The leg length, in turn, depends on the knee angle θ_2 . Fig. 3.12 shows a plot of the resulting torque profiles in relation to the *hip a/a* joint angle for a series of leg lengths.

The results of these torque estimations will be a base for the joint actuation design described in the next two sections. Note that I only estimated the torque of the *knee f/e* joint but not of the *hip f/e* joint. Luther Palmer presents in his dissertation the simulation results of the trotting quadruped robot *KOLT* with similar mass and leg kinematics as HyQ (see a brief description of *KOLT* in section 2.4.1). The results show that the magnitude of the peak torques in the *hip f/e* joint are only half of the ones in the *knee f/e* joint [Palmer, 2007].

3. ROBOT SPECIFICATIONS AND DESIGN STUDIES

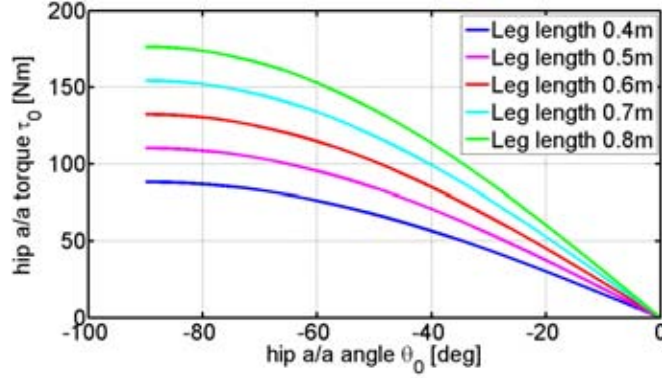


Figure 3.12: Plot with the results of the torque estimation of the *hip a/a* joint: torque vs. joint angle for different leg lengths.

3.4 Joint Actuation Design and Kinematics

3.4.1 Hydraulic Joints

Based on section 3.2.3, both *hip f/e* and *knee f/e* joints are actuated by hydraulic cylinders. Since a cylinder is a linear actuator, its linear motion has to be converted into a rotation. This is accomplished by a lever arm, on which the cylinder force acts to create a torque. The design of such an actuator unit is not straight-forward and several parameters such as cylinder stroke, cylinder diameter and maximum lever arm have to be selected accordingly to meet the specifications. This section provides some guidelines in achieving this.

3.4.1.1 Torque Profile Selection

Let us first of all discuss the relation between joint torque and joint angle and how to obtain the responsible geometric design parameters. Fig. 3.13 shows a sketch of a cylinder with three geometric parameters that form a triangle: variable cylinder length c , fixed lever arm b and length a which is the fixed distance between cylinder attachment and joint axis.

The effective lever arm length l_{el} depends on the dimension of this triangle. With

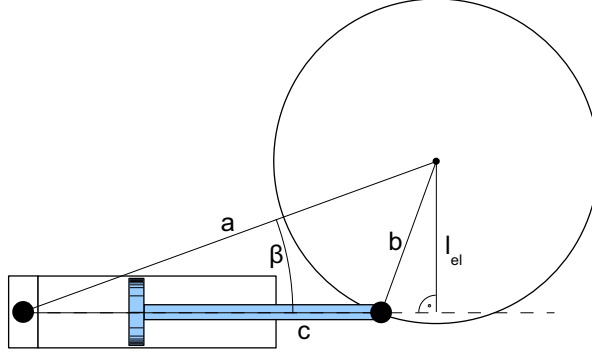


Figure 3.13: Sketch of a cylinder with the geometric parameters necessary to calculate the effective lever arm l_{el} . The fixed lengths a and b and the variable length c form a triangle. The effective lever arm l_{el} is always perpendicular to the cylinder length c .

the *law of cosines*:

$$b^2 = a^2 + c^2 - 2ac \cos(\beta) \quad (3.15)$$

$$\beta = \arccos\left(\frac{a^2 + c^2 - b^2}{2ac}\right) \quad (3.16)$$

we obtain the effective lever length:

$$l_{el} = a \sin(\beta) = a \sin\left(\arccos\left(\frac{a^2 + c^2 - b^2}{2ac}\right)\right) \quad (3.17)$$

This leads to the joint torque τ :

$$\tau = F_{cyl} l_{el} = F_{cyl} a \sin\left(\arccos\left(\frac{a^2 + c^2 - b^2}{2ac}\right)\right) \quad (3.18)$$

The cylinder stroke, the rotational joint range and the lever arm (proportional to joint torque) are related parameters of the actuator unit:

for a given cylinder stroke: $leverarm \sim \frac{1}{jointrange}$

for a given joint range: $cylinderstroke \sim leverarm$

for a given lever arm: $cylinderstroke \sim jointrange$

Before selecting suitable values for the parameters a , b (the lever arm) and c (related to cylinder stroke), we have to take a look at the torque output profiles in relation to cylinder position. Equation (3.18) showed that this relation is non-linear. Maximum torque is obtained if the triangle is right-angled and $l_{el} = b$:

$$\tau_{max} = F_{cyl} b \quad (3.19)$$

3. ROBOT SPECIFICATIONS AND DESIGN STUDIES

The position of this torque maximum (and therefore also maximum of effective lever length) in the torque vs. cylinder position plot depends on the selection of the parameters a , b and c . Fig. 3.14 shows three different cases with fixed values for b , c_{min} and c_{max} and increasing values of a : (a) with the torque maximum shifted to the side with cylinder extension $<50\%$ of the stroke; (b) the torque maximum at half extended cylinder and (c) the torque maximum shifted to the side with cylinder extension $>50\%$ of the stroke. The sketch in the left side of the figure shows the geometry of the given configuration, with the cylinder shown in three positions (completely retracted $c = c_{min}$, half extended $c = c_{min} + \frac{1}{2}l_{cs}$ and fully extended $c = c_{max}$). The right side of the figure shows two plots each: (top) the normalized effective lever length (proportional to torque) vs. normalized cylinder position; and (bottom) the delta of joint rotation γ that is created by a delta of linear cylinder extension. The last plot is related to the Jacobian matrix presented in section C.1.

For certain configurations the Jacobian matrix can be singular, in our case this happens when the joint rotational axis crosses the motion axis of the cylinder (the effective lever arm is zero). Configurations close to these singularities lead to a large change in angular position for a tiny change in cylinder length. The *delta* γ plots of Fig. 3.14(a) and 3.14(b) show this for maximum and minimum cylinder extension, respectively. Since joint position control is increasingly difficult near the singularities, these configurations should lie outside the joint workspace and therefore joint kinematics should be designed accordingly. More information about this topic can be found in [Sciavicco and Siciliano, 2001].

The plots have been normalized by setting the stroke length of the cylinder $l_{cs} = 1$. A joint range of $\varphi_{jr} = 2rad$ has been assumed. Due to this normalization, the cylinder position and effective lever length are unitless and the values of delta γ are expressed in [rad].

Fig. 3.14(b) shows a symmetric torque profile. Let us use this example to explain how to calculate values for the length a and b . To obtain a symmetric torque profile, the effective lever arm at $c = c_{min}$ and at $c = c_{max}$ have to be equal. Therefore the rod end has to be on the same line for both cases as shown in the sketch of Fig. 3.15(a).

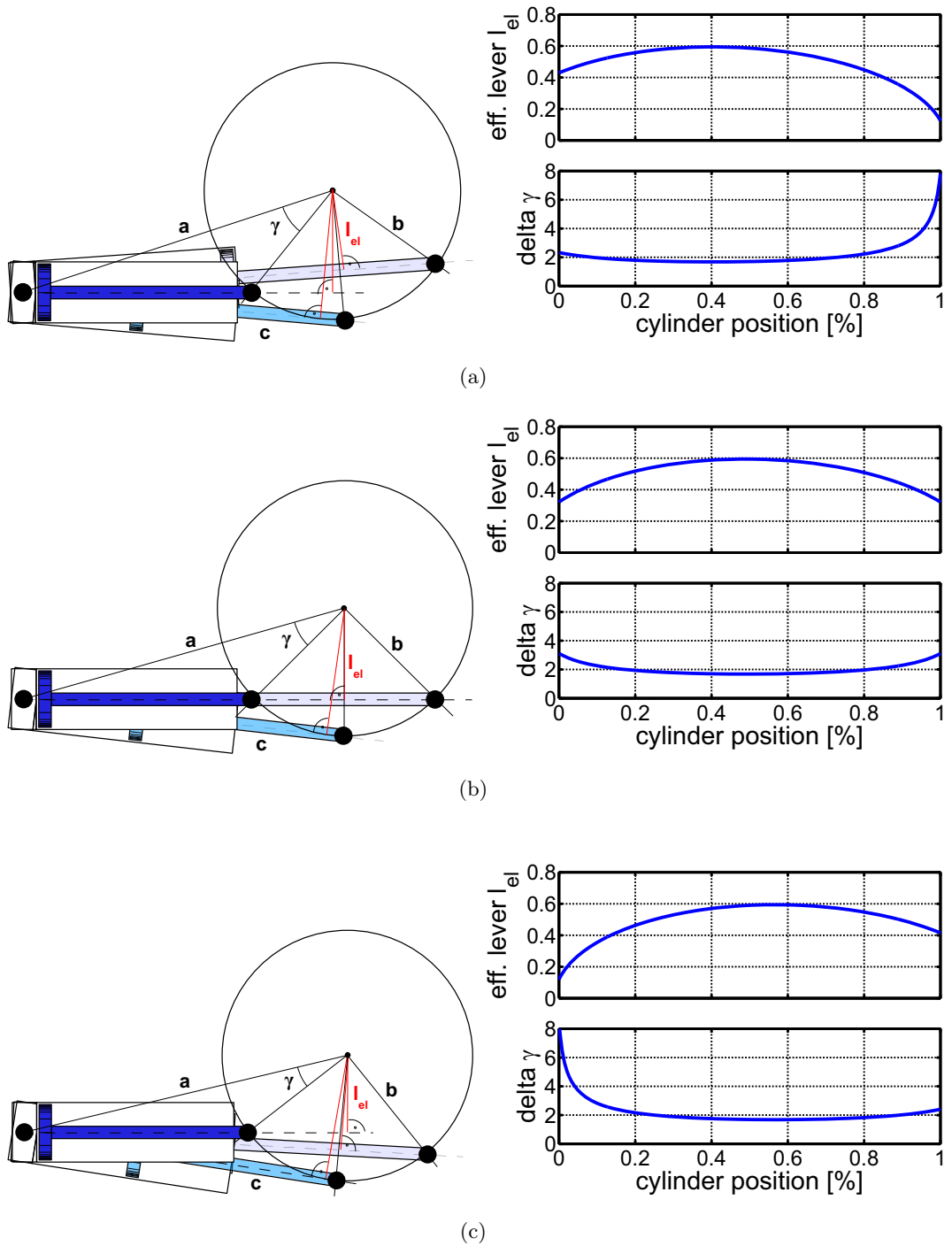


Figure 3.14: Study of different torque profile shapes with same parameter b for all plots and parameter a first small, medium then big with resulting torque maximum: (a) shifted to the left; (b) in the centre and (c) shifted to the right inside the cylinder position plot.

3. ROBOT SPECIFICATIONS AND DESIGN STUDIES

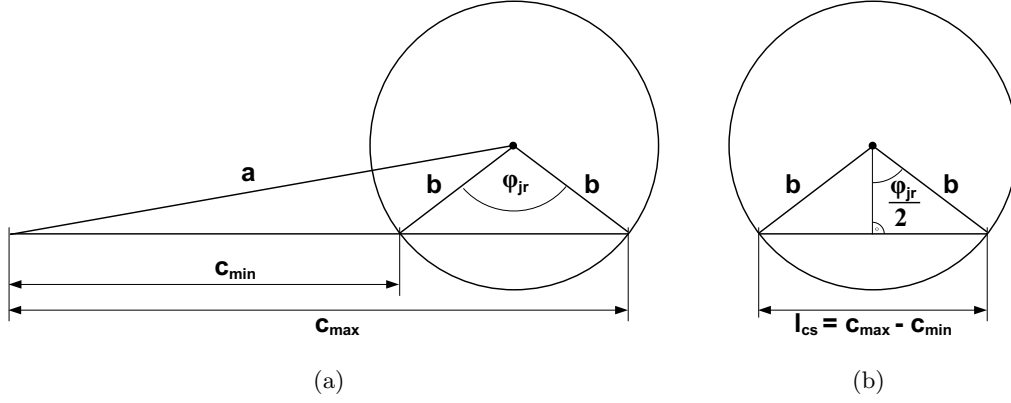


Figure 3.15: Sketch of the hydraulic joint geometry to calculate the parameters a and b , based on the joint range φ_{jr} , cylinder stroke l_{cs} and maximum extended cylinder length c_{max} .

If the maximum joint range φ_{jr} , the cylinder maximum length c_{max} and the cylinder stroke l_{cs} are known, we can calculate the values for a and b . Fig. 3.15(b) shows that b only depends on φ_{jr} and l_{cs} :

$$\cos\left(\frac{\pi}{2} - \frac{\varphi_{jr}}{2}\right) = \frac{0.5l_{cs}}{b} \quad (3.20)$$

and therefore:

$$b = \frac{l_{cs}}{2 \cos\left(\frac{\pi}{2} - \frac{\varphi_{jr}}{2}\right)} = \frac{l_{cs}}{2 \sin\left(\frac{\varphi_{jr}}{2}\right)} \quad (3.21)$$

The second step is to calculate a . With the law of cosines we obtain:

$$a^2 = b^2 + c_{max}^2 - 2bc_{max} \cos\left(\frac{\pi}{2} - \frac{\varphi_{jr}}{2}\right) \quad (3.22)$$

and finally:

$$a = \sqrt{b^2 + c_{max}^2 - 2bc_{max} \sin\left(\frac{\varphi_{jr}}{2}\right)} \quad (3.23)$$

3.4.1.2 Cylinder Selection

We are now ready to select a suitable cylinder, its stroke and piston diameter, according to the above mentioned estimations, specifications and design rules. Let me summarize them:

- torque profile based on Fig. 3.10
- leg segment length $l_{ls} = 0.35m$ (section 3.3)
- joint range $\varphi_{jr} = 120^\circ$ (section 3.2.5)
- low weight (**SP2.5** in section 3.1.2)

Most hydraulic cylinders found on the market are not compact enough for a legged robot like the one presented in this dissertation. The major part of hydraulic components manufacturers sells cylinders starting from a bore diameter of 25mm, which is too large for the robot. The company *Hoerbiger Micro Fluid GmbH* is one exception, since they produce double-acting asymmetric *micro-cylinders* with bore diameters ranging from 8 to 32mm with stroke lengths of up to 1m for the largest model. Their specified operating pressure is up to 16MPa. Fig. 4.16 shows a picture of a 16mm bore cylinder of *Hoerbiger*.

With the information of the cylinder's data sheet [Hoerbiger, 2008], we can now calculate and confront the properties of cylinders with different diameters (12/8, 16/10, 20/12, 25/16, 32/20 [in mm]) and stroke lengths (50, 60, 70, 80, 90, 100 [in mm]). The diameter is written as (piston (bore) diameter D)/(rod diameter d).

Table 3.3 lists the parameters a and b in [mm] based on (3.23) and (3.21), respectively. Table 3.4 lists the maximum torques based on (2.7) and (3.19) for the extending piston motion with a maximum pressure difference in the chambers of 16MPa. Finally, Table 3.5 lists the measured and estimated weights of the cylinder (empty, without oil). Since the information about the weight is not provided in the manufacturer's data sheet, I measured the three available cylinder models in our laboratory and extrapolated the weights for the remaining sizes.

Since a cylinder weight greater than 1kg is not suitable, only the 12/8 and 16/10 type remain. Furthermore, type 12/8 and the two shortest lengths of 16/10 do not provide enough torque. In terms of geometrical length a , the longer, the more difficult to fit inside the mechanical structure. Therefore, type 16/10 with 70mm and 80mm are the most suitable models. We chose type 16/10 with 80mm, since it is a normalized

3. ROBOT SPECIFICATIONS AND DESIGN STUDIES

stroke [mm]	12/8	16/10	20/12	25/16	32/20	b [mm]
50	247.9	282.3	304.3	346.3	377.8	27.7
60	263.0	297.5	319.4	361.4	392.9	33.5
70	278.2	312.6	334.6	376.5	408.0	39.3
80	293.4	327.8	349.7	391.6	423.1	45
90	308.5	342.9	364.9	406.8	438.2	50.8
100	323.7	358.1	380.1	421.9	453.4	56.6

Table 3.3: List of geometric parameter a in [mm] (column 2-6) and b in [mm] (column 7) for a selection of hydraulic cylinders with different stroke lengths and diameters.

stroke [mm]	12/8	16/10	20/12	25/16	32/20
50	50.1	89.1	139.2	217.7	356.5
60	60.5	107.7	168.2	263.1	430.8
70	71	126.3	197.2	208.4	505.1
80	81.4	144.8	226.2	353.8	579.3
90	91.9	163.4	255.3	399.1	653.6
100	102.3	182	284.3	444.5	727.8

Table 3.4: List of maximum torques in [Nm] for a selection of hydraulic cylinders with different stroke lengths and diameters.

stroke [mm]	12/8	16/10	20/12	25/16	32/20
50	0.33	0.55	1.01	1.43	2.75
60	0.36	0.59	1.07	1.5	2.89
70	0.39	0.62	1.14	1.59	3.02
80	0.41	0.67	1.2	1.66	3.16
90	0.44	0.7	1.26	1.75	3.3
100	0.46	0.74	1.33	1.83	3.44

Table 3.5: List of component weight (empty, no oil) in [kg] for a selection of hydraulic cylinders with different stroke lengths and diameters.

stroke according to ISO-4393.

3.4.1.3 Cylinder Attachment on Leg

The last step in the hydraulic joint actuation design is the selection of the cylinder attachment on the leg. I will explain this on the example of the knee joint and a symmetric torque profile according to Fig. 3.14(b).

First we have to move the cylinder rod to half of its maximum extension (this is where the torque maximum will be) and we move the knee joint to its central position within its range of motion ($\theta_2 = 80^\circ$ according to Table 3.2). We now have various possibilities to attach the cylinder between the upper and lower leg segment. Fig. 3.16 shows three possible configurations. Since the joint has to provide maximum torque in these configurations, a right angle is needed between the cylinder axis and the lever arm (shown in green). ϵ_{21} and ϵ_{22} are design angles as defined in Fig. B.2. Their sum is always equal for all possible configurations of a joint.

We selected configuration 2 with the cylinder parallel to the upper leg segments because it fitted well into the mechanical structure. Configuration 1 is not possible because of space problems and interference with other components (*hip f/e* encoder and hip cylinder). The CAD¹ software allows moving the joint inside its complete range of motion. This way any interference between two parts can be identified. Configuration 3 moves the cylinder bottom attachment too far from the upper leg.

The attachment of the hip is obtained in a similar way based on the constraints given by the mechanical structure. The final values of these parameters for both joints are shown in Fig. B.2.

¹Computer Aided Design (CAD)

3. ROBOT SPECIFICATIONS AND DESIGN STUDIES

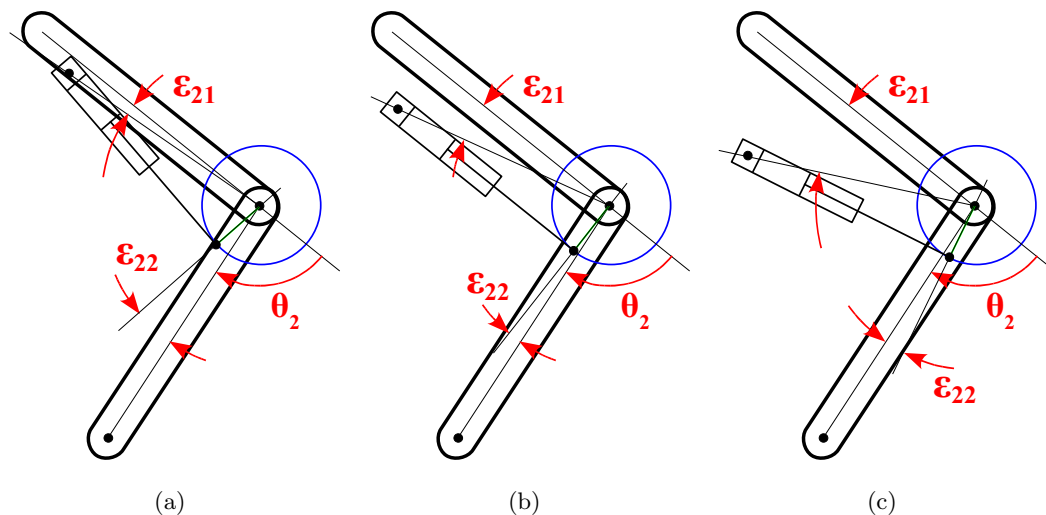


Figure 3.16: Three different cylinder attachment configurations shown for the knee joint: (a) configuration 1 with ϵ_{22} positive; (b) configuration 2 with the cylinder parallel to the upper leg segment and (c) configuration 3 with ϵ_{22} negative.

3.4.2 Electric Joints

The *hip a/a* joint is actuated by an electric motor according to section 3.2.3. Other than the linear output force of cylinders, electric motors already provide a rotation, so no geometric parameters have to be selected for the actuation design. We need to select a motor-gear combination with suitable torque and speed output.

As for the hydraulic joint design, let me summarize the above mentioned estimations and design rules for the *hip a/a* joint:

- torque profile based on Fig. 3.12
- compact overall dimensions (section 3.2.3)
- low weight (**SP2.5** in section 3.1.2)

The selection of motor and gear and the mechanical design of the joint are strongly influenced by the actuator design of the lower body of the humanoid robot *iCub*, which

3.4 Joint Actuation Design and Kinematics

has been designed in our laboratory [Tsagarakis et al., 2007]. iCub is actuated by frameless DC brushless motors in combination with harmonic gears. As stated in section 2.2.1 DC brushless motors have higher speed and torque capabilities, higher power density, low maintenance and improved efficiency in comparison with DC brushed motors. The frameless option allows an excellent integration of the stator and rotor into the mechanical structure of the robot and minimises size and weight. The harmonic gears have no backlash, high reduction ratios, very compact (flat) dimensions and low weight [Tsagarakis et al., 2007]. Therefore, the combination of DC brushless motors with harmonic gears build a powerful and compact electric actuator for legged robots providing higher performance than other electric motor and gear types. Their major disadvantage however is the low resistance against peak torques, as mentioned in section 2.2.1. For HyQ, they are therefore only powering the *hip a/a* joints, which are least affected by impact peak forces during normal running (radial bearings take most of the load).

We selected *emotiq* HT series frameless three-phase DC brushless motors, mainly because they have a high torque and power density, are available in an extensive range of standard designs and because they are the replacement of the *Kollmorgen* motors used for iCub. Table 3.6 lists the specifications of a selection of these motors. For the harmonic gears, we selected the CSD series of *Harmonic Drive*, because they are especially flat and available with high reduction ratios (1:50, 1:100 and 1:160). Table 3.7 contains the specifications of a selection of these gears.

The specifications of the motors and gears show that the limiting factor in terms of torque limits are the gears: the type CSD25 (1:100) is a suitable match for the torques of above estimation and has acceptable dimensions and weight. For the motor we selected the HT2301 since it is a good compromise between weight, torque and power/weight ratio. The combination leads to the following specifications: torque limit of 152Nm, no-load speed of $4.34 \frac{rad}{s}$, diameter of 85mm (without frame) and a weight of 0.57kg (without frame).

3. ROBOT SPECIFICATIONS AND DESIGN STUDIES

Model	weight	max no-load speed ω	max rated torque τ_R	max continuous stall torque	max continuous power
HT2000	0.12kg	$995 \frac{rad}{s}$	1.33Nm	0.114Nm	48W
HT2001	0.22kg	$628 \frac{rad}{s}$	3.16Nm	0.229Nm	63W
HT2002	0.32kg	$523 \frac{rad}{s}$	4.95Nm	0.326Nm	73W
HT2300	0.17kg	$607 \frac{rad}{s}$	2.32Nm	0.215Nm	56W
HT2301	0.33kg	$434 \frac{rad}{s}$	4.76Nm	0.413Nm	81W
HT2302	0.48kg	$356 \frac{rad}{s}$	7.31Nm	0.620Nm	97W

Table 3.6: Specifications of a selection of frameless DC brushless motor *emoteq*. The weight is without frame (only rotor+stator), the maximum no-load speed is obtained from the speed-torque curves and the maximum rated torque τ_R is the amount of torque that the motor can produce without danger of demagnetizing the rotor [Emoteq Inc., 1998].

Model	diameter	weight	max input speed ω	torque limit (1:50)	torque limit (1:100)	torque limit (1:160)
CSD20	70mm	0.13kg	$1047 \frac{rad}{s}$	69Nm	76Nm	76Nm
CSD25	85mm	0.24kg	$785 \frac{rad}{s}$	127Nm	152Nm	152Nm
CSD32	110mm	0.51kg	$733 \frac{rad}{s}$	268Nm	359Nm	359Nm

Table 3.7: Specifications of a selection of harmonic gears of the company *Harmonic Drive* with different reduction ratios. The torque limits are *limits for momentary peak torque* [Harmonic Drive Inc., 2009].

3.5 Leg Prototype with 2 DOF

An important part of the design studies was to construct a first leg prototype (*Leg V1*) early in the design process for experimental testing of the mechanical structure, sensors and electronics, but especially to evaluate the design and performance of the hydraulic actuator units (cylinder and valve). Fig. 3.17 shows a picture and CAD model of the prototype with two hydraulic DOF: *hip f/e* and *knee f/e*, presented in

[Semini et al., 2008]. This robotic leg has been used for a series of experimental studies that are presented in chapter 5.

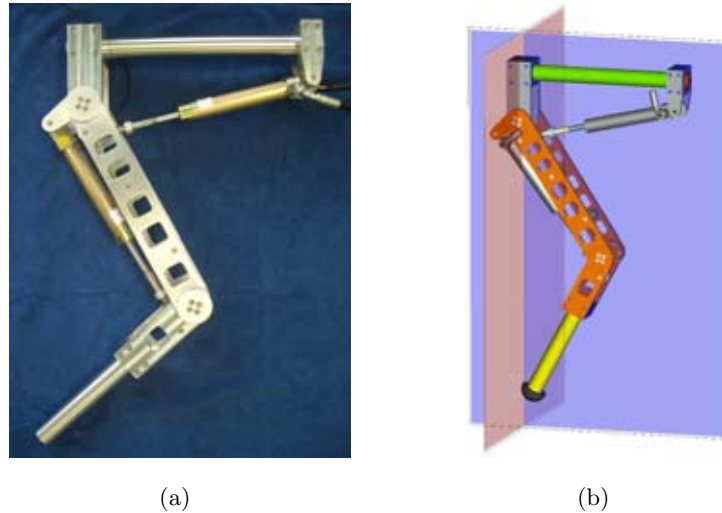


Figure 3.17: Picture and CAD model of the leg prototype (*Leg V1*) with the two hydraulic cylinders of the *hip f/e* and *knee f/e* joint.

Since the leg design is similar to the one of the final leg, its construction and materials are explained more in details in section 4.2. The specifications and geometric parameters of the prototype are reported in section 5.6 where the experimental setup is presented. Finally, the differences and improvements between the leg prototype and final leg are discussed in section 6.1.

3.6 Passive Compliant Ankle Joint

Running or hopping animals temporarily store energy in compliant tendons and muscles to increase their energy-efficiency (see section 2.5.2). Kangaroos for example can store up to 38% of energy from one hop to the other [Alexander, 1988].

Since one of the goals of building HyQ is to study different running gaits, it is crucial to build a certain degree of compliance into the legs of the robot. While the hydraulic

3. ROBOT SPECIFICATIONS AND DESIGN STUDIES

actuation naturally adds some compliance to the system (due to oil compressibility and expanding tubes), an additional passive joint with a compliant element (e.g. a spring) has to be added to the leg. This joint is located between the lower leg and the foot and is therefore like an *ankle joint*. It can either be linear or rotational. Fig. 3.18 shows the two possible extensions of the kinematic structure that was presented in section 3.2.2.

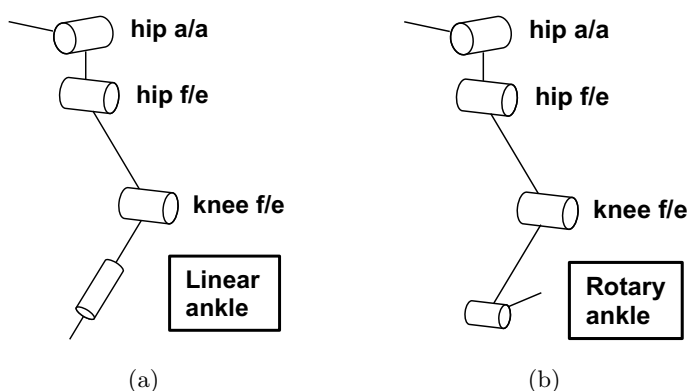


Figure 3.18: Kinematic Structure of the leg including a passive ankle joint with compliance. Two design options are possible: (a) with a **linear** joint or (b) with a **rotational** joint.

The most promising candidates for the selection of a compliant element are either a mechanical spring or a pneumatic spring. Since mechanical springs are commercially available in various designs, materials and sizes, they are the simpler solution than the pneumatic spring. The remainder of this section presents a study on a linear ankle joint with a mechanical spring. The focus lies on the selection of a suitable spring.

A very important criterion for the selection of the spring is its weight, because its location on the leg is far from the torso and hip joint and therefore adds considerably to the inertia of the leg (see design rule **SP2.5** in the beginning of this chapter). Additionally, the spring's maximum compression length and the spring stiffness have to be chosen. Its natural (uncompressed) length and internal and external diameter are parameters that are important for the mechanical integration of the spring.

To estimate the specifications of the springs, it is useful to calculate the amount of energy that the spring needs to be able to store. Let us assume that the robot drops from a height of 0.15m on a diagonal foot pair (see **SP1.7**) with the lower legs vertical (or nearly vertical) to the ground plane, Fig. 3.19(a). We can model the robot as a simple spring-mass system as shown in Fig. 3.19(b) and explained in section 2.5.2). Let us assume that in an ideal case (neglecting air resistance and energy losses due to the impact) all potential energy E_{pot} of the robot at the start of the fall (uncompressed spring, Fig. 3.19(b), left) will be converted and stored equally inside the two leg springs when the robot reaches its lowest position (maximally compressed spring, Fig. 3.19(b), right). Since the mass spring model contains one spring, we will consider half of the robot's mass for this simulation and call it $m_{sim} = \frac{m_{robot}}{2}$.

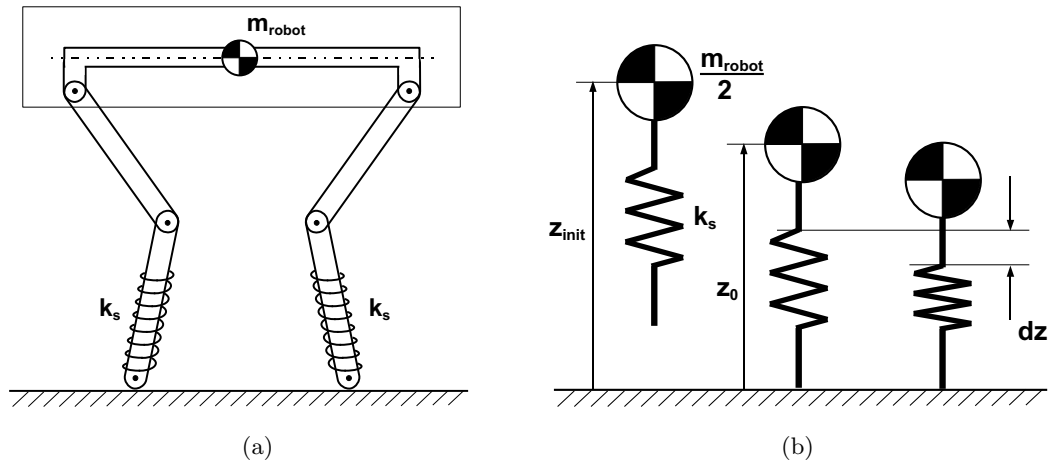


Figure 3.19: Robot sketch and model used for spring dimensioning: (a) Sketch of the robot with linear springs in lower leg and (b) spring-mass model of the robot in the air (left), at the moment of touch-down (centre) and with maximally compressed spring (right).

In this ideal case, the energy conversion between the potential energy E_{pot} and spring energy E_{spring} can be written as follows:

$$E_{pot} = m_{sim}g(z_{init} - z_0 + dz) = E_{spring} = \frac{1}{2}k_s dz^2 \quad (3.24)$$

where m_{robot} is the total robot mass, g the gravitational acceleration, z_{init} the height

3. ROBOT SPECIFICATIONS AND DESIGN STUDIES

of the robot COM at the start of the fall, z_0 the height of the robot COM at the instant when the feet touch the ground, dz the maximum spring compression and k_s the spring stiffness.

Regrouping (3.24) we obtain the following quadratic equation for dz :

$$\frac{1}{2}k_s dz^2 - m_{sim}g dz - m_{sim}g(z_{init} - z_0) = 0 \quad (3.25)$$

Solving (3.24) for dz , we obtain two solution:

$$dz_{1,2} = \frac{m_{sim}g \pm \sqrt{(m_{sim}g)^2 + 2k_s m_{sim}g(z_{init} - z_0)}}{k_s} \quad (3.26)$$

Only the solution with the + sign makes physically sense. With the initial estimation of section 3.1.2 the upper limit of m_{robot} is 90kg and therefore $m_{sim} = 45kg$. Fig. 3.20 shows the spring compression to spring stiffness plot for a series of initial start positions ($z_{init} - z_0$) of the robot, including the static case with ($z_{init} - z_0$) = 0m.

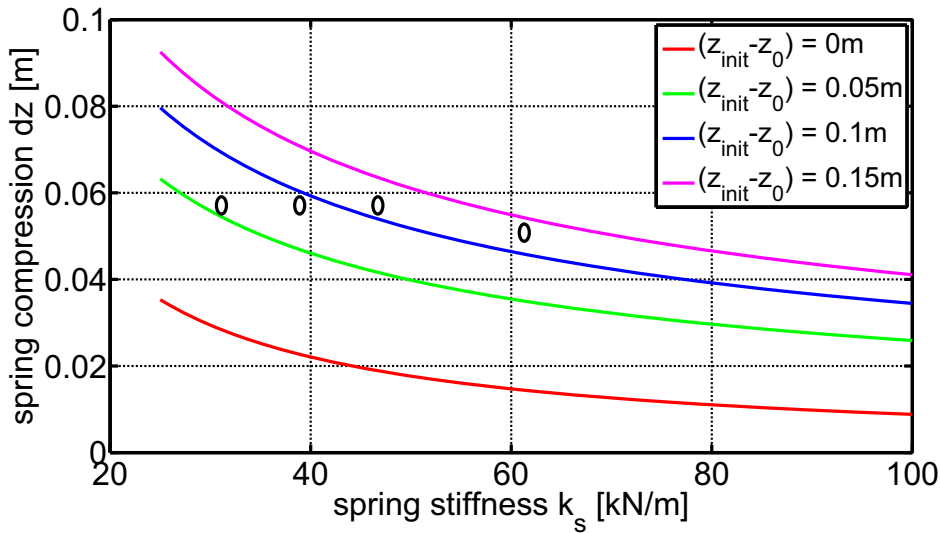


Figure 3.20: Plot of spring compression vs. spring stiffness for different initial robot heights ($z_{init} - z_0$). Black circles indicate the properties of selected titanium springs.

The next task is to find a light-weight and compact spring that is commercially available. The springs used for the rear suspension systems of mountain bikes are

3.6 Passive Compliant Ankle Joint

interesting candidates. Like in the field of robotics, low weight is crucial for the construction of high-performance bikes. Literally *every 100 gram on the bike is too much*. Additionally, the available springs have stiffness values in a suitable range, since the market offers springs for different body weights of the riders. The dimensions match the size of the robot's legs. Fig. 3.21 shows the picture of a titanium spring by *Nuke Proof*.

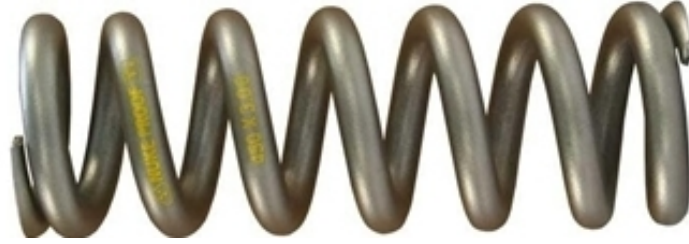


Figure 3.21: Picture of *Nuke Proof Shokwave Ti* compression spring made of Titanium.

Table 3.8 lists the specifications of a selection of four *Nuke Proof* titanium springs. According to their stiffness and maximum compressible length, these four types have been added to the plot in Fig. 3.20 with black circles.

Property	type 1	type 2	type 3	type 4
stiffness [kN/m]	31	39	47	61
uncompressed length [m]	0.124	0.125	0.13	0.124
compressible length [m]	0.057	0.057	0.057	0.051
max. energy storage [J]	51	64	76	79
weight [kg]	0.224	0.242	0.343	0.318
energy density [J/kg]	227	263	222	249
internal diameter [m]	0.036	0.036	0.036	0.036
external diameter [m]	0.053	0.055	0.056	0.056

Table 3.8: List of specifications of mountain bike rear suspension springs *Nuke Proof*.

For the particular case of the above simulation, spring type 4 is the most suitable one, because it has the highest stiffness and energy storage capability.

3. ROBOT SPECIFICATIONS AND DESIGN STUDIES

Besides increasing energy-efficiency, passive compliance in the legs also helps to protect the robot from damage. The compliant element dampens the peak forces that act on the joints and actuators during the impacts at foot touch-down. Additionally, a layer of visco-elastic rubber around the foot increases this effect.

3.7 Spring-Mass Model Simulation

The physical behaviour of a hopping robot with compliant legs, can be modelled with a simple spring-mass system as presented in section 2.5.2. The dynamic models defined in (2.11) to (2.14) can be used to simulate the study of the previous section 3.6. Let us assume the following simulation parameters listed in Table 3.9, which correspond to the parameters of the above study and spring type 4. Furthermore, damping coefficient and external forces are zero. The simulation environment is based on a 4th order Runge-Kutta integrator with an integration step of 0.1ms. The ground is considered as hard.

Simulation Parameter	Variable	Value
mass	m	45kg
COM position at start	z_{init}	0.65m
uncompressed leg length	z_0	0.5m
COM velocity at start	v_{init}	$0\frac{m}{s}$
spring stiffness	k	$61\frac{kN}{m}$
damping coefficient	c	$0\frac{Ns}{m}$
external force	F	0N

Table 3.9: List of simulation parameters for the spring mass model with zero damping and no external force. Spring parameters correspond to the spring type 4 of Table 3.8.

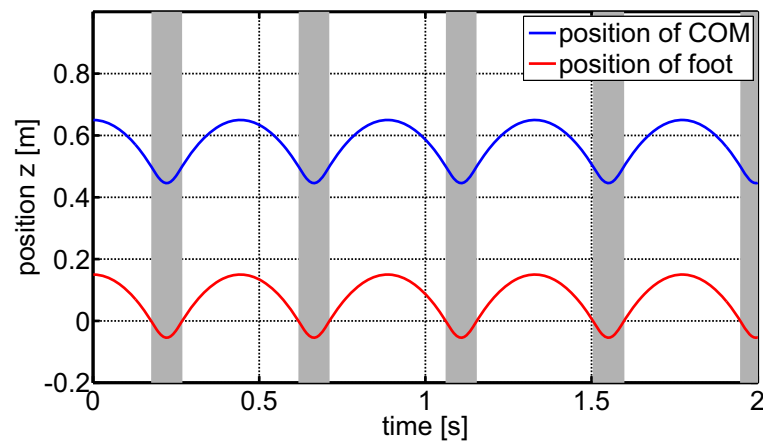
The initial state of \mathbf{Z} is:

$$\mathbf{z}_{init} = \begin{pmatrix} 0.65 \\ 0 \end{pmatrix} \quad (3.27)$$

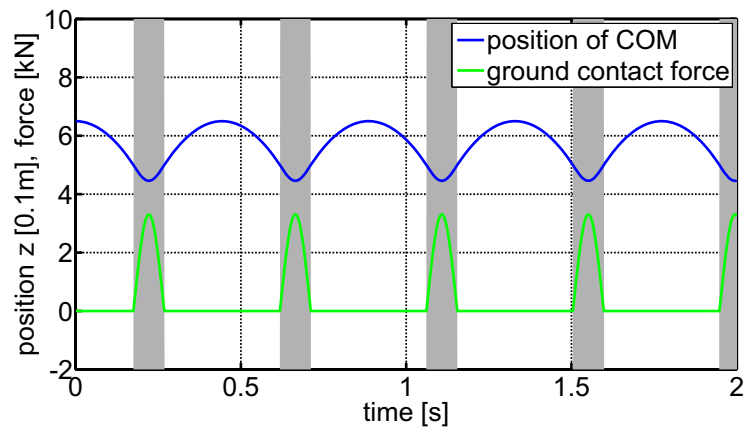
Fig. 3.22 shows the resulting time plot of the COM position and ground contact force. Without any loss of energy ($c = 0$) and external forces ($F = 0$), this simulation results in a continuous hopping motion with constant hopping height. Note that

3.7 Spring-Mass Model Simulation

during the stance phase (marked with a grey background) the foot position penetrates the ground, which represents the compression length of the spring. According to the 0.15m-curve in Fig. 3.20, we expect a maximum spring compression during stance phase slightly higher than the one of the spring type 4. The hopping of this simulation results in a 55mm compression, which confirms our expectations.



(a)



(b)

Figure 3.22: Plots of the hopping robot simulation: **(a)** Resulting COM position vs. time plot for the hopping robot simulation with spring-mass model. The stance phase is marked with a grey background. The foot position penetrates the ground during the stance phase and represents the spring compression. **(b)** Ground contact forces vs. time plot.

3.8 Power System and Energy Source Comparison

This chapter ends with a case study of the comparison between the performance of commercial AC motors and combustion engines to drive the pump on board of the robot (see development stage 2 and 3 of section 3.1.3). AC motors widely used in industry are for example the *ABB general performance aluminium motors*. We selected the *ABB M2AA series* with 2-poles and 400V AC and estimated their power-to-weight ratio according to the output power and motor weight of the data sheet [ABB, 2008]. In a range of 1-4 kW, the motors have a power-to-weight ratio of approximately 0.15kW/kg (excluding electronics and power supply).

For this study, we analysed the 4-stroke internal combustion engine *Honda GX-series* [Honda, 2009]. In a range of 1-4 kW, these engines feature a power-to-weight ratio of 0.28 kW/kg (with full gasoline and oil tanks).

In this study, the power density of commercial combustion engines is almost double the one of commercial AC motors. While this difference is already significant, it is crucial to also have a look at the energy density of the energy source that powers the two solutions (if evaluating power autonomy of robots or machines in general). Two possible onboard energy sources for mobile robots are batteries (in case of electric actuation) or fuel (in case of a combustion engine). Table 3.10 summarizes the energy densities of batteries (lithium ion type) and fossil fuel (petrol). I also added the titanium spring of section 3.6 as a reference.

Energy storage	energy density [$\frac{kJ}{kg}$]
battery (e.g. lithium ion)	1300
fossil fuel (e.g. petrol)	46000
mechanical coil spring (e.g. <i>Nuke Proof</i>)	0.26

Table 3.10: List of energy densities of batteries, fossil fuel and mechanical springs.

3.9 Conclusions

This chapter presented the robot specifications including design rules, performance and physical specifications: The robot has an expected length of about 1m and a weight up to 90kg. The chapter then continued with the explanation of a series of design studies that build the foundation of the robot design and components selection. In particular, I presented the considerations to define the robot structure, including the number of legs and leg length, number of joints and type of actuation (electric/hydraulic), joint range of motion, kinematic leg structure and the leg configuration on the torso.

Next, the joint torque requirements were estimated based on simulations of a jumping and standing robot. This led to the design of the joint actuation and kinematics including the selection of the hydraulic and electric actuator components. After the presentation of the leg prototype that has been used for experimental testing and design evaluation, I discuss compliant ankle joints and spring-mass model simulations. The chapter ends with a short comparison of energy sources and a case study of power systems to drive the onboard hydraulic pump.

3. ROBOT SPECIFICATIONS AND DESIGN STUDIES

4

Robot Design and Components

This chapter presents the mechanical design and components of the robot. I named the robot *HyQ*, which is the abbreviation for *Hydraulic Quadruped* and pronounced [hai-kju:] [Semini et al., 2008]. Fig. 4.1 shows a 3D view of HyQ with empty torso.

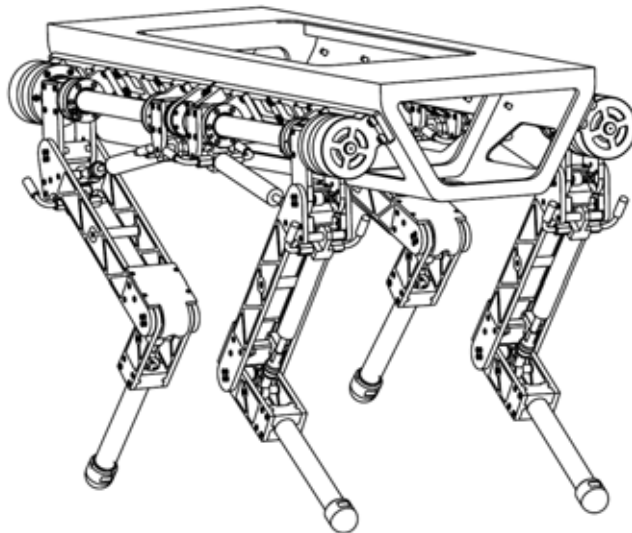


Figure 4.1: 3D model of HyQ with empty torso.

After a system overview, this chapter presents the mechanical design of the robot, with a focus on its kinematic structure, construction materials and the design of torso, legs and feet. It continues with an explanation of the hydraulic and electric actuation system, sensory system and the real-time control structure.

4. ROBOT DESIGN AND COMPONENTS

4.1 System Overview

HyQ is a quadruped robot with both electrically and hydraulically actuated leg joints. It has the size of a large dog or small pony and is designed to carry the entire hydraulic actuation system on board. Its mechanical structure is mainly built in a strong and light-weight aluminium alloy and stainless steel. Each of the four legs features three active DOF with a range of 120° . The modular design of the legs allows easy mounting and dismounting for maintenance or repair. The legs have built-in compliance to allow energy-efficient locomotion and to protect the mechanical structure from strong impacts. All joints are controlled by an onboard Pentium computer connected to motor and valve drivers. Gait control and robot balance is accomplished by the onboard position, force sensors and inertial measurement unit (IMU).

Table 4.1 gives a summary of the most important robot specifications.

Property	Value
dimensions (fully stretched legs)	1.0m x 0.5m x 0.98m (LxWxH)
weight	48kg (stage 1), 90kg (stage 2)
active DOF	12; 3 per leg (2 hydraulic, 1 electric)
joint range of motion	120°
hydraulic actuation	double-acting asymmetric cylinders
electric actuation	DC brushless motors + harmonic gear
max. torque [elec]	152Nm (torque limit of gear)
max. torque [hydr]	145Nm (peak torque at P_{max})
max. pressure P_{max}	16MPa
onboard sensors	position, force, pressure, IMU
onboard computer	PC104 Pentium with real-time Linux
control frequency	1kHz

Table 4.1: Summary of the most important system specifications of HyQ.

Fig. 4.2 shows the CAD model of the complete robot with all components.

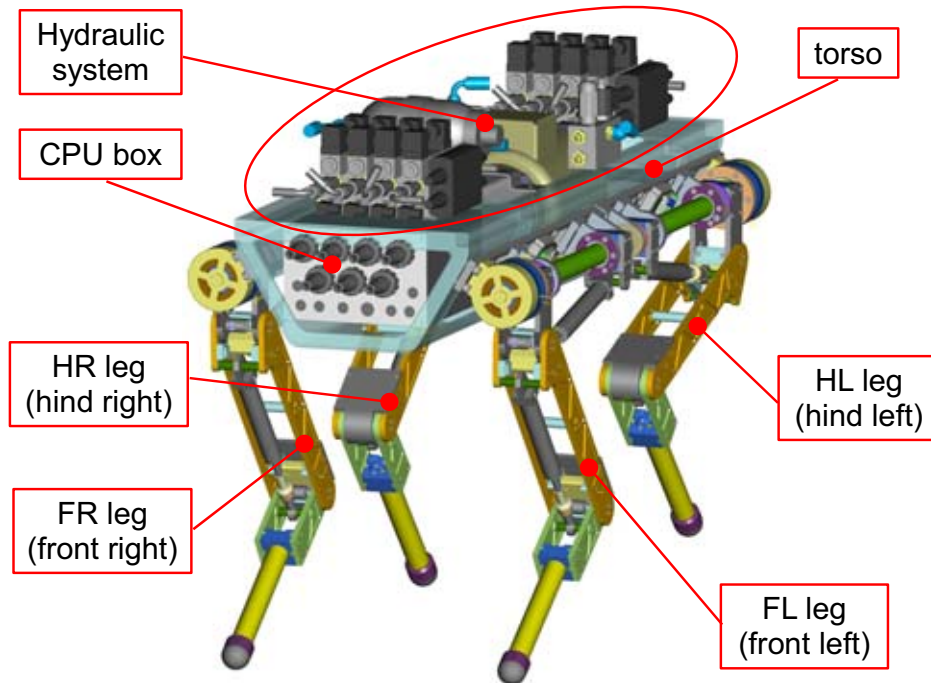


Figure 4.2: 3D CAD model of HyQ with a description of the components.

Table 4.2 shows the list of the weights of all parts and components of the complete robot for stage 1 and for stage 2 (see section 3.1.3 for details on the development stages).

4.2 Mechanical Design

4.2.1 Kinematic Structure

The HyQ robot has four identical legs. They are mounted to the torso in a way that the knees of the front and of the hind legs face each other as shown in Fig 4.3. Each leg features three active DOF and one passive DOF in the foot (the latter is not implemented in the first version): hip abduction/adduction (*hip a/a*), hip flexion/extension (*hip f/e*), knee flexion/extension (*knee f/e*) and the ankle joint. The studies presented in section 3.2 explain the reasons and advantages of choosing this particular kinematic structure.

4. ROBOT DESIGN AND COMPONENTS

Robot part/component	Weight
Torso	10.2kg
Four legs (see note below)	31.6kg
CPU box	3.5kg
Central manifold	1.0kg
Hydraulic hoses to legs	2.0kg
Total weight for robot stage 1	48.3kg
Pump unit (see note below)	20.2kg
Two valve manifolds (see note below)	13.2kg
Accumulator	3.1kg
Hydraulic hoses inside torso	3.0kg
Heat exchanger	1.6kg
Oil Filter	1.0kg
Total weight for robot stage 2	90.4kg

Table 4.2: List of all robot parts and components with their weight, including the total weight for robot stage 1 and robot stage 2. The weight of the legs includes the hydraulic cylinders, electric motor unit and the leg-torso attachment. The pump unit includes the pump motor, pump, manifold, valves and full oil tank. The valve manifolds include the four valves, eight pressure sensors and quick-release couplings.

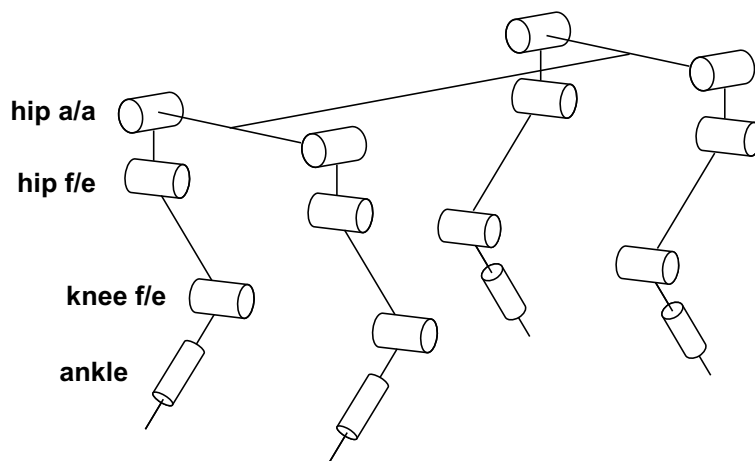


Figure 4.3: Kinematic structure of HyQ with joint names: *hip a/a*, *hip f/e*, *knee f/e* and ankle joint.

4.2.2 Construction Materials

A crucial element in designing a robot is to keep its total weight low. Especially the segments (leg or manipulator) that have to be accelerated the most, e.g. the foot and the lower segments of a leg (see also **SP2.5** in section 3.1.2). It is important to keep the leg inertia as low as possible to reduce joint torques. Marathon runners choose very light shoes for this reason; each 100 gram of weight has to be carefully looked at. Therefore, an appropriate selection of the material for the robot's mechanical structure is very important.

The second crucial requirement for robot construction materials is to be strong and capable to resist impacts. A requirement that is generally in direct conflict with the first one. A general engineering practice is to add some additional material to be on the safe side in terms of structural robustness. This practice however is not suitable for designing a high performance legged robot.

Other requirements to consider are manufacturability (to achieve the necessary dimensional and geometric tolerances), corrosion-resistance and cost.

We decided to use a combination of stainless steel and aluminium alloys for the construction of HyQ. Most parts of the robot including the torso are made in *Ergal*, an aluminium alloy (type 7075) that is widely used in the aerospace industry due to its excellent strength-to-weight ratio. It has a mass density of 2810kg/m^3 and yield stress of up to 520MPa. For critical parts that need a higher strength, such as attachment shafts of the cylinders and bearings, we used stainless steel of the type *AISI 303* and *17-4 PH* that are stronger but almost three times heavier than *Ergal*. *AISI 303* has superior machinability across a wider range of operations and cutting conditions compared to other steel types. *17-4 PH* has a very high yield stress. For a few parts of the torso, a cheaper aluminium alloy (*Anticorodal 60*) has been used. Table 4.3 lists the properties of these four materials.

Composite materials based on e.g. carbon and Kevlar have excellent strength to weight ratio and are widely used for aerospace components (including wings, fuselages

4. ROBOT DESIGN AND COMPONENTS

Material	Code	Density	Elastic Modulus	Yield Stress
Aluminium (Anticorodal 60)	6060	2700kg/m ³	69GPa	80-160MPa
Aluminium (Ergal 55)	7075	2810kg/m ³	72GPa	420-520MPa
Stainless Steel	AISI 303	8020kg/m ³	196GPa	515-655MPa
Stainless Steel	17-4 PH	7800kg/m ³	196GPa	760-1240MPa

Table 4.3: Comparison of Material Properties.

and propellers), boat and scull hulls, bicycle frames and racing car bodies. They are becoming more and more popular also in robotics. While the first version of HyQ is built in Ergal and stainless steel, some parts (including the torso) could eventually be replaced by composite materials in future versions.

Let us now focus on the mechanical design of the torso, the legs and feet.

4.2.3 Robot Torso

The main function of the torso of the robot, besides carrying most robot components, is to act as a rigid chassis for the four legs. The optimal torso has minimal (axial and torsional) deflection¹, handles well all sorts of impacts, provides a rigid platform to easily mount the robot legs and the other robot components and is lightweight, while preferably looking good at the same time.

We preferred a structure based on a folded aluminium sheet (Fig. 4.4) to a welded structure of tubes (often seen in small car or motorbike chassis). The advantages of a construction with a folded sheet are: simplicity, rigidity, light-weight and easy manufacturability. In addition it has great ability to mount and accommodate components. The torsional robustness of the folded sheet is increased by four internal walls perpendicular to the longitudinal axis of the torso (see Fig. 4.4(a)). The weight of these walls

¹In nature, the spinal cord in the torso of cursorial mammals, allows a considerable deflection and together with the tendon and muscles provides elastic energy storage during high speed running. For simplicity, the first version of HyQ has a rigid torso.

is reduced as much as possible by removing material in their centre, which leaves only their frames. The material of the sheet is Ergal.

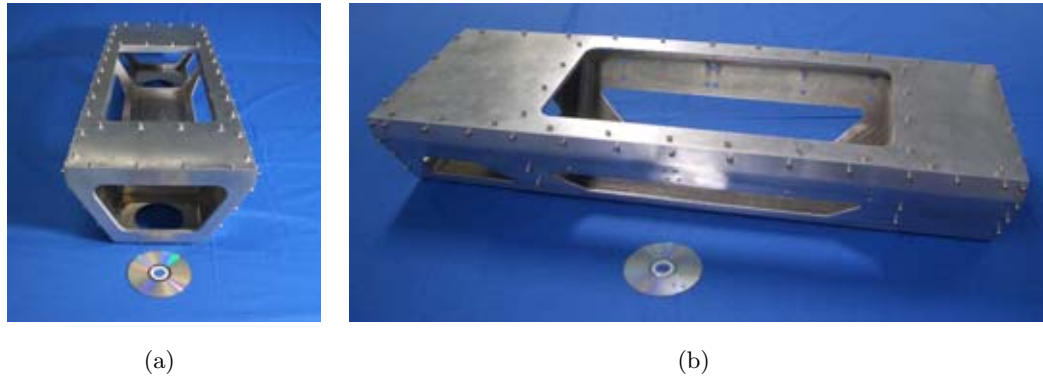


Figure 4.4: Picture of the empty robot torso with a standard-size compact disc to indicate the size: (a) front view and (b) side view.

To estimate the effectiveness of the internal walls and mainly to determine the thickness of the aluminium sheet, a series of finite element model (FEM) analysis have been performed. Since this study has not been performed by me, the details of this study are reported in Appendix D.1.

The final torso has a sheet thickness of 3mm and contains 4 internal walls with a thickness of 10mm. Ergal turned out to be not very suitable for folding. Therefore, instead of bending the sheet at four positions to create a closed shape, two parts were manufactured: a U-shaped bottom part with two bends and a flat cover plate. 102 M4-screws connect the bottom with the top part and the internal walls. The total weight of the torso including screws is 10.2kg. Its dimensions are 1.0m x 0.34m x 0.17m (LxWxH) with 30° inclined side walls.

4.2.4 Robot Leg (V2)

The most important parts of the robot structure are the legs. Their properties (dimensions, weight and inertia of leg segments, joint actuation) determine the performance of the legs and therefore of the whole robot. For initial testing of the structure and the

4. ROBOT DESIGN AND COMPONENTS

actuation system, a prototype leg (let us call it *Leg V1* for version 1) has been built; see section 3.5 and chapter 5. Based on these experiments, I was able to improve the leg design, which resulted in the final leg (*Leg V2*). This section explains the design and geometry of the final leg version. Differences between the two leg designs are reported in the *Discussion* chapter in section 6.1.

The design studies of the previous chapter resulted in a leg segment length of 350mm, a joint range of 120° for all three joints and cylinder with 80mm stroke. With this information first of all we need to determine the maximum cylinder length. Since we placed a load cell with adapter between the rod and the rod end clevis (44mm length), the total cylinder length with completely extended rod increased to a value of 361mm (157mm+80mm+44mm+80mm). If we consider a margin of 1mm on each end of the stroke, we obtain a usable stroke length of 78mm and therefore $c_{max} = 360mm$. To obtain a torque profile with the torque maximum in the centre, we can now calculate the parameters b and a according to (3.21) and (3.23), with all values in [mm]:

$$b = \frac{l_{cs}}{2 \sin(\frac{\varphi_{jr}}{2})} = \frac{78}{2 \sin(60^\circ)} = 45.0 \quad (4.1)$$

$$\begin{aligned} a &= \sqrt{b^2 + c_{max}^2 - 2bc_{max} \sin(\frac{\varphi_{jr}}{2})} \\ &= \sqrt{45^2 + 360^2 - 2 \cdot 45 \cdot 36 \sin(60^\circ)} = 321.8 \end{aligned} \quad (4.2)$$

Both *hip f/e* and *knee f/e* joints have the same parameters a , b and output torque profiles, as shown in the left of Fig. 4.5. However they have different values for ε_1 and ε_2 . Table 4.4 lists the geometric parameters for both joints.

Parameter	hip f/e	knee f/e
a	321.9mm	321.8mm
b	45.0mm	45.0mm
ε_1	6.24°	8.04°
ε_2	0°	6.0°

Table 4.4: List of the geometric parameters of the *hip f/e* and *knee f/e* joint.

The relation between the cylinder extensions c_1 and c_2 and the joint angle θ_1 (*hip f/e*) and θ_2 (*knee f/e*) is expressed as follows:

$$c_1 = \sqrt{a_1^2 + b_1^2 - 2a_1b_1 \cos\left(\frac{\pi}{2} + \theta_1 + \varepsilon_{11}\right)} \quad (4.3)$$

$$c_2 = \sqrt{a_2^2 + b_2^2 - 2a_2b_2 \cos(\pi - \theta_2 - \varepsilon_{21} - \varepsilon_{22})} \quad (4.4)$$

with the definition of the joint angles according to Fig. B.2. The joint angle vs. cylinder position based on (4.3) and (4.4) is shown in Fig. 4.5.

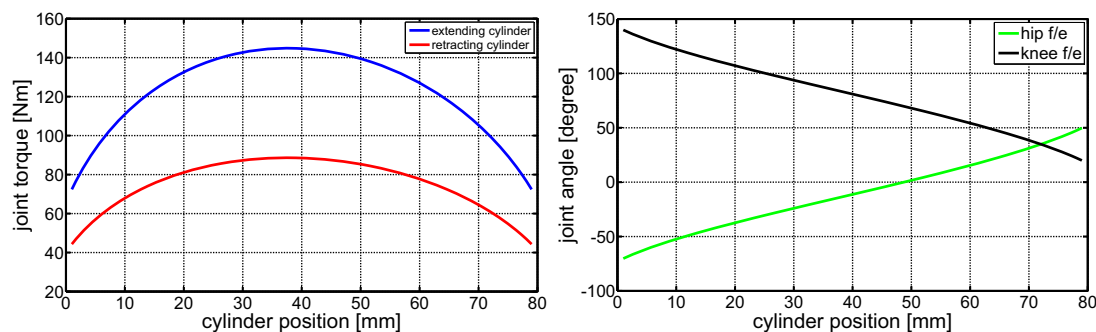


Figure 4.5: Joint torque and angle vs. cylinder position plots for the *hip f/e* and *knee f/e* joint: Joint torque vs. extending and retracting cylinder position are identical for both joints (left) and joint angle vs. cylinder position plot (right).

Since the brushless DC motor is frameless we had to design the motor case with integrated harmonic gear, bearings and encoder. The mechanical design is strongly influenced by the design of the electric motor units of iCub, designed by Nikos Tsagarakis [Tsagarakis et al., 2007]. Fig. 4.6 shows a cross-section of the CAD model with the description of the components.

The connection between the motor unit and the leg is constructed by 6 stainless steel pins with a diameter of 6mm, evenly aligned on a circle with a diameter of 32mm. The robustness of this design has been checked and improved based on the results of a series of finite element model (FEM) analyses reported in Appendix D.2.

4. ROBOT DESIGN AND COMPONENTS

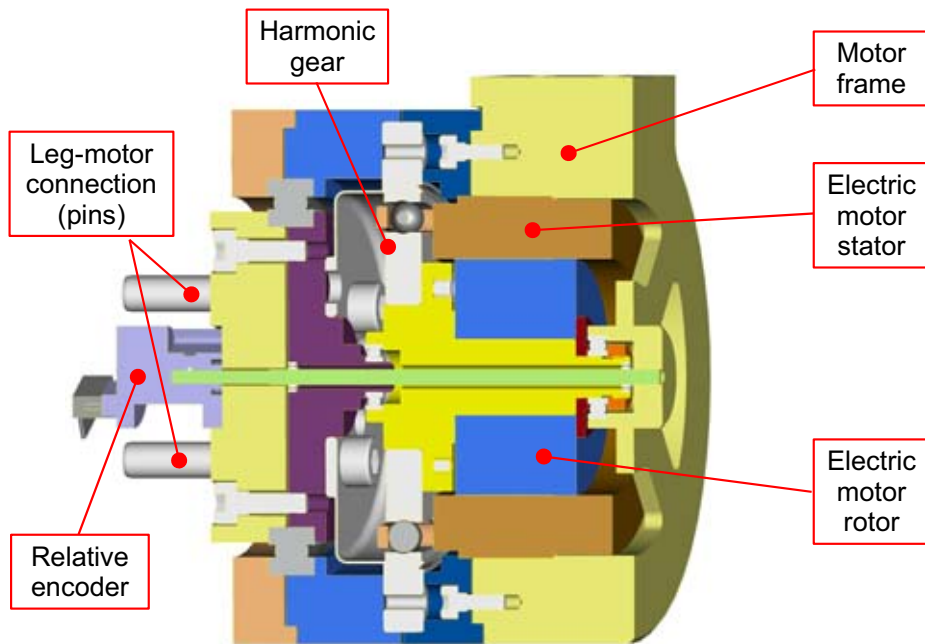


Figure 4.6: Cross-section of the CAD model of the electric motor unit with the description of the components.

The final design of the leg with a description of the parts and leg segments, is shown in Fig. 4.7(a). Fig. 4.7(b) displays a cross-section through the leg-sagittal plane to show the construction details between the leg plates.

A third FEM analysis has been performed to study the structural robustness of the leg. One goal was to determine how much material can be removed from the big leg plates while keeping the mechanical structure strong enough. The results of the study are shown in Appendix D.3. As shown in Fig. 4.7(a) the leg plates of the upper and lower leg are designed in a light-weight fashion with as much material removed as possible (3mm depth on each side of the plates), leaving 45° rims for torsional strength. The two plates of the upper legs are 8mm thick and weigh 0.234kg each, as opposed to 0.32kg before material removal. With an upper leg segment weight of 1.0kg (without knee cylinder), this is a reduction of over 17%.

Table 4.5 lists the weights of the leg segments (as illustrated in Fig. 4.7(a)) and their inertia with respect to the axis of rotation. The values are estimations based on

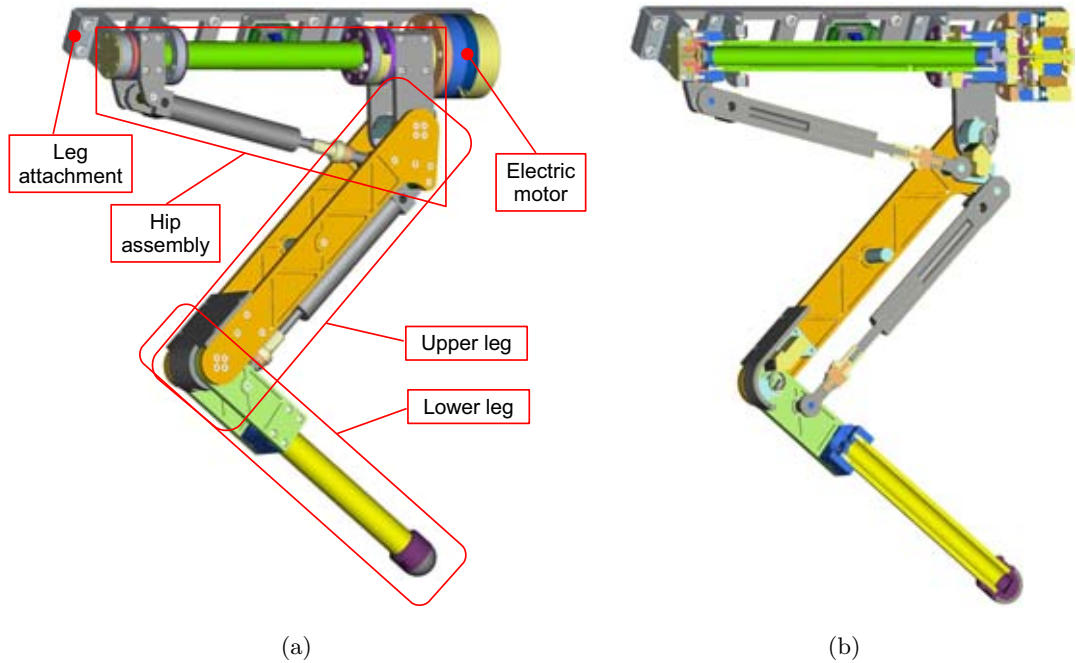


Figure 4.7: CAD models of HyQ robot leg (V2) with the description of the leg parts: (a) complete and (b) cross-section.

the CAD model. No inertia data is given for the leg attachment and electric motor unit, since they are fixed to the torso and therefore not in motion.

Leg Part	Weight	Inertia
leg attachment	1.31kg	-
electric motor unit	1.53kg	-
hip assembly (with hip cylinder)	2.48kg	$0.00745kg \cdot m^2$
upper leg (with knee cylinder)	1.77kg	$0.0713kg \cdot m^2$
lower leg (with basic foot)	0.81kg	$0.0218kg \cdot m^2$
Total weight	7.9kg	

Table 4.5: List of weight and inertia of the 5 main leg parts based on the estimation of the CAD software. The inertia is with respect to the corresponding joint axis of rotation: *hip a/a* for hip assembly, *hip f/e* for upper leg and *knee f/e* for lower leg.

4. ROBOT DESIGN AND COMPONENTS

4.2.5 Robot Foot and Ankle Joint

The robot foot is an important part of the robot since the interaction with the environment (the ground) is happening there: The complete motion of the robot is determined by the forces acting at the feet. The robot foot has two main functions: establish good traction between the robot leg and the ground to avoid slipping. The other task is to dampen the impact force peaks to a certain extend to protect the mechanical structure and to reduce vibrations. A layer of visco-elastic rubber meets both of these requirements.

The passive ankle is either a rotational or linear joint with a mechanical spring. This joint and the foot of HyQ are designed in a modular way to easily test different designs: rotational or linear, with or without mechanical spring (with different spring stiffnesses), different rubber types, with or without damping elements, contact switches and other sensors like spring compression (position) or multi-axis contact force sensors. A simplified mechanical drawing of the lower leg with the most important parts are shown in Appendix E.1 as a reference for future ankle joint and foot designs.



Figure 4.8: Pictures of the basic HyQ foot: **(a)** disassembled and **(b)** assembled.

To reduce the complexity of the first version of HyQ, a basic foot with fixed ankle joint without sensors, mechanical spring or damper has been designed as shown in Fig. 4.8. However, some degree of elasticity and damping has been added by coating the semi-spherical foot with a layer of visco-elastic rubber from a squash ball. We expect that depending on the roughness of the ground, this rubber has to be replaced frequently because it wears off. The material of car/bike tires and the soles of sport shoes

are other promising materials for robot feet since they are designed to be less affected by wear. A second design with the titanium spring presented in section 3.6 is currently being constructed.

4.2.6 Assembled HyQ Robot

Finally, Fig. 4.9 and 4.10 show a side and front view picture of the assembled mechanical structure with torso and four legs, without electric and hydraulic components.

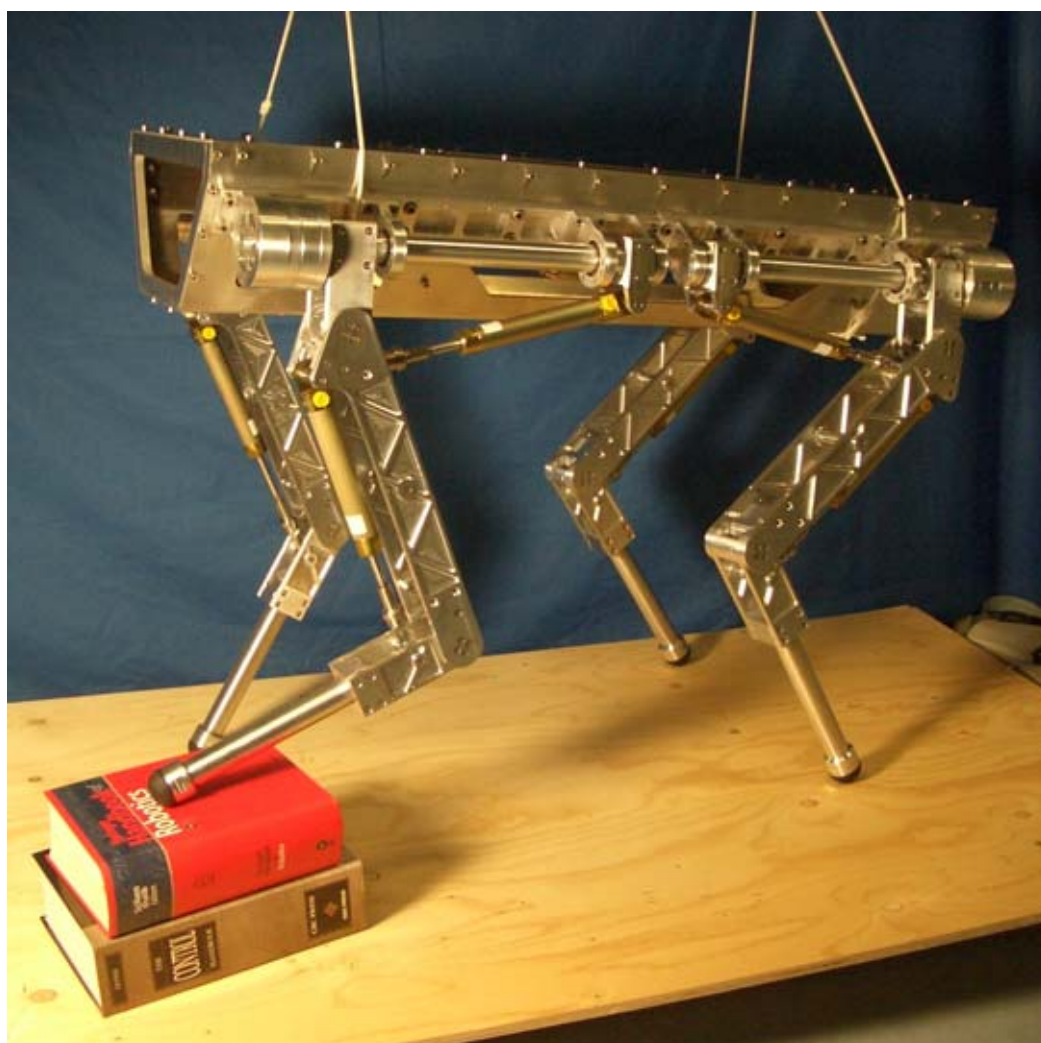


Figure 4.9: Picture of the mechanical structure of HyQ (side view).

4. ROBOT DESIGN AND COMPONENTS

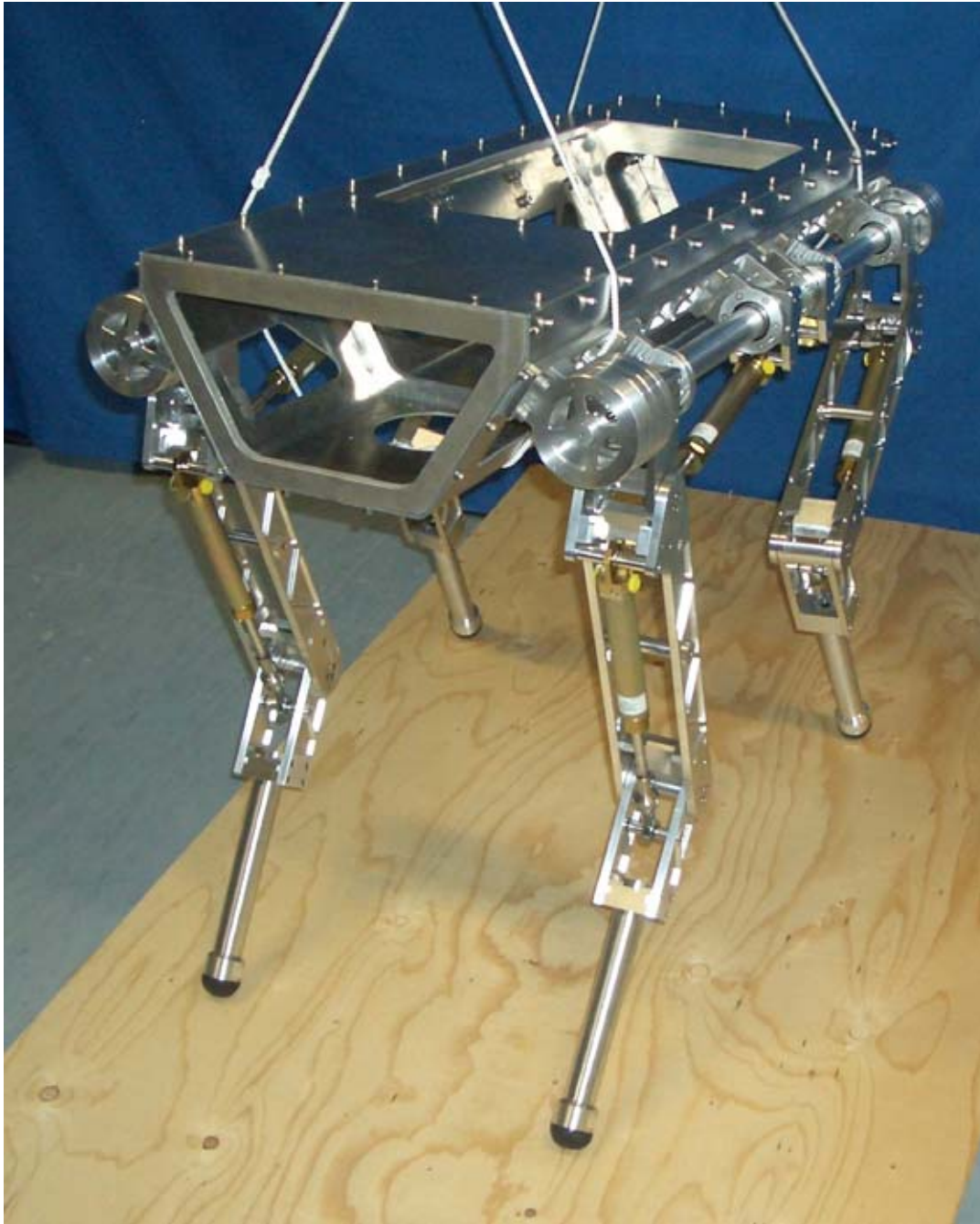


Figure 4.10: Picture of the mechanical structure of HyQ (front view).

4.3 Actuation Systems

This section explains both the actuation systems for the electrically and hydraulically actuated joints of HyQ. After a short system overview, the single components and their specifications are presented.

4.3.1 Electric System

4.3.1.1 Electric System Overview

The *hip a/a* joints of the robot are actuated by DC brushless motors in combination with harmonic gears based on the actuator design study of section 3.4.2. Each motor is controlled and powered by its own controller board located on the attachment plate between torso and leg. Two separate CAN¹ busses establish the communication between two of these boards and the CPU box.

4.3.1.2 Motor Controller

Each of the four DC brushless motors is controlled and powered by an *ELMO Whistle Solo* board, as explained more in details below in section 4.5.3. The communication with the CPU box is established via CAN bus.

4.3.1.3 Brushless Motor and Harmonic Gear

The brushless DC motor *Emotiq HT2301* and the harmonic gear *Harmonic Drive CSD-25-100* of the electrically actuated joints are selected and described in detail in section 3.4.2. Fig. 4.11 shows a picture of the stator and rotor of the frameless motor and a picture of the harmonic gear.

¹CAN: Controller Area Network

4. ROBOT DESIGN AND COMPONENTS

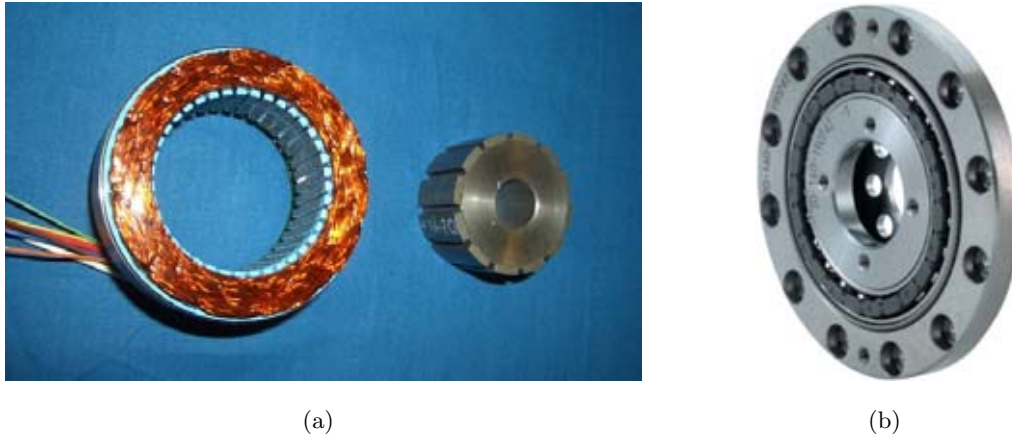


Figure 4.11: Pictures of (a) the *Emoteq* brushless DC motor and (b) the *Harmonic Drive* harmonic gear [Harmonic Drive Inc., 2009].

4.3.2 Hydraulic System

This section describes the hydraulic system. After a short overview including the hydraulic schematic of the system, the single components and their specifications are presented.

4.3.2.1 Hydraulic System Overview

Fig. 4.12 shows the CAD model of the torso with all components of the hydraulic system (with the exception of the hydraulic cylinders). Besides the CPU box, the main space inside and on the robot torso are occupied by the hydraulic system.

The hydraulic schematic of the system is displayed in Fig. 4.13. Note that only one of the two *Valve manifolds* is shown, since both front and hind leg manifolds are identical: they both host four valves, eight pressure sensors and eight quick-release couplings).

4.3.2.2 Hydraulic Pump Units

For the robot development stage 1, the hydraulic actuators of HyQ are powered by an external hydraulic pump unit as shown in Fig. 4.14(a). For stage 2, an onboard

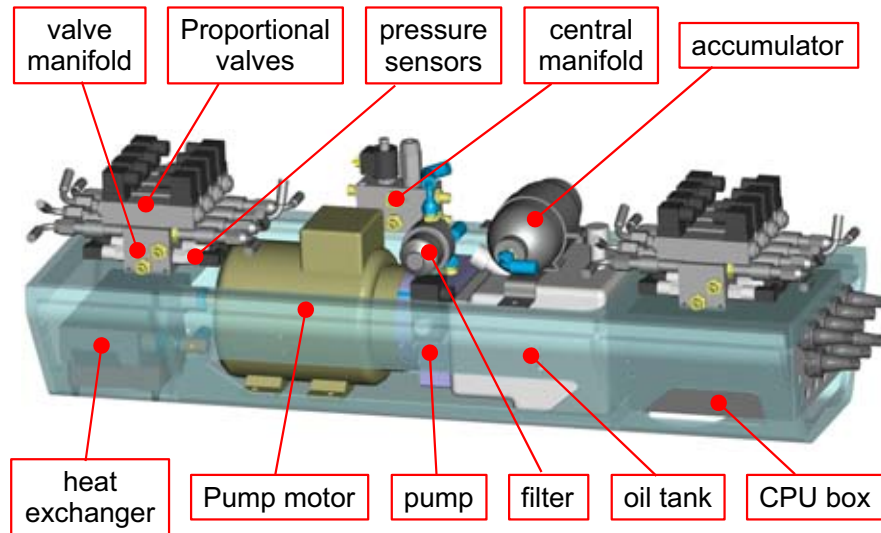


Figure 4.12: CAD model of robot torso with the components of the hydraulic system and the CPU box.

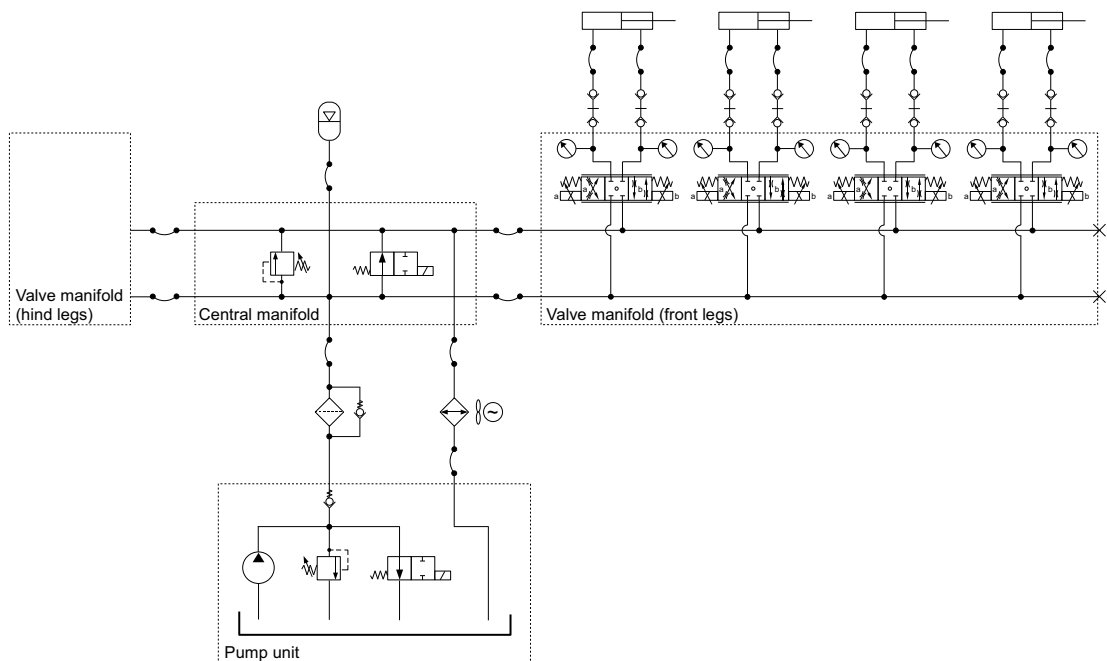


Figure 4.13: Schematic of complete hydraulic system. The *Valve manifold (hind legs)* in the left of the schematic is identical to the *Valve manifold (front legs)*.

4. ROBOT DESIGN AND COMPONENTS

mobile pump unit (*Brevini FPAB*) [Brevini, 2009] with an AC motor is used instead. The motor is a general performance aluminium 2-poles 400V AC motor with a nominal speed of 3000 rpm (*ABB M2AA-90S*) [ABB, 2008]. The complete unit with motor is shown in Fig. 4.14(b). A frequency inverter allows for an AC motor frequency variation of 50% around the nominal frequency of 50Hz, which is directly related to motor speed and therefore to pump flow. Together with an accumulator, this allows the testing of several locomotion gaits and robot velocities with varying flow requirements. The specifications of both pump units are listed in Table 4.6.



(a)



(b)

Figure 4.14: Pictures of the hydraulic pump units: (a) stationary laboratory pump unit (for robot stage 1) and (b) mobile onboard pump unit (for robot stage 2).

Property	laboratory pump unit	mobile pump unit
motor power	2.2kW	1.5kW
pump flow <i>l/min</i>	6 <i>l/min</i>	5 <i>l/min</i>
adjustable pressure range	2-21MPa	6-18MPa
tank size	50l	4l
hydraulic oil type	VG46	VG46

Table 4.6: List of specifications of the laboratory and mobile hydraulic pump units.

The mobile pump unit weighs 17kg (without oil) and consists of standard components. Its dimensions of 0.52m x 0.18m x 0.22m (LxWxH) are considered very compact

in the world of hydraulics. In the field of mobile robotics, however, where every centimetre and kilogram of system components has to be carefully looked at, this pump unit is rather big. Part of the future work is to reduce the size of all system components as much as possible. Especially for the 13kg-AC motor, there is a potential for a considerable reduction in size and weight.

4.3.2.3 Proportional Valve

Each hydraulic cylinder is controlled by a proportional valve. Fig. 4.15 shows a picture of the solenoid-operated proportional spool valve *Wandfluh WDPFA03-ACB-S5-G24* used to control the flow to the cylinder chambers of the hydraulic joints of HyQ [Wandfluh, 2007]. Table 4.7 lists the most important specifications of the valve.



Figure 4.15: Picture of the proportional spool valve *Wandfluh WDPFA03-ACB-S5-G24* with a metric ruler with centimetres.

We selected this valve, based on its relatively compact dimensions and weight. Furthermore, it has a low price, low internal leakage and an appropriate nominal flow rate and working pressure. As the datasheet does not include any information about the dynamic behaviour of the valve (e.g. frequency response), we performed several tests to assess the valve dynamics. The results are presented in chapter 5.

4. ROBOT DESIGN AND COMPONENTS

Property	Value
Designation	4/3-way proportional directional valve
Construction	Direct operated spool valve
Solenoids	Proportional
Nominal volume flow	5 l/min
Maximum volume flow	8 l/min
Maximum working pressure	31.5MPa
Weight	0.77kg
Dimensions (without electric connectors)	140mm x 30mm x 30mm (LxWxH)
Leakage volume flow	$\leq 25\text{cm}^3/\text{min}$ at 21MPa

Table 4.7: List of specifications of the hydraulic valve *Wandfluh WDPFA03-ACB-S5-G24*.

4.3.2.4 Hydraulic Cylinder

The selection of the hydraulic cylinders *Hoerbiger LB6-1610-0080-4M* has been described in the cylinder selection in section 3.4.1.2. Fig. 4.16 shows a picture of the cylinder.



Figure 4.16: Picture of hydraulic cylinder *Hoerbiger LB6-1610-0080-4M* with bore diameter of 16mm and a stroke length of 80mm.

Table 4.8 lists the most important specifications of the cylinder. Its dimensions are presented in Appendix E.3.

Property	Value
Bore diameter	16mm
Rod diameter	10mm
Stroke length	80mm
Piston area A_P	2.01cm^2
Piston ring area A_R	1.23cm^2
Maximum operating pressure	16MPa
Weight (empty)	0.67kg

Table 4.8: List of specifications of the hydraulic cylinder *Hoerbiger LB6-1610-0080-4M*

4.3.2.5 Accumulator, Filter and Heat Exchanger

The hydraulic system contains an accumulator, oil filter and heat exchanger. Fig. 4.17 shows pictures of these components. The accumulator is a *Fox serie 250* model based on compressed nitrogen gas with a hydraulic volume of 0.7l. The oil filter is an *OMT serie MHP220* with a filter degree of $10\mu\text{m}$. The heat exchanger is a *Sesino AP 178* with a performance up to $35\text{W}/^\circ\text{C}$ depending on flow rate.

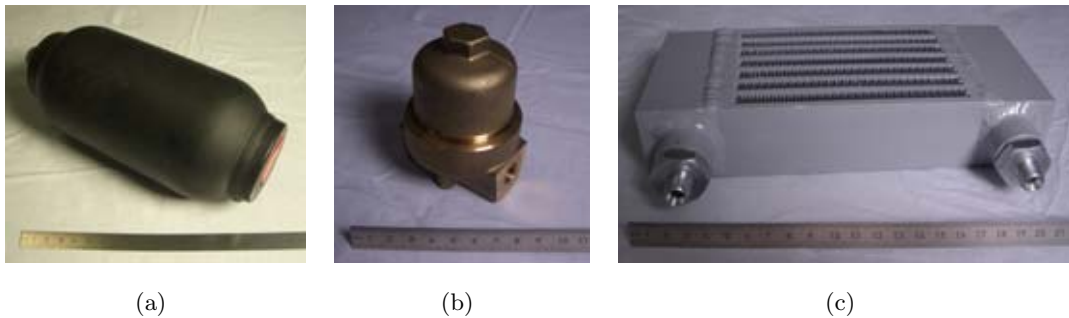


Figure 4.17: Pictures of hydraulic system components: (a) accumulator; (b) filter and (c) heat exchanger.

4.3.2.6 Manifolds, Fittings and Tubing

The hydraulic system contains two types of manifolds: one *central manifold* and two *valve manifolds*, see Fig. 4.18. The central manifold distributes the high pressure line

4. ROBOT DESIGN AND COMPONENTS

(**P**) and the low pressure line (**T**) to the two valve manifolds and the accumulator. It also contains a pressure relief valve and the electrically controlled venting valve (**EV02**).

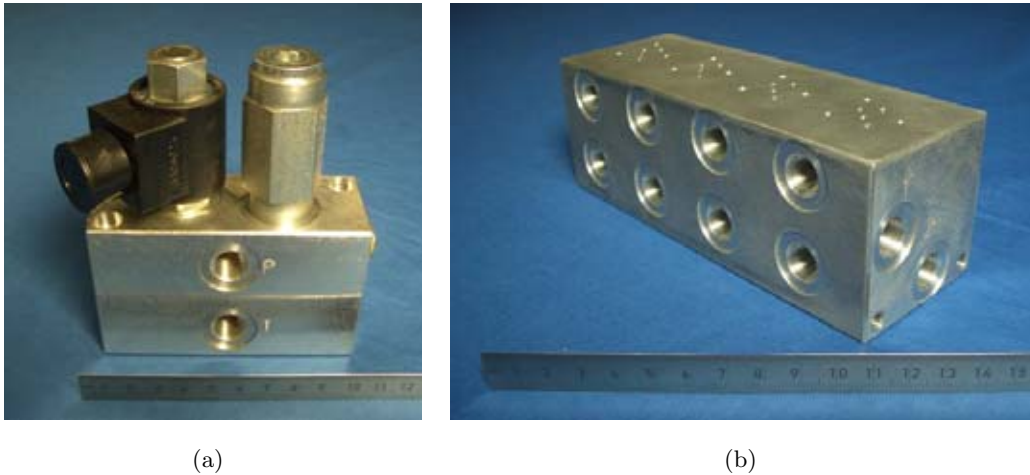


Figure 4.18: Picture hydraulic manifolds of the robot: **(a)** central manifold with venting valve (left) and pressure relief valve (right) and **(b)** valve manifold with space for 4 valves and 8 pressure sensors.

Each valve manifold hosts 4 valves. Each valve is internally connected to **P** and **T** and each of the two valve outputs **A** and **B** has two ports: one for a pressure sensor and one for the hose to the cylinder. The dimensions of the valve manifold are as much reduced as possible: 60mm x 60mm x 170mm (LxWxH) with a weight of 1.6kg. It is built in aluminium alloy instead of the more common steel to reduce its weight. This weight reduction is discussed in section 6.3.

To guarantee the modularity of the leg (specification **SP2.4** of section 3.1.2), the hoses between the valve manifold and the cylinders need to be easily connected and disconnected without spilling oil. This is especially important for machine prototypes. For these fittings I therefore decided to use hydraulic quick-release couplings (size 1/8inch) as shown in Fig. 4.19. Each part of the coupling contains a poppet valve that keeps the oil back if they are not connected. This reduces the spilled oil to a minimum during connection and disconnection phases. These couplings are heavier than standard connectors. The total weight of 16 quick-release couplings is 1.9kg. The obvious advantage

of these couplings, however, outweighs the increased weight.



Figure 4.19: Pictures of *Faster* quick release coupling, size 1/8inch, with a 2Euro coin (diameter 26mm) as reference.

All tubes on the robot are *Dunlop hiflex* flexible hoses. The hose sizes are either 1/4inch or 1/8inch. The connection between the valve manifold and the cylinders is made by thin and extremely flexible 1/8inch hoses. All other hoses are size 1/4inch. They do need to be very flexible since they are not connected between moving parts and a larger diameter means less pressure drop.

4.4 Sensory System

The robot is equipped with over 50 sensors: Relative and absolute encoders measure the position of each joint, pressure sensors the hydraulic oil pressure of each cylinder chamber, load cells the output force of the cylinders, an inertial measurement unit the accelerations of the robot torso and a few other sensors measuring the state of the hydraulic system. This section presents these sensors in detail.

4.4.1 Position

The position of each joint of the robot's legs is measured by two sensors: a relative (incremental) and an absolute encoder. While the relative encoder acquires the position with a high resolution and is therefore suitable for a smooth control, it cannot return

4. ROBOT DESIGN AND COMPONENTS

the absolute position of the joint. Therefore a low-resolution absolute encoder is used during the start-up phase of the robot to initialize the position of each joint. Note that electrically actuated robot joints usually have their encoders mounted directly on the fast rotating motor shaft (before the gear box), which results in a multiplication of the encoder resolution by the gear ratio.

Robot joints with only relative encoders are usually initialized by a so-called *homing* routine. The joint is either slowly moved until the *index* signal of the encoder is reached or it is blocked by its mechanical limit, whose positions are well-known. These approaches however are time-consuming and not convenient for heavy robots like HyQ, since they have to be lifted completely off the ground. Absolute encoders allow the robot to initialize its current joint configuration immediately after powering-up the CPU, without moving any joint.

4.4.1.1 Relative Encoder

The relative encoder is an *Avago AEDA3300 BE1*, a three-channel optical incremental encoder [Avago, 2006]. Channel A and B to measure position and rotating direction and the index channel I for joint homing. It features a high resolution of up to 80000 counts per revolution if connected to a electronic acquisition board supporting *quadrature decode*, which results in a resolution of 0.0045° per count. Fig. 4.20(a) shows a picture of the encoder. Its compact cylindrical dimensions are 17 mm in diameter and 24mm in length.

4.4.1.2 Absolute Encoder

The absolute encoder is an *austriamicrosystems AS5045*, a contactless magnetic rotary encoder chip [austriamicrosystems AG, 2006]. Its output signal is 12 Bit (4096 positions per revolution), which corresponds to a resolution of 0.0879° . Fig. 4.20(b) shows an image of the electronic chip with the magnet on top. As these encoders are only used for joint initialization, they are read one after the other via a serial communication bus. They are not used to close the fast position control loop, so communication speed is not important. This way the number of data acquisition boards can be reduced, refer to section 4.5.2.2.

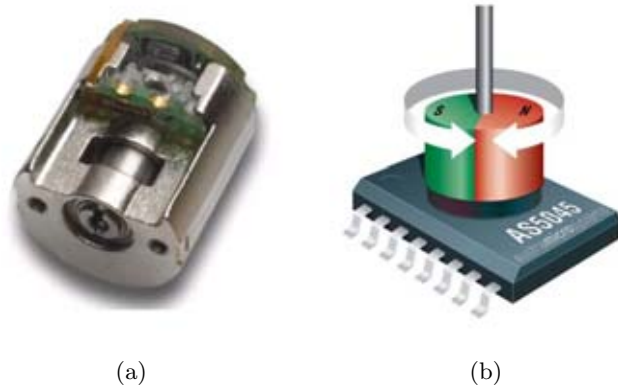


Figure 4.20: Picture of (a) relative encoder *Avago AEDA3300 BE1* [Avago, 2006] and (b) model of absolute encoder *austriamicrosystems AS5045* [austriamicrosystems AG, 2006].

4.4.2 Pressure

The hydraulic pressure sensor (transducer) is a *Trafag 8251-74-2517*, a piezoresistive strain gauge (thin film) sensor [Trafag, 2008]. It measures relative pressures of up to 25MPa and creates an output signal of 0-10V. Its accuracy is $\pm 0.5\%$ of the full scale. Fig. 4.21(a) shows a picture of the sensor.

4.4.3 Force

The force acting on the cylinder rod is measured by a *Burster 8417*, a tension and compression load cell based on strain gauges [Burster GmbH, 2009]. The force range is 0-5kN and its accuracy is $\pm 0.5\%$ of the full scale. Its cylindrical body is 20mm in diameter and 12mm in length. Fig. 4.21(b) shows a picture of the load cell.

4.4.4 Inertial Measurement Unit

The inertial measurement unit (IMU) is a *HiBot Attitude Sensor*, featuring three modules: A 3-axis accelerometer, a 3 axis gyroscope sensor and a compass module [HiBot Corp., 2009]. Fig. 4.21(c) shows a picture of the sensor board. Its compact

4. ROBOT DESIGN AND COMPONENTS

dimensions of 50mm x 25mm x 8mm (LxWxH), analogue voltage outputs and configurable acceleration range make it especially suitable for HyQ.

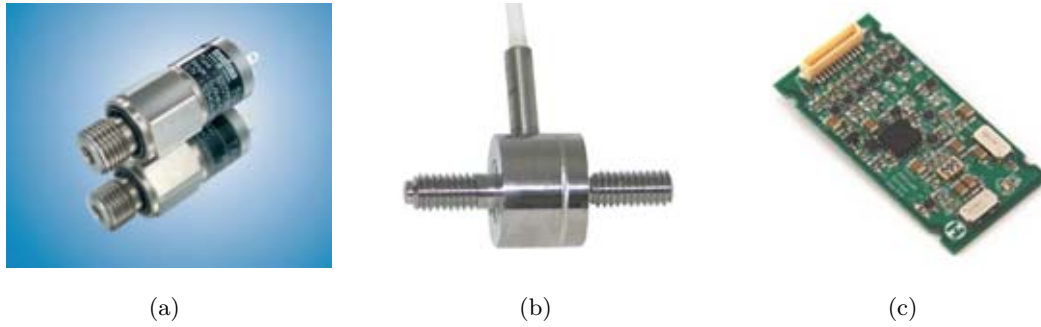


Figure 4.21: Picture of (a) pressure sensor *Trafag 8251-74-2517* [Trafag, 2008], (b) load cell *Burster 8417* [Burster GmbH, 2009] and (c) inertial measurement unit *HiBot Attitude Sensor* [HiBot Corp., 2009].

4.4.5 Summary

Table 4.9 summarizes the specifications of the sensors.

Sensor	Model	Input Range	A/D	Resolution	Output Range
Absolute Encoder	AMS5045	360°	D	0.0879°	-
Relative Encoder	AEDA3300	360°	D	0.0045°	-
Pressure	Trafag8251	0-25MPa	A	-	0-10V
Force	Burster8417	0-5 kN	A	-	0-10V
IMU	HiBot AS	1.5-6g 300°/s (Roll, Pitch) 100°/s (Yaw)	A	-	0-3.3V

Table 4.9: Summary of the sensors used on HyQ with specifications (A/D: analogue or digital output).

4.5 Robot Control System

4.5.1 System Overview

The control system architecture of HyQ is shown in Fig. 4.22. It can roughly be divided into three main parts: the *CPU box*, the components of one *Valve Unit for 1 Leg* and one *Leg Unit*. The latter two parts are connected to one multifunction I/O board (Sensoray board 1-4) and exist for each leg, but are not repeated in the figure. The *CPU box* shown in the left side of the figure is the central processing unit of the robot. It communicates with one or several external PCs via Ethernet bus, samples sensor signals, calculates and generates the low-level control signals for the actuators, communicates with the motor controller via CAN bus, monitors system states and logs data.

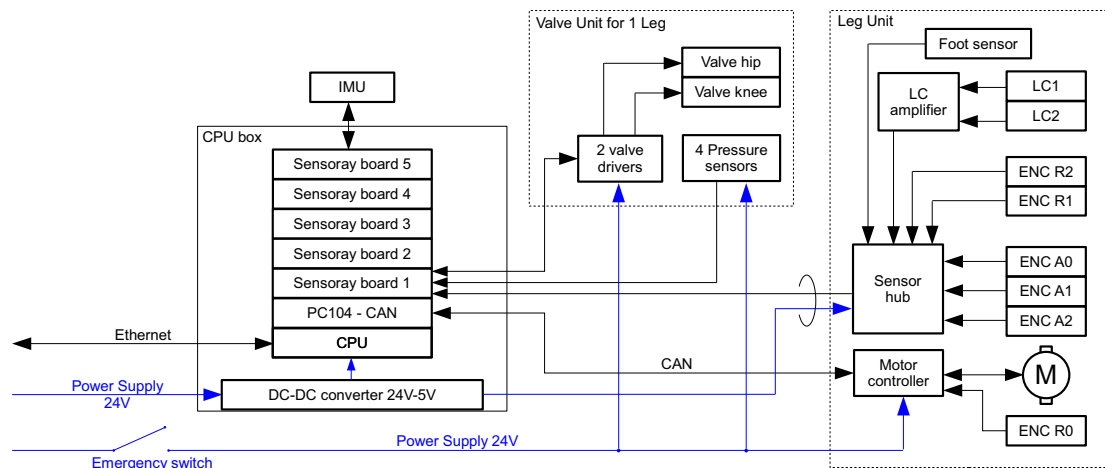


Figure 4.22: Control system architecture of HyQ. Each *Sensoray* board is connected to one *Valve Unit for 1 Leg* and one *Leg Unit*. Explanation of abbreviations: **LC** load cell, **ENC R** relative encoder and **ENC A** absolute encoder.

The *Valve Unit for 1 Leg* consists of two valves, 4 pressure sensors and 2 valve driver boards, which are either part of the front legs manifold or the hind legs manifold located on the robot torso. (As shown in Fig. 4.12 each manifold serves two legs.) The pressure sensors and valve driver boards are connected to their *Sensoray* board (one per leg), which samples the sensor signals at 1kHz, communicates to the CPU board

4. ROBOT DESIGN AND COMPONENTS

and finally creates a PWM¹ signal for controlling the valves.

Each of the four *Leg Units* consists of a sensor hub board, relative and absolute encoders (*ENC R* and *ENC A*), load cells (*LC*) with amplifier board, a foot sensor, a motor controller and a motor (*M*). The hub board is connected to its Sensoray board with a single cable containing all sensor signal and power supply wires. The motor controller communicates via CAN bus with a PC104-CAN board that is connected to the CPU board. The motor controller is directly connected to its corresponding relative encoder. Note that unlike the valve control loop, the motor control output is calculated and generated by the motor controller, which receives trajectory set-points from the CPU board.

An external power supply of 24V leads both to the valve and motor controllers and the pressure sensors. An emergency switch triggered by several STOP buttons immediately disconnects the power from the valves and the motors.

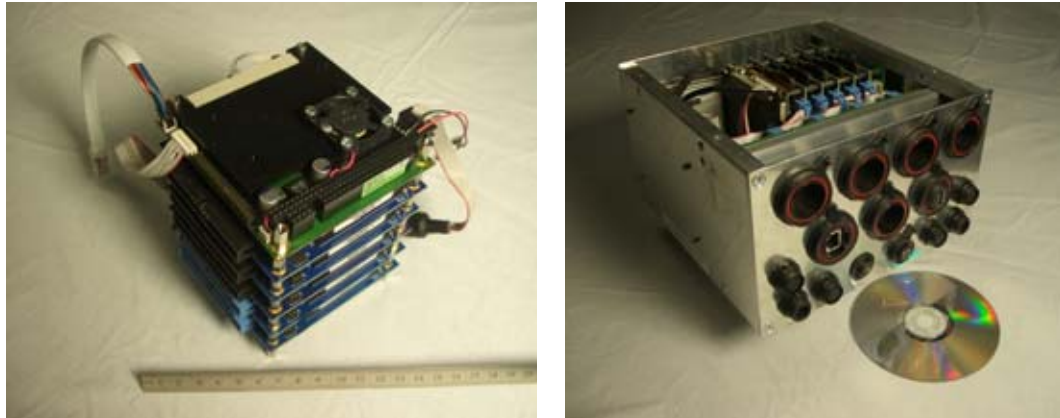
4.5.2 CPU Box

The central processing unit (CPU) of the robot is located in a shock absorbing box and contains the following components:

- 1 Pentium CPU board
- 5 Multifunction I/O boards
- 1 PC104 to CAN communication board
- 1 DC-DC converter board

The following three sections present these boards, their specifications and usage on the HyQ robot. The cable connectors to the CPU box are built in a strong plastic and can be screwed tightly to the box. This guarantees a reliable electric connection despite vibrations and impacts on the robot body.

¹PWM: Pulse Width Modulated



(a)

(b)

Figure 4.23: Picture of the on-board computer of HyQ: **(a)** PC-104 stack with CPU board on top and 5 data acquisition boards below and **(b)** shock absorbing computer box with integrated DC-DC voltage converter and fan. The picture shows the front panel with various electric connectors.

4.5.2.1 Pentium CPU Board

The compact CPU board of the onboard computer features a high-performance and low power Pentium-M processor of *Intel*. It is a *Kontron MOPSPM104* board with a PC104 form factor and PC104 ISA bus, suitable for the data acquisition boards. MOPS stands for *Minimized Open PC System*. Fig. 4.24(a) shows a picture of the board [Kontron, 2008] and Table 4.10 lists its most important specifications.

The board runs a real-time patched version of Linux, as described in section 4.6. The operating system and user programs can either be stored on a common 3.5inch hard disc (offboard software testing) or on a compact flash memory (on robot). The selection of the board is not only based on its small dimensions, strong processing power and single power supply voltage, but mainly by the PC104 interface of the data acquisition board presented next.

4.5.2.2 Multifunction I/O Board

The requirements for a data acquisition and output board for HyQ are the following:

4. ROBOT DESIGN AND COMPONENTS

Property	Value
form factor	PC104
CPU	Intel Pentium-M
CPU clock	1.4 GHz
internal bus	33 MHz PCI bus
external bus	ISA and PCI
RAM	up to 1GB
interfaces	USB, Ethernet, 2 serial ports, 1 parallel port, IDE interface, VGA, PS/2 mouse and keyboard
cooler	passive heat dissipation and CPU fan
power supply	5V
watchdog timer	available

Table 4.10: Summary of the most important specifications of the Pentium CPU board *Kontron MOPSPM104* [Kontron, 2008].

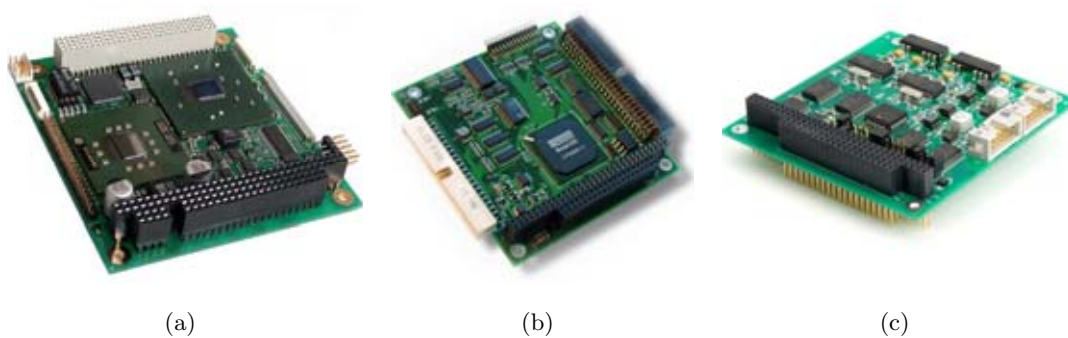


Figure 4.24: Picture of the three PC104 board types used in the CPU box: (a) Pentium CPU board *Kontron MOPSPM104* [Kontron, 2008]; (b) multifunction I/O board *Sensoray 526* [Sensoray, 2002] and (c) *Peak* dual channel PC104-CAN board [Peak, 2008].

- analogue to digital conversion of multiple channels
- encoder pulse counting of multiple channels
- PWM output signal generator for multiple channels
- fast communication with CPU board

The *Sensoray 526 multifunctional I/O* board (Fig. 4.24(b)) generally meets these requirements, however it has only a limited number of 8 analogue inputs and 4 counters. The latter can either be used as encoder pulse counters or PWM output signal generators. Table 4.11 lists the specifications of the board.

Property	Value
A/D converter	8-channel (multiplexed) differential 16-bit (± 10 V)
D/A converter	4-channel 16-bit (± 10 V)
digital I/O	8 channels (capable of generating interrupts)
counters	4 24-bit counters (either encoder or PWM)
power supply	5V
watchdog	available

Table 4.11: Summary of the specifications of the multifunction I/O board *Sensoray 526* [Sensoray, 2002].

There are five Sensoray boards inside the CPU box. Sensoray board 1-4 are connected to one leg each. Table 4.12 lists the port usage of these four boards. Sensoray board 5 is mainly responsible for sensors not related to the legs: it reads the data of the IMU and supply pressure sensor (8 analogue inputs) and switches the multiplexers of the pressure/current signals from the pressure sensors and valve driver boards. These multiplexers are necessary due to the limited number of analogue inputs on the Sensoray board.

Port	Usage
Analogue Inputs	4 multiplexed channels of either pressure or current sensors 2 for the load cells 1 for the foot sensor
Digital I/O	2out, 1in: serial communication with absolute encoders 2out: multiplexer selection for solenoid A or B
Counters	2in: relative encoders 2out: PWM signals for the 2 valves

Table 4.12: Connection list of Sensoray board 1-4, one per leg.

4. ROBOT DESIGN AND COMPONENTS

4.5.2.3 PC104-CAN Board and DC-DC Converter Board

Besides the CPU and multifunction I/O boards, the PC104 stack contains also a PC104-to-CAN communication board. The *Peak PCAN-PC/104 dual channel* board shown in Fig. 4.24(c) features two independent CAN networks channels. Each CAN network communicates with two motor controllers. This way, the load on the bus is spread, which leads to shorter latency times and higher data bandwidth.

The DC-DC converter board is a custom designed board of our laboratory. It converts 24V to 2 separate outputs of 5V. The first output is the power supply of the PC104 boards and the second one supplies the sensors with 5V. This separation guarantees a more stable power supply for the sensors and therefore cleaner sensor output signals with less noise.

4.5.3 Valve Driver Board and Motor Controller

The valve driver boards *M30* are custom designed boards of our laboratory. Each board controls the 2 solenoids of one valve. The core elements of the board are two *Burr Brown DRV102 PWM solenoid/valve driver* ICs ¹. It features a wide supply voltage range from 8-60V with a high output of up to 2.7A [Burr Brown, 1999]. The board has one multiplexed low-power PWM input port, a digital port to select the active solenoid and two analogue output signals proportional to the solenoid currents.

The motor controllers are *ELMO Whistle Solo* boards, Fig. 4.25. It delivers up to 1600W of continuous power or 3200W of peak power in a very compact package of 58.25 x 28.5 x 46.5 mm (LxWxH). Its power supply voltage is 12-95V and it can control different types of electric motors including DC brushless motors. It either communicates via serial (RS232) or a CAN bus (CANopen) [ELMO Motion Control, 2009].

4.5.4 Sensor Hub Board

The sensor hub boards are custom designed by our laboratory. Each leg has one hub board mounted on the upper leg segment between *hip f/e* and *knee f/e* joint. The board

¹IC: Integrated Circuit



Figure 4.25: Picture of the *ELMO Whistle Solo* motor controller board [ELMO Motion Control, 2009].

gathers all sensor wires of the leg sensors at one central point on the leg. One single cable brings all wires to the CPU box. This increases the reliability of the system and reduces its complexity. All cables between the sensors and the hub board have connectors on both ends for easy maintenance, component replacement and debugging. This meets specifications **SP2.1** and **SP2.4** of section 3.1.2.

4.6 Real-Time Control Software

The CPU board runs a Linux kernel patched with real-time *Xenomai*. The robot control software environment is *SL*, named after its original purpose *Simulation Laboratory*. Today, SL is both a general robot control and rigid body dynamics simulation framework. It is developed by Stefan Schaal and collaborators at the Computation Learning Motor Control Lab at the University of Southern California (USC). It has a special aim for hard real time control of robots. With its roots in the early days of MIT and CMU Leg Labs, more than 15 years of development are behind SL and its core has been deployed on more than a dozen platforms including very powerful and possibly dangerous hydraulic robots, where accurate and reliable control is of utmost importance.

It features all the commonly used elements in modern robotic control, such as forward and inverse kinematics and dynamics, position and inverse dynamics controllers, data logging and visualization. It contains modern control algorithms such as floating

4. ROBOT DESIGN AND COMPONENTS

base inverse dynamics control. SL is divided into three main software components: 1) the generic code that is shared by the actual robot and the simulation, 2) the robot specific code, and 3) the simulation specific code. [Schaal, 2006]

A new SL simulation environment has recently been implemented for HyQ in collaboration with the Computation Learning Motor Control Lab at USC. Fig. 4.26 shows a screenshot of SL with the OpenGL visualization of the robot model on the left and the user consoles on the right of the screen.

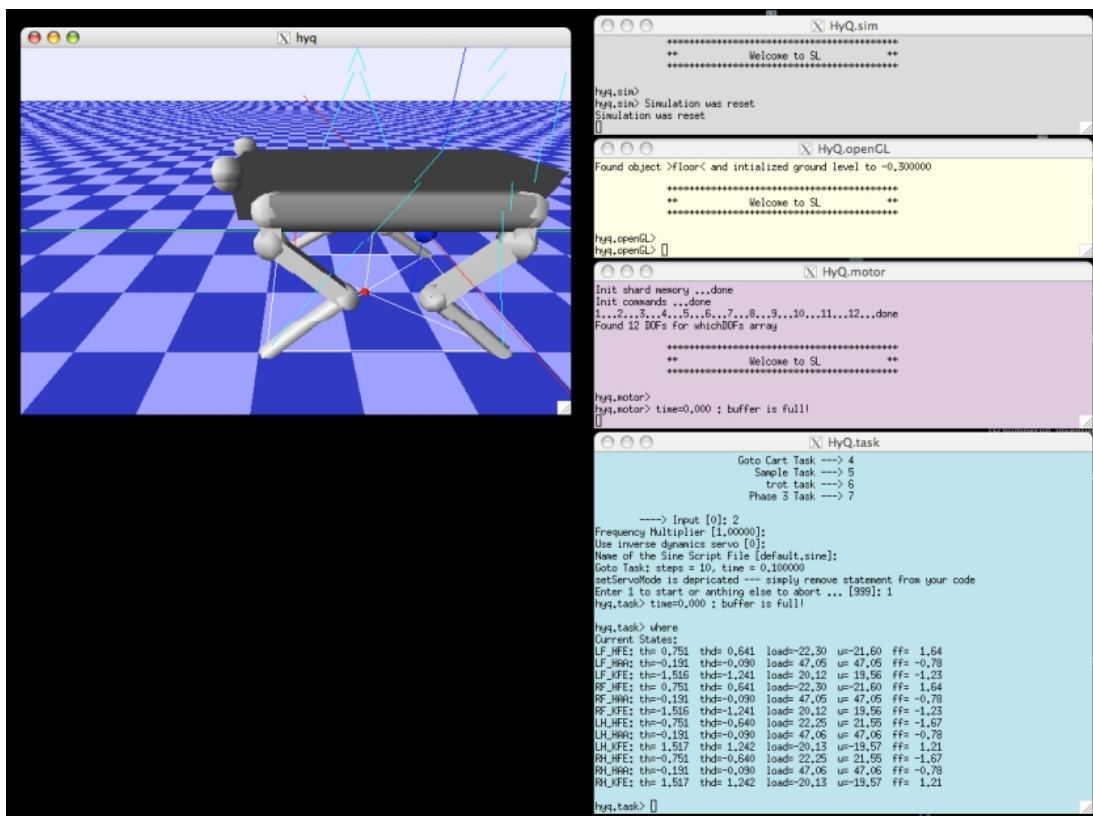


Figure 4.26: Screen shot of SL software environment with the OpenGL visualization of the robot model on the left and the user consoles on the right.

4.7 Conclusions

This chapter presented the design of the electrically and hydraulically actuated quadruped robot HyQ with 12 active DOF. The robot with fully stretched legs has the following dimension: 1.0m x 0.5m x 0.98m (LxWxH) and weighs 48kg with external hydraulic power supply and 90kg with complete hydraulic system onboard. After a short system overview and robot specifications, I discussed the mechanical structure of the robot torso and legs in detail, including the description of the aluminium alloy and stainless steel of the mechanical parts. It followed the explanation of the hydraulic and electric actuation systems with schematics, component descriptions and specifications.

Next, I presented all different sensor types used on the robot (encoders, pressure transducers, load cells and IMU), followed by the description of the robot control system. This included a detailed explanation of the electronic boards, their specifications and how they are connected with each other. The chapter ends with a short presentation of the real-time operating system and the robot control software *SL*, which incorporates also a rigid body dynamics simulator.

4. ROBOT DESIGN AND COMPONENTS

5

Experimental Studies

This chapter presents the experimental studies that I have conducted during the design process of the robot. These studies are centred on the leg prototype (*Leg VI*) presented earlier in section 3.5 and its hydraulic actuation system. Since the complete quadruped robot was not yet operational when I was writing my dissertation, no experimental results are included in this dissertation. Planned experiments are described in the future work section 7.2.

In a first study, I evaluated the performance of the selected hydraulic actuation system, focussing on the valve first and then on the valve in combination with the cylinder. Further studies involved the leg prototype: first fixed to the table with freely moving upper and lower leg segments; later fixed to a vertical slider with contacts between foot and ground.

5.1 Hydraulic Valve Frequency Response

The first study evaluated the dynamic performance of the valve, since this information is not stated in the data sheet. First of all, we are interested in obtaining the frequency response of the valve. Usually spool position is compared with input voltage. However, we cannot measure the spool position inside the valve, so we will analyse the valve input voltage in relation to the output pressure. Since for this experiment the cylinder is not needed and only the valve has to be tested, the valve output ports A and B have

5. EXPERIMENTAL STUDIES

been closed as shown in the hydraulic schematic in Fig. 5.1.

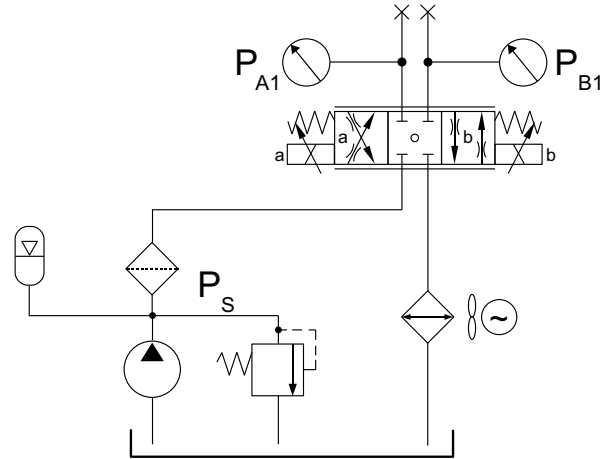


Figure 5.1: Hydraulic schematic of the valve test experiments. The valve ports A and B are closed to evaluate the performance of the valve only.

The frequency response of the valve was assessed as follows:

1. Create sinusoidal input voltage (with constant frequency) for the valve with positive values leading to solenoid A and negative values to solenoid B. This way the valve spool is moved constantly from one side to the other.
2. Sample the signals of solenoid input voltage, solenoid currents, pressures of valve port A and B (Sample frequency 1kHz)
3. Remove DC part of the signals, process them with fast Fourier transform and get the magnitude and phase of the principle frequency
4. Repeat above steps for a desired frequency range, e.g. 1-200Hz
5. Create Bode magnitude and phase plot with the above values of step 3. For example for the Pressure/Voltage (P/V) transfer function divide the magnitude of the pressure by the magnitude of the voltage (for Bode magnitude plot) and subtract the phase of the voltage from the phase of the pressure (P-V) for the Bode phase plot.

5.2 Hydraulic Valve+Cylinder Frequency Response

Fig. 5.2 shows the resulting Bode plot for both the output pressure to solenoid input voltage (P/V) and output pressure to solenoid input current (P/I) transfer function. The supply pressure was set to 16MPa. The resulted bandwidth (cut-off frequency) is approximately 35Hz. Additional results showed that the bandwidth of the solenoid (current to input voltage) is above 100Hz.

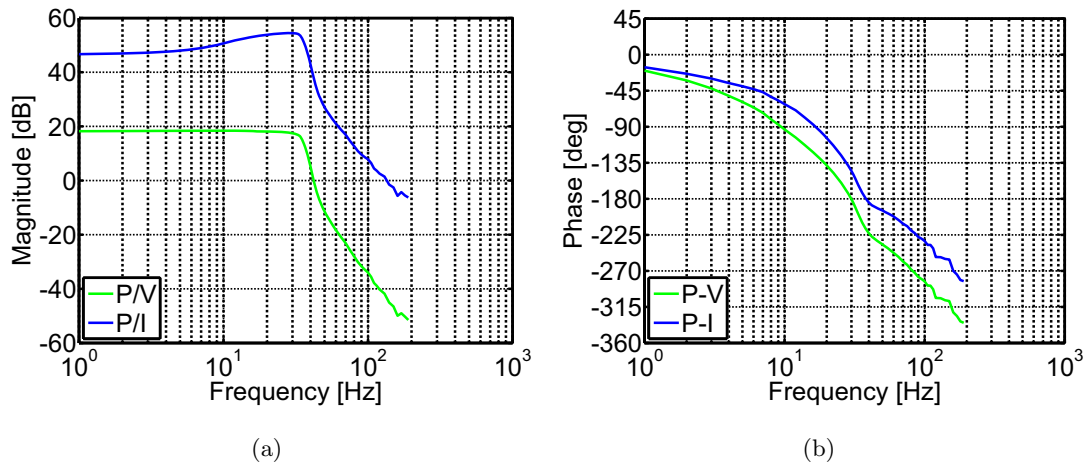


Figure 5.2: Bode plot of valve frequency response for Pressure/Voltage (P/V) and Pressure/Current (P/I) transfer function: (a) magnitude plot and (b) phase plot.

The same frequency response tests have been repeated for different supply pressures and different input voltage levels. A comparison of the bode plots showed that the variation of these conditions does not considerably influence the resulting bandwidth.

5.2 Hydraulic Valve+Cylinder Frequency Response

To evaluate the performance of the cylinder in combination with the valve, an actuator test-bench has been designed and constructed. Since the cylinder can generate forces exceeding 3000N, the test bench had to be robust and safe. Fig. 5.3 shows a picture of the test bench including the cylinder. The top of the picture shows the cover part of the setup with a linear potentiometer to measure the cylinder extension. The model of the potentiometer is *Burster 8710* with a range of 0.1m.

5. EXPERIMENTAL STUDIES



Figure 5.3: Picture of the hydraulic cylinder test bench, showing the base with cylinder in the bottom of the picture and the top part with linear potentiometer in the top of the picture.

The setup can be used in two different configurations: For measurements of the cylinder displacement, the cylinder is fixed only on one side with the rod free to move. For measurement of the cylinder output force, both cylinder ends are fixed to the structure and a load cell is mounted between the rod and the rod end. The latter configuration has been used for the frequency response described next.

Fig. 5.4 shows the hydraulic schematic of the experiment. The cylinder is fixed inside the test bench with half extended rod, indicated in blue in the figure. The connection between the valve and the cylinder ports are two flexible tubes with a length of 0.8m and an internal diameter of 4.8mm.

The same test procedure as explained for the valve frequency response test (section 5.1) has been used to obtain the Bode plot shown in Fig. 5.5. The figure shows the plot of the output pressure to solenoid input voltage (P/V) transfer function measure for three different supply pressures: 5MPa, 10MPa and 16MPa. The measured bandwidth (cut-off frequency) was 20Hz, 18Hz and 16Hz, respectively.

The resulting bandwidth of the hydraulic valve with attached cylinder is roughly half of the bandwidth of the valve alone. The hydraulic tubes and the cylinder cham-

5.2 Hydraulic Valve+Cylinder Frequency Response

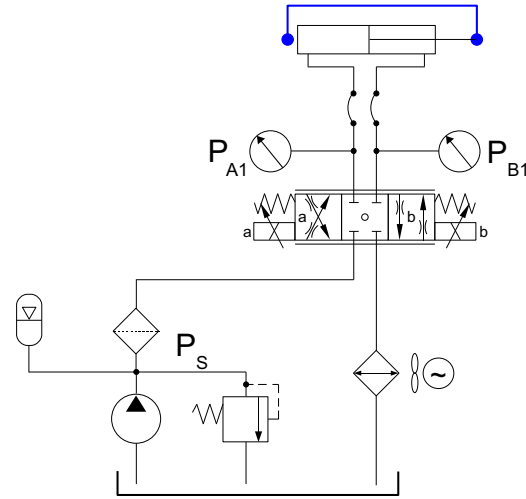


Figure 5.4: Hydraulic schematic of the valve+cylinder test experiments. The cylinder is rigidly fixed inside the actuator test-bench with half extended rod (indicated in blue).

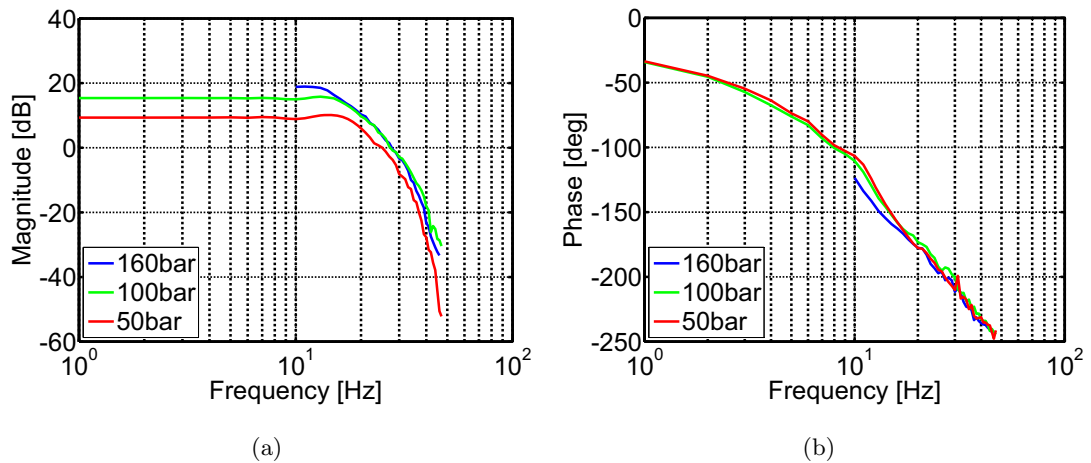


Figure 5.5: Bode plot of valve+cylinder frequency response for Pressure/Voltage for three different supply pressures (5MPa, 10MPa and 16MPa): (a) magnitude plot and (b) phase plot.

ber are an additional volume for the oil after the valve. Since the oil is considered compressible under dynamic conditions (as this frequency response test), the increased volume acts like an electric capacitance and reduces the bandwidth. Moreover, the expansion of the hydraulic hoses adds to this effect.

5. EXPERIMENTAL STUDIES

It is not yet clear if the final bandwidth of approximately 18Hz is enough to achieve the desired overall dynamic performance of the robot. However, we expect that the disturbances created by the position tracking error during the flight phase, can be handled by robust locomotion algorithms. Corrective action during the stance phase should lead to the desired locomotion performance of the robot.

5.3 Hydraulic Cylinder Speed Test

The next study was to measure the maximum speed of the cylinder rod without load. We used the cylinder test bench of Fig. 5.3 with the cylinder fixed on one side and the rod free to move (no-load condition). The cylinder position was measured with a linear potentiometer. The maximum speed was assessed as follows:

1. Start with the cylinder in an almost completely retracted position.
2. Create a step signal for the valve solenoid voltage to open the valve as fast as possible.
3. While the cylinder rod accelerates and extends, sample the position (Sample frequency 1kHz)
4. Close valve before the cylinder rod reaches maximum extension.
5. Differentiate the position signal to obtain the cylinder velocity profile.

Fig. 5.6 shows the test results showing the cylinder position, cylinder speed, valve signal in percentage of nominal valve voltage and supply pressure (set to 16MPa). The experiment was performed with and without the hydraulic accumulator to analyse the drop in supply pressure.

The experiment with the accumulator resulted in an average maximum cylinder rod speed of 1.1m/s under no-load conditions. The result shows that explosive motions with this kind of actuator are possible. This property is especially important for legged robots since it enables a fast retracting leg motion during the flight phase of running and therefore allows good clearance between the foot and the ground to avoid stumbling.

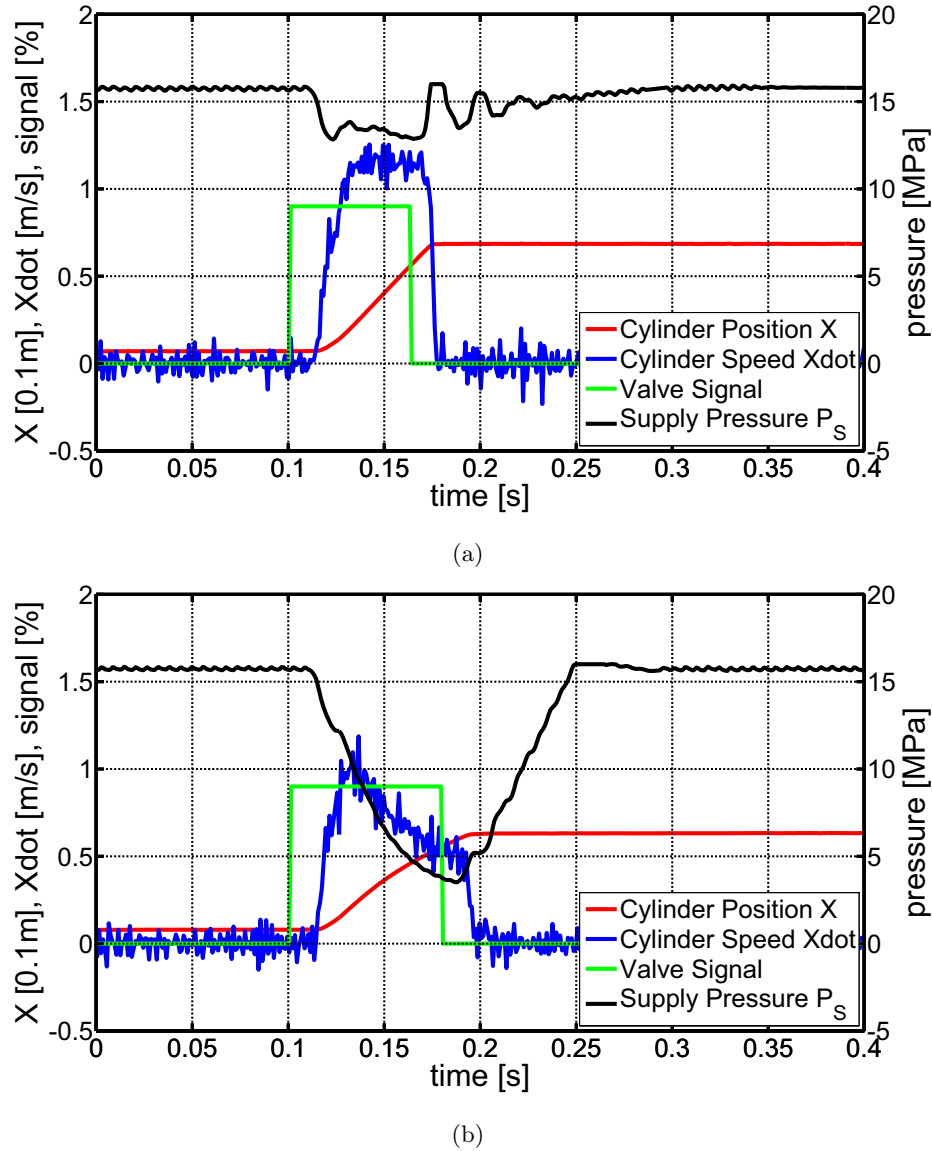


Figure 5.6: Plot of cylinder speed experiments for a supply pressure of 16MPa under no-load conditions: (a) with accumulator and (b) without accumulator. Note that the valve signal is shown as a percentage of the nominal voltage of the valve.

Based on the resulting plot, it would take less than 100ms for the rod to move over the complete stroke length of 80mm (no-load conditions). The estimated cylinder force based on pressure measurements is 1200N during the maximum cylinder speed, which results in a peak output power of 1320W.

5. EXPERIMENTAL STUDIES

The comparison between the tests with and without the accumulator clearly shows the contribution of the accumulator to keep the pressure high and to provide hydraulic flow in case of peak demand.

5.4 Leg Prototype Trajectory Following

The next series of experiments have been performed with the 2-DOF leg prototype (*Leg V1*) introduced in section 3.5. For first tests, I attached the prototype leg to a vertical slider as shown in the pictures on Fig. 5.7(a) and blocked its motion on the slider high enough that the foot never touched the ground. In this configuration, I performed first system tests and started tuning the gains of the implemented PID¹ position controller.

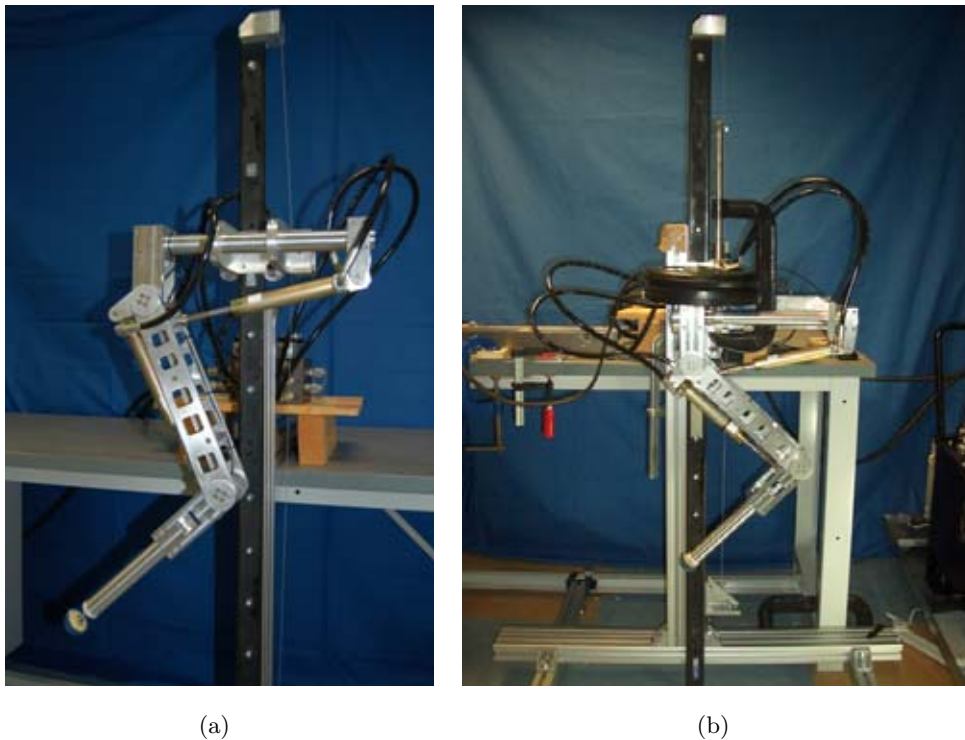


Figure 5.7: Pictures of leg prototype *Leg V1* on vertical slider: **(a)** leg fixed at a certain height of the slider and **(b)** leg on slider with 10kg additional weight clamped to it.

¹Proportional, Integral and Derivative (PID)

Fig. 5.8 shows the schematic of the hydraulic system of the leg prototype with the two cylinders, valves and pump unit.

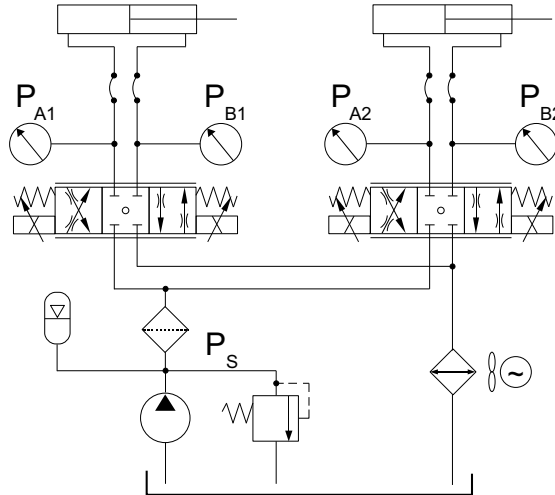


Figure 5.8: Hydraulic schematic of the 2-DOF prototype leg showing two double acting cylinders.

To test the tracking performance I implemented the so-called composite cycloid foot trajectory [Sakakibara et al., 1990] that results in a bio-inspired walking trajectory for the foot position with smooth joint trajectories for both velocity and acceleration. Fig. 5.9 shows the angle vs. time plot for the *hip f/e* and *knee f/e* joint.

The tracking performance of the two hydraulic joints in the air is quite poor. The implemented PID position controller is not optimal for tracking. Especially the hip joint suffers from the coupling between the two joints. Additionally, the leg inertia (the combination of lower and upper leg), that is acting on the hip joint, depends on the knee joint position. Research to find a more suitable controller for the hydraulic joints is ongoing. My colleagues evaluated several options from gain scheduling to feedback linearisation [Cunha et al., 2009, Focchi et al., 2010].

We believe however that the position tracking performance during the flight phase is not crucial for the overall locomotion behaviour of the robot, as mentioned above in section 5.2.

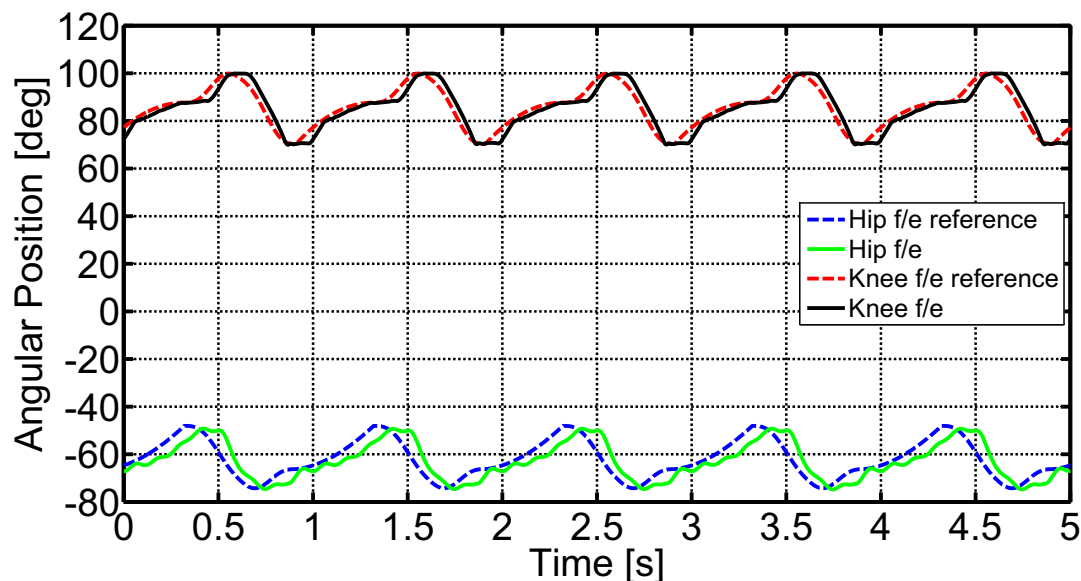


Figure 5.9: Plot of angle vs. time for the *hip f/e* and *knee f/e* joint for a bio-inspired walking trajectory.

5.5 Leg Impact Studies

A series of important tests involve the experimental testing of the mechanical structure in combination with the hydraulic actuators. As mentioned in section 2.2.3 hydraulic actuators are very well suited for dynamic legged robots, because the compressibility of the oil and the expanding tubes naturally add damping to the system. It therefore protects the mechanical structure from dangerous impact force peaks.

For these experiments the leg prototype was free to move up and down on the vertical slider. To measure the involved forces and pressures in the cylinder chamber, I dropped the leg from different initial heights (measured from ground to the lowest point of the foot). The foot was coated by a 4mm layer of visco-elastic rubber for initial impact damping, but no spring in the ankle joint was present. The tests have been performed with different leg weights, to increase the impact energy. The weight of the leg is 4.4kg and the slider carriage 3.1kg. As shown in Fig. 5.7(b) one, two or three 5kg-weights have been clamped to the slider carriage at the top of the leg. The clamp weighs 2.5kg.

The first series of experiments were performed with actively controlled joint position: The two joints were PID controlled at a reference of $\theta_1 = -45^\circ$ and $\theta_2 = 90^\circ$.

Fig. 5.10 shows the summary of the experiments. The time plots show the slider height (from the ground) on the left and the time plot of the force of the knee cylinder on the right. The force has been measured with the load cell and calculated based on the chamber pressure sensors according to (2.7) with the piston areas listed in Table 4.8.

A second series of impact experiments have been performed with closed valves during impact to assess the passive leg behaviour. The position control was turned off just before impact. As before the joint angles were $\theta_1 = -45^\circ$ and $\theta_2 = 90^\circ$. This time the leg was always dropped from a height of 0.15m, but with varying leg weights of 10kg, 15kg, 20kg and 25kg.

The top of Fig. 5.11(a) shows the time plot of the vertical position of the leg on the slider. The dashed horizontal line indicates the height where the foot hits the ground for the first time. The bottom part of the plot shows the vertical ground reaction forces, calculated with (3.18) and (C.4) based on measured joint position and cylinder force. These plots show clearly how the compliance (both stiffness and damping) in the hydraulic system damps the impact peaks and even makes the leg bounce off the floor like an elastic ball. The ground force profile shows this elastic contact.

Next, we are considering the resulting force in the knee cylinder based on the load cell (solid lines) and cylinder chamber pressures (dashed line) as shown in Fig. 5.11(b). The plot shows that the load cell saturates at around 3.5kN. The leg prototype *Leg V1* has different load cells with a lower range (*Honeywell Sensotec Model 11*) than the final leg. For lower values the force profiles are almost identical, but for static measurements the curves differ due to the neglected static cylinder friction. We conclude that the pressure sensor data is sufficient to accurately estimate the cylinder force during dynamic motions. Whether the pressure sensor data will permit smooth force control (and as a consequence the load cell can be eliminated) is part of future work.

5. EXPERIMENTAL STUDIES

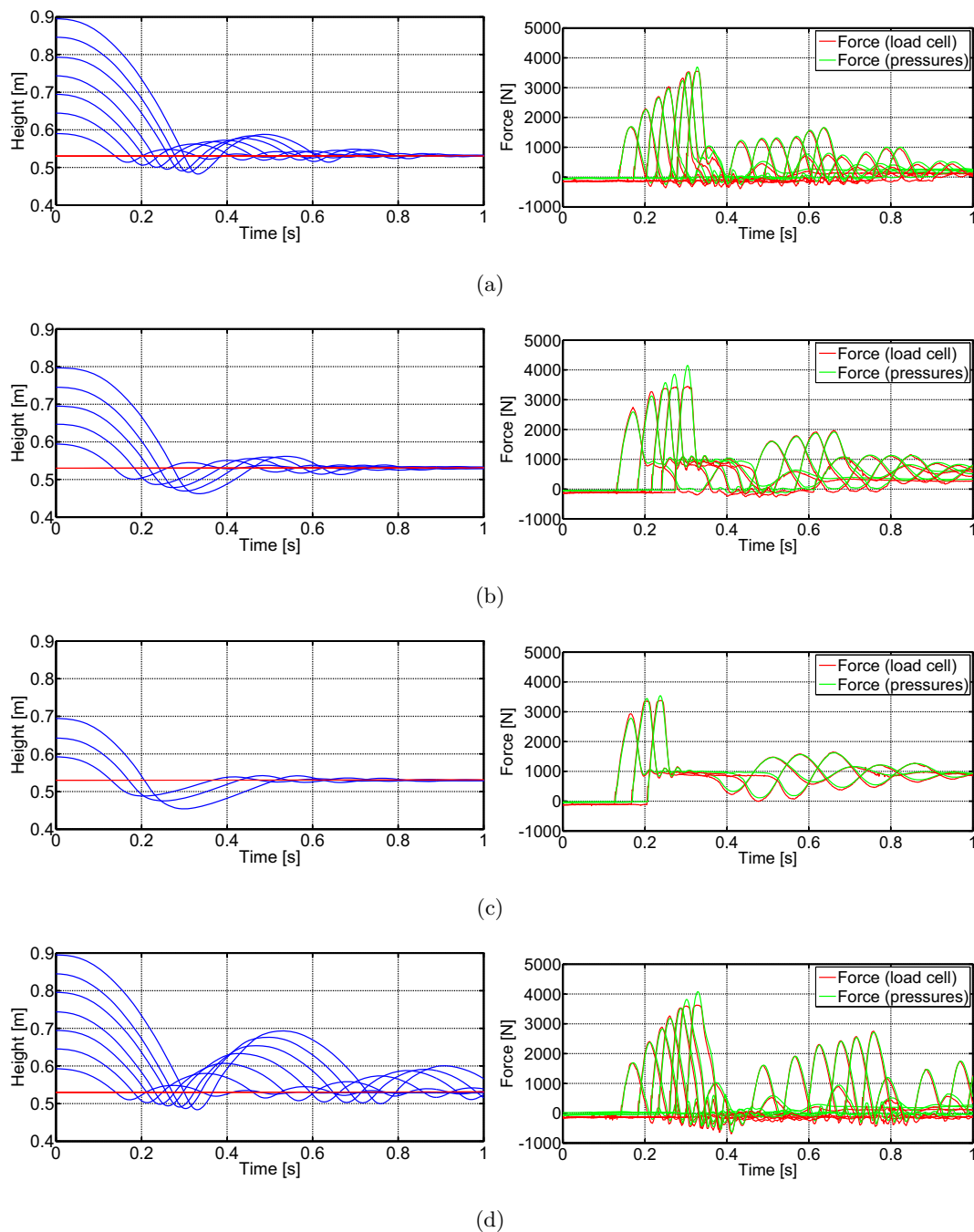
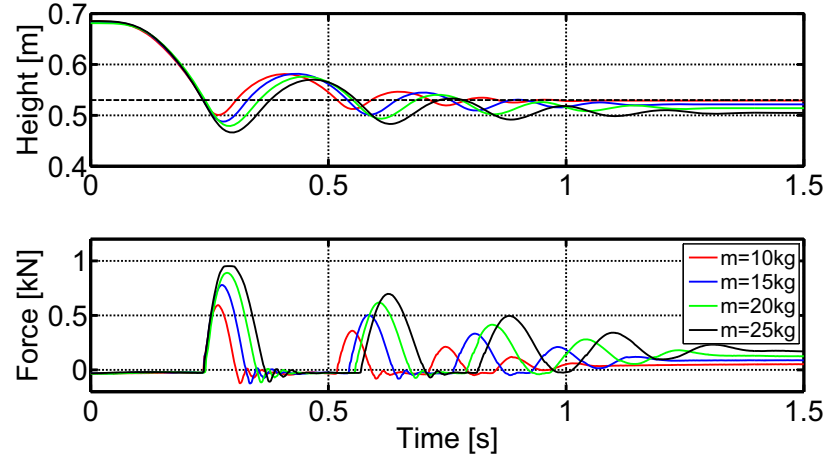
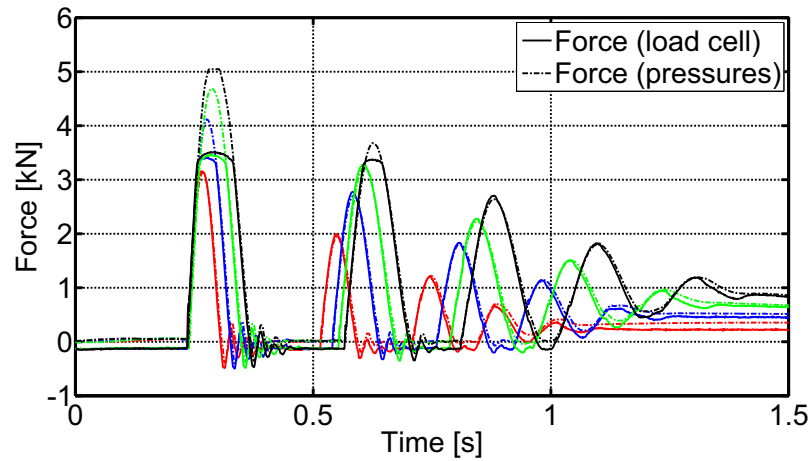


Figure 5.10: Result plots of the leg impact experiments (active control) with varying leg weights m_{leg} , supply pressures P_s and initial heights $\{0.05\text{m}, 0.1\text{m}, 0.15\text{m}, 0.2\text{m}, 0.25\text{m}, 0.3\text{m}, 0.35\text{m}\}$. The plots show the slider height (left) and the knee cylinder force (right). Increasing height results in increasing force peaks. **(a)** $m_{leg}=7.5\text{kg}$, $P_s=5\text{MPa}$; **(b)** $m_{leg}=15\text{kg}$, $P_s=5\text{MPa}$; **(c)** $m_{leg}=20\text{kg}$, $P_s=5\text{MPa}$; **(d)** $m_{leg}=7.5\text{kg}$, $P_s=16\text{MPa}$.



(a)



(b)

Figure 5.11: Result plots of the leg impact experiments (valves closed) from a drop height of 0.15m and with varying leg weights m_{leg} of 10kg, 15kg, 20kg and 25kg. (a) slider height (top) and vertical ground reaction force (bottom); (b) force in the knee cylinder measured by the load cell or estimated based on the pressure sensor data.

5.6 Periodic Hopping with Leg Prototype

During the leg impact experiments, we noticed that above a certain leg weight and supply pressure, the leg started to hop continuously. Independent of the initial drop height, after only a few cycles the system converged to a limit cycle with constant

5. EXPERIMENTAL STUDIES

frequency [Slotine and Li, 1991]. We decided to further investigate this behaviour as a sidetrack to the actual development of the quadruped robot.

This behaviour mainly depends on the dynamic performance of the valve and the PID controller. The valve spool dynamics create flow delays: No oil can flow through the valve until the spool moves far enough to open the valve. Fig. 5.12 shows a zoom into the cylinder speed test plot of Fig. 5.6(a) and shows that the minimum valve delay is approximately 15ms. During this period, no controller action corrects the error in position, which is constantly growing due to the compliance in the joint. Depending on the controller gains, the valve can open too much and create an overshoot. Enough energy is then given back into the system to make the leg lift off the ground again. At the next touch down of the foot, the behaviour starts over again.

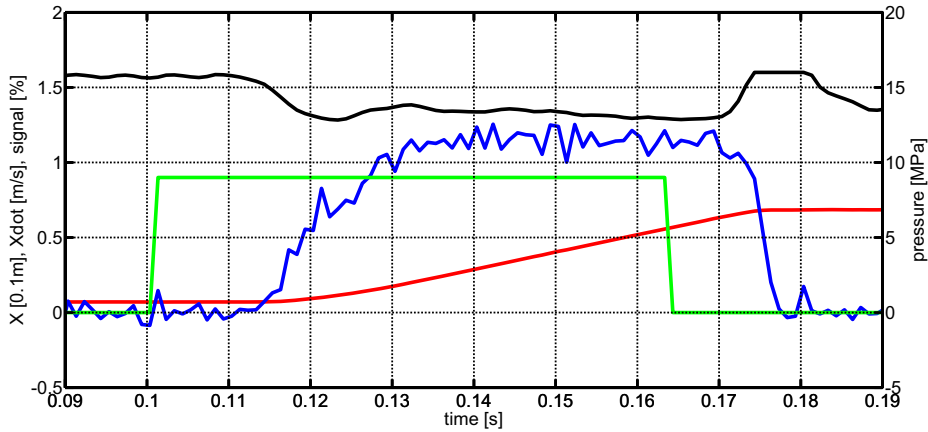
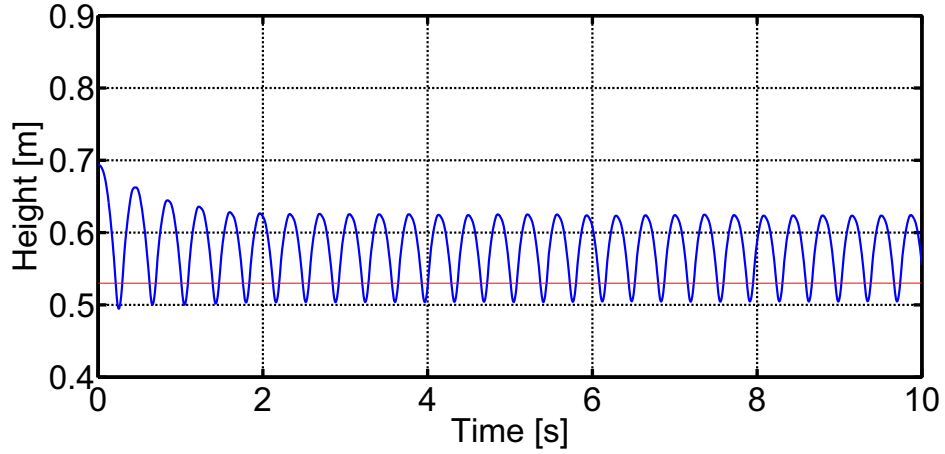
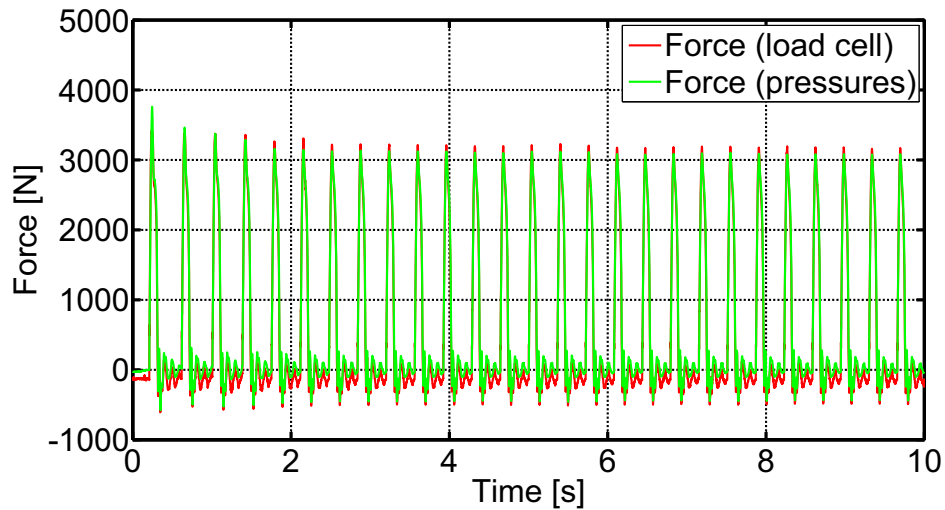


Figure 5.12: Zoom into cylinder speed test plot of Fig. 5.6(a). The delay between the input signal (green) and cylinder speed (blue) is approximately 15ms.

Fig. 5.13(a) shows the time plot of the slider height after dropping the leg from 0.16m (distance from ground to the lowest point of the foot). The supply pressure was set to 16MPa, the total leg weight was 15kg and the joints were position controlled with the same reference angles as in the leg impact study: $\theta_1 = -45^\circ$ and $\theta_2 = 90^\circ$. Fig. 5.13(b) shows the time plot of the force of the knee cylinder, either measured with the load cell or calculated based on the pressure sensors as explained in section 5.5.



(a)



(b)

Figure 5.13: Time plots of position and force during 10s of continuous hopping motion after a drop from 0.16m, with following parameters: total leg weight of 15kg, supply pressure of 16MPa, joint angle reference at $\theta_1 = -45^\circ$ and $\theta_2 = 90^\circ$ and a knee controller P-gain of 3.0. **(a)** slider height vs. time plot and **(b)** knee cylinder force vs. time plot with the force either measured with the load cell or calculated based on the pressure sensors as explained in the end of section 5.5.

5. EXPERIMENTAL STUDIES

To further investigate this behaviour, I started to do a series of experiments with varying conditions. As explained above, the overshoot is related to the size of the PID controller gains (especially the P-gain). Therefore, I tried the same experiments with different values of the P-gain that controls the knee joint. Next, I changed the supply pressure, since it is related to the amount of energy that is given back to the system and finally added more weight to the leg to investigate the influence of leg mass.

To group all plots of one test series into one figure, I plotted them in a *phase plot of vertical hopping* according to [Raibert, 1986], where the slider position is plotted against the slider velocity: position on the ordinate and velocity on the abscissa. Time progresses in the counter-clockwise direction. The cycle shown in the plot can be divided into the flight phase (top) and stance phase (bottom). The top represents the highest position during the flight phase and the bottom the lowest position during stance phase. The left-most part of the plot represents touch-down and the right-most part lift-off. The velocity signals have been low-pass filtered with a 10th-order Butterworth filter with cut-off frequency at 100Hz.

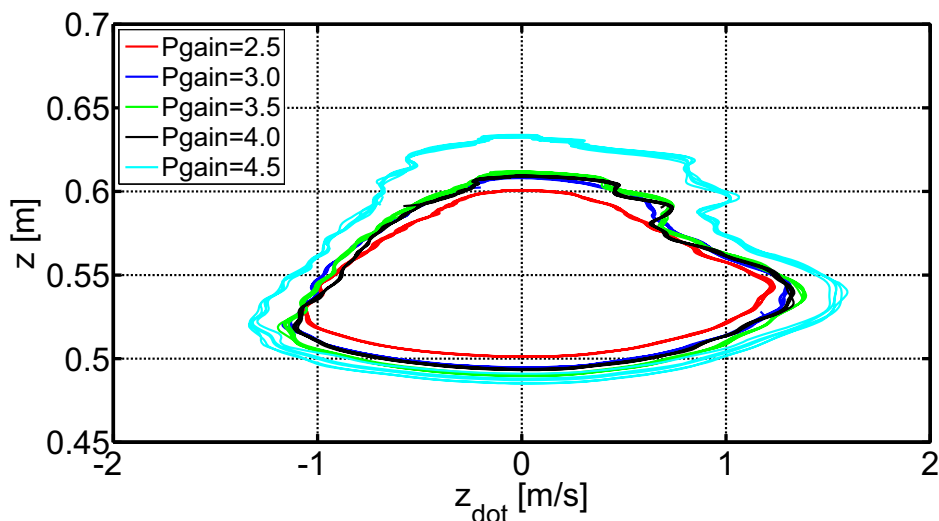


Figure 5.14: Phase plot of vertical hopping for different P-gains, with the supply pressure set to 12MPa, a total leg weight of 15kg and the joint angle reference at $\theta_1 = -45^\circ$ and $\theta_2 = 90^\circ$. The foot hits the ground at a height of 0.53m.

Fig. 5.14 shows the phase plot of vertical hopping for a series of P-gains {2.5, 3.0,

5.6 Periodic Hopping with Leg Prototype

3.5, 4.0, 4.5}, with the supply pressure set to 12MPa, a total leg weight of 15kg and the joint angle reference at $\theta_1 = -45^\circ$ and $\theta_2 = 90^\circ$. Lower P-gains did not result in a continuous hopping motion. Higher values made the system unstable (large vibrations) and the experiment was stopped immediately. The leg length and therefore also the slider height at the moment of impact was 0.53m.

Fig. 5.15 shows the phase plot of vertical hopping for a series of supply pressures {8MPa, 10MPa, 12MPa, 14MPa, 16MPa}, with the P-gain set to 3.0, a total leg weight of 12.5kg and the joint angle reference at $\theta_1 = -45^\circ$ and $\theta_2 = 90^\circ$. Lower pressures do not result in a continuous hopping motion. Higher pressures would exceed the operating pressure of the cylinders, see Table 4.8.

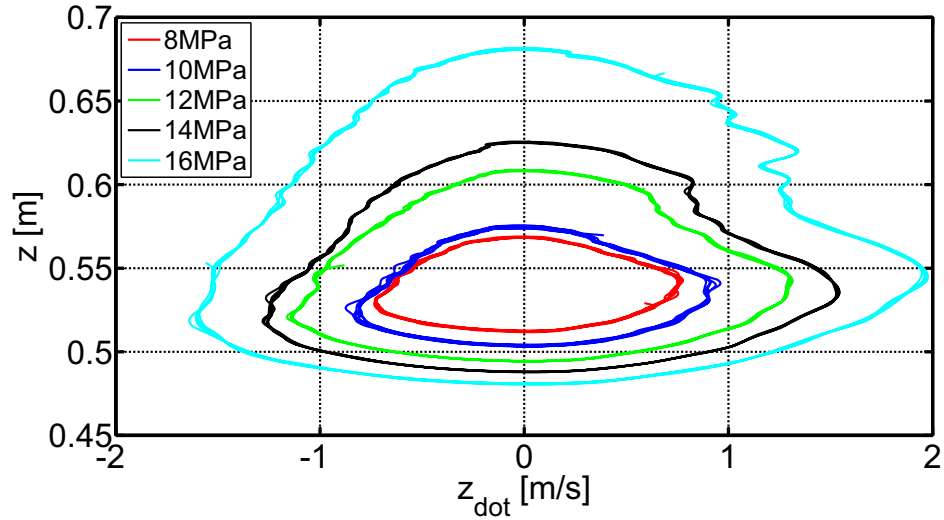


Figure 5.15: Phase plot of vertical hopping for different supply pressures, with the P-gain set to 3.0, a total leg weight of 12.5kg and the joint angle reference at $\theta_1 = -45^\circ$ and $\theta_2 = 90^\circ$.

Fig. 5.16 shows the phase plot of vertical hopping for a series of leg weights {7.5kg, 15kg, 20kg}, with the P-gain set to 3.0, a supply pressure of 10MPa, and the joint angle reference at $\theta_1 = -45^\circ$ and $\theta_2 = 90^\circ$. Note that the experiment with a leg weight of 7.5kg did not result in a continuous hopping after a drop from 21cm height.

5. EXPERIMENTAL STUDIES

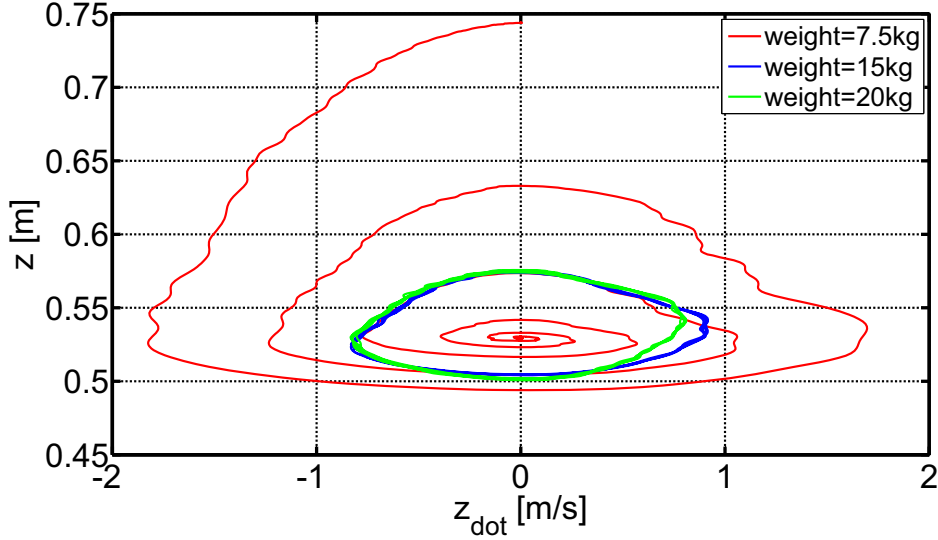


Figure 5.16: Phase plot of vertical hopping for different weights, with the P-gain set to 3.0, a supply pressure of 10MPa, and the joint angle reference at $\theta_1 = -45^\circ$ and $\theta_2 = 90^\circ$.

A picture sequence of one complete hopping cycle is shown in Fig. 5.17, frame order: top left to bottom right. For this experiment I used following settings: supply pressure of 16MPa, leg weight of 12.5kg, knee controller Pgain of 3.0 and the joint angle reference at $\theta_1 = -45^\circ$ and $\theta_2 = 90^\circ$. The time between two frames is 40ms. The first and last frame are at the same point of the cycle. The duration of the complete cycle is 440ms, which results in a hopping frequency of approximately 2.3Hz.

5.7 Conclusions

The section summarizes the conclusions of the experiments presented in this chapter:

- A frequency response test of the valve with cylinder (rigidly fixed to a test bench with half extended rod) resulted in a bandwidth of 18Hz (output pressure to solenoid input voltage). The bandwidth is mainly determined by the dynamic properties of the valve and the bulk modulus of the oil. Whether this bandwidth is high enough to achieve the desired overall dynamic performance of the robot,

5.7 Conclusions

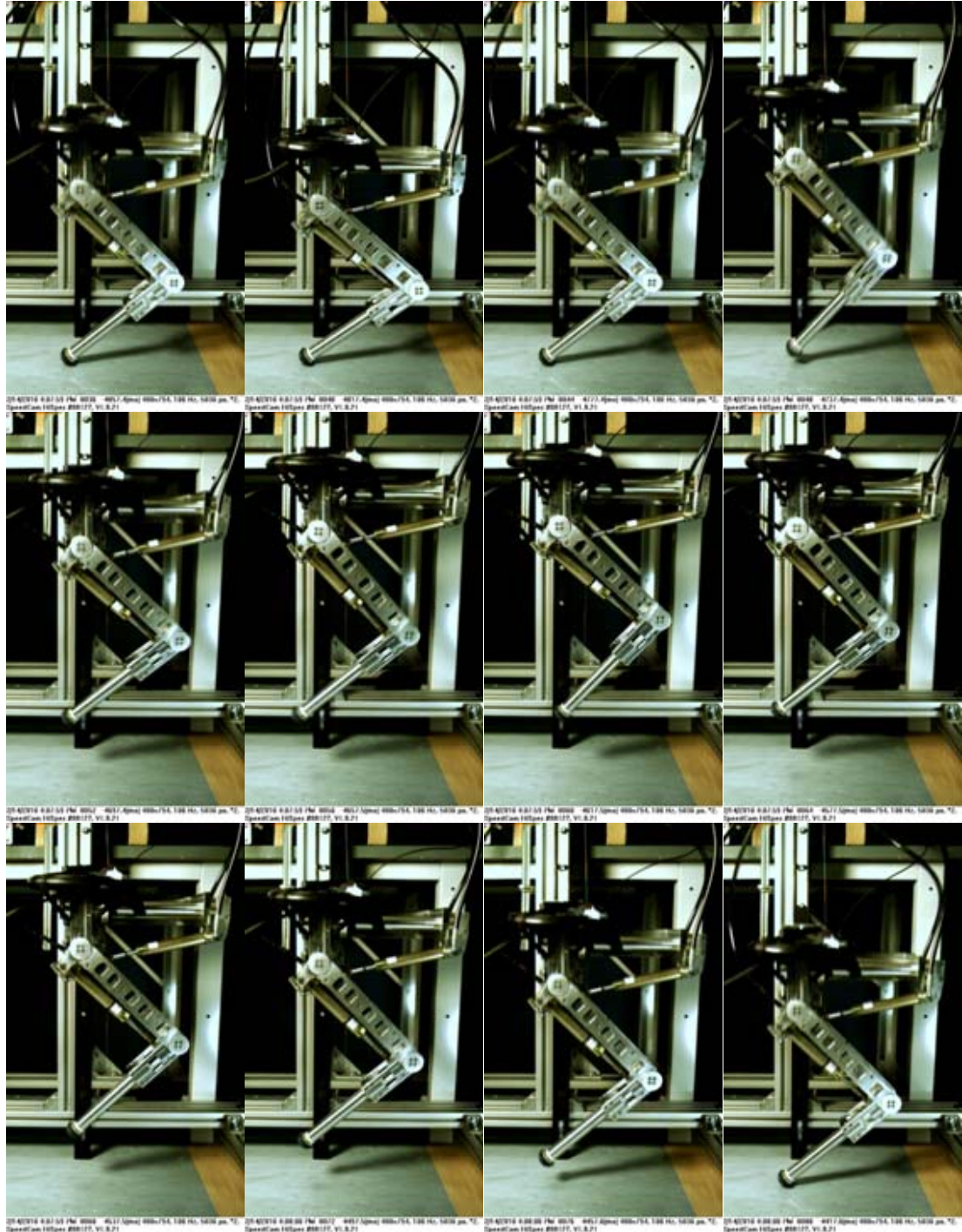


Figure 5.17: Picture sequence of hopping leg prototype. Time between frames: 40ms.

5. EXPERIMENTAL STUDIES

is not clear yet. However, we expect that the disturbances created by the position tracking error during the flight phase, can be handled by robust locomotion algorithms. Corrective action during the stance phase should lead to the desired locomotion performance of the robot.

- A cylinder performance test measuring the maximum rod speed with fully opened valve resulted in 1.1m/s under no-load conditions. The result shows that explosive motions with this kind of actuator are possible. This property is especially important for legged robots since it enables a fast retracting leg motion during the flight phase of running and therefore allows good clearance between the foot and the ground to avoid stumbling. The estimated cylinder force based on pressure measurements is 1200N during the maximum cylinder speed, which results in a peak output power of 1320W.
- The hydraulic accumulator is an important system component that keeps the pressure high and provides hydraulic flow in case of peak demand.
- A trajectory following experiment of the two PID-position controlled hydraulic joints of the prototype leg resulted in a quite poor performance. Especially the hip joint suffers from the variable inertia and the coupling between the two joints. More sophisticated controllers than PID (e.g. model-based) have to be implemented to increase tracking performance.
- The prototype leg with additional weights was attached to a vertical slider and dropped from different heights to evaluate the leg impact behaviour. The tests showed clearly how the intrinsic compliance (both stiffness and damping) of the hydraulic actuation is able to damp the impact peaks. It even makes the leg bounce off the floor several times like an elastic ball. Hydraulic actuation is therefore well suited for dynamic legged robots that need to cope with high force peaks at foot touch-down.
- The load cell data of the knee cylinder was confronted with the force data obtained by the cylinder chamber pressure sensors. The results showed that the pressure sensor data is sufficiently accurate to estimate the cylinder force during dynamic motions. Static conditions give worse results due to the neglected cylinder friction.

Whether the pressure sensor data will permit sufficiently smooth force control (and whether the load cell can be eliminated), is part of future work.

- The prototype leg (attached to a vertical slider) can be forced to start continuously hopping after empirical tuning of some system parameters (controller gains, supply pressure etc.). After an initial excitation (e.g. drop from different heights), the leg enters a parameter-dependent limit cycle with a constant hopping frequency and amplitude.

5. EXPERIMENTAL STUDIES

6

Discussion

This chapter discusses the differences between the design of the prototype leg and the final leg. It continues with a comparison study of the specifications of the hydraulic and electric actuator units of HyQ. General comments about hydraulic actuation for mobile robots conclude this chapter.

6.1 Leg Prototype (Leg V1) vs. Final Leg (Leg V2)

As mentioned before in section 4.2.4, the final leg (*Leg V2*) is an improved version of the leg prototype (*Leg V1*). The following list describes the improvements made to the design:

- Improved torque profile as shown in Fig. 6.1.
- Increased maximum joint torque based on longer lever arm and cylinder stroke length as shown in Table 6.1.
- Reduced cylinder margin (distance between the mechanical stop of the leg joint and the internal stop of the cylinder) to increase the lever arm and output torque.
- Stronger mechanical stops of the leg joints. The stops of *Leg V1* were too weak and got easily damaged.
- More robust load cells with a higher range (5kN instead of 3.5kN), adapters to connect them to the cylinder rod and more resistant rod ends.

6. DISCUSSION

- Increased leg segment length (distance between the axes of the *hip f/e* and *knee f/e* joint).
- Removed material from the main leg plates based on FEM analysis to reduce the leg weight.
- Addition of absolute encoders to each joint to remove the necessity to initialize the joints by moving them.

Table 6.1 summarizes the geometric parameters of the leg prototype *Leg V1* and the final leg *Leg V2* as defined in Fig. B.2.

Property	Leg V1	Leg V2
distance <i>hip f/e</i> to <i>knee f/e</i> axis	300mm	350mm
cylinder stroke	70mm	80mm
cylinder margin (each side)	5mm	1mm
usable cylinder stroke	60mm	78mm
a1	304.4mm	321.9mm
a2	304.1mm	321.8mm
b1	37.7mm	45.0mm
b2	39.0mm	45.0mm
ε_{11}	6.03°	6.24°
ε_{12}	24.0°	0°
ε_{21}	9.46°	8.04°
ε_{22}	-20.0°	6.0°

Table 6.1: List of geometric design parameters of the leg prototype *Leg V1* and the final leg *Leg V2*.

Fig. 6.1 shows the torque profiles of the two leg versions. The maximum of the torque profile of *Leg V1* is shifted towards the left to smaller cylinder lengths. The reasoning behind this initial choice was to increase the torque for the robot in a squat posture, where more torque is required. This decision turned out to be problematic since the controllability of the joint for almost extended leg joints, was drastically

6.1 Leg Prototype (Leg V1) vs. Final Leg (Leg V2)

reduced as can be seen in the plot of $\delta \gamma$. A small change in cylinder position, resulted in a large change in joint position. The configuration approaches a singularity of the Jacobian matrix J (C.3), as described in [Sciavicco and Siciliano, 2001]. This has been improved in the design of *Leg V2* by putting the torque maximum into the centre of the cylinder extension.

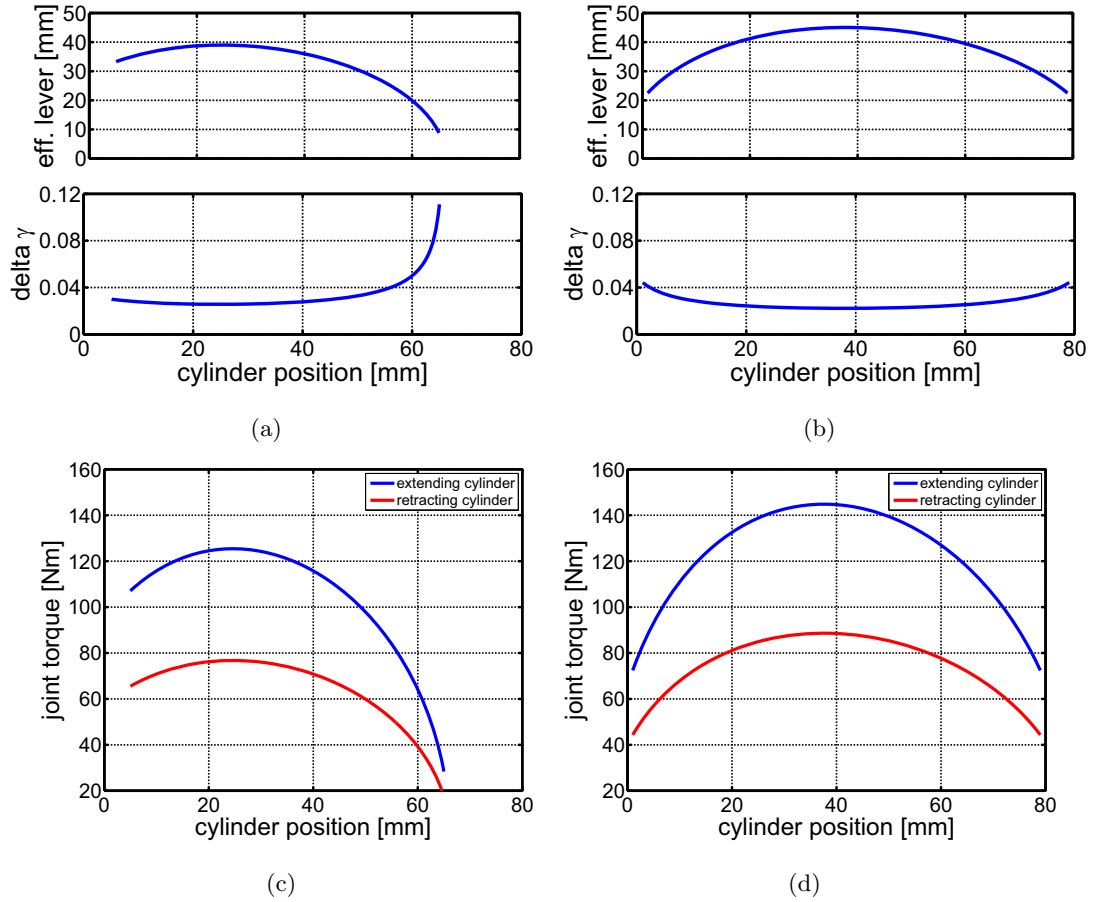


Figure 6.1: Confrontation of the torque output profiles of: (a) + (c) *Leg V1*; and (b) + (d) *Leg V2*. The plots on the top show the effective lever length and $\delta \gamma$ (as shown in Fig. 3.14) vs. cylinder position. The bottom plots show the torque output profile for both extending and retracting cylinder motions. The unit of $\delta \gamma$ is expressed in $\frac{rad}{mm}$.

6. DISCUSSION

6.2 HyQ's Electric and Hydraulic Actuator Comparison

This section presents a comparison between the hydraulic and electric actuator units of HyQ. Actuator comparisons usually tend to be biased towards the technology the author is most familiar with. Since we selected both actuators types for HyQ, I try to give an unbiased confrontation of the specifications of these two actuator units.

The electric actuator is a brushless DC motor (*Emoteq HT2301*) with harmonic gear (*Harmonic Drive CSD-25-100*). They are described more in details in section 3.4.2. Their datasheets can be found following these references: [Emoteq Inc., 1998, Harmonic Drive Inc., 2009].

The hydraulic actuator unit consists of a hydraulic cylinder *Hoerbiger LB6-1610-0080-4M* and proportional spool valve *Wandfluh WDPFA03-ACB-S5-G24*, as described in section 4.3.2.3 and 4.3.2.4. Their datasheets can be found following these references: [Hoerbiger, 2008, Wandfluh, 2007].

Table 6.2 summarizes the results of the comparison, followed by a detailed explanation of each property.

Property	Electric	Hydraulic	Unit
weight	1.530	2.276	kg
volume	460	528	cm ³
peak torque	152	145 (89)	Nm
cont./mean torque	41	123 (75)	Nm
no-load speed	4.3	24.4	rad/s
output power	81	1320	W
power/weight ratio	53	580	W/kg
joint range	unlimited	2.1	rad
price	2680	940	€

Table 6.2: Comparison of the two actuator units studied for HyQ: Brushless DC motor (Electric) and hydraulic cylinder based rotary joint (Hydraulic).

6.2 HyQ's Electric and Hydraulic Actuator Comparison

- The **weight** of the electric actuator includes the frameless motor (stator and rotor), the harmonic gear, the motor frame built in Ergal and stainless steel and the leg-motor attachment (Fig. 4.6), excluding the encoder and the 6mm pins. The mass of the hydraulic actuator includes the cylinder, rod end, proportional valve, one quarter of the valve manifold, two hydraulic hoses of 0.8m length, four hydraulic connectors and the oil inside the cylinder and hoses.
- The **volume** of both actuators is based on the parts used to calculate the mass.
- The **peak torque** of the electric motor is limited by the *momentary peak torque* of the harmonic gear, since the *maximum rated torque* of the electric motor is much higher. The torque maximum of the hydraulic actuator is given by the maximum force output of the extending (retracting) cylinder multiplied by the maximum lever length.
- The **cont./mean torque** of the electric motor is the *maximum continuous stall torque* and the mean value of the non-linear joint torque/angle curve for extending (retracting) cylinder for the hydraulic actuator.
- The **no-load speed** of the electric actuator is the maximum motor speed with zero load divided by the reduction ratio of the gear (1:100). The no-load speed of the hydraulic actuator is the maximum speed measured for the cylinder rod (section 5.3) multiplied by the lowest value of $\delta\gamma$ of Fig. 6.1(b).
- The **output power** of the electric motor is given by its *maximum continuous power output*. The power of the hydraulic actuator is estimated by multiplying the maximum speed of the cylinder rod with the cylinder force (based on pressure measurements and (2.7)) during the cylinder speed experiment.
- The **power/weight ratio** is the ratio between the *weight* and *output power* of this comparison.
- The **joint range** is unlimited for the electric actuator and based on the definition of section 3.2.5 for the hydraulic actuator.
- The **price** of both actuators is based on the market price in 2009 (ordered quantity: 5) and includes all parts and components used to calculate the mass.

6. DISCUSSION

Some general comments about this comparison: For a meaningful comparison we decided not to confront the rotary electric motor with the linear hydraulic cylinder, but rather the resulting rotary hydraulic joint including the non-linear torque/angle characteristics. At the time of writing this dissertation, the electric motor unit was not ready for experimental trial. Therefore speed, torque and power data mentioned in this comparison is taken from the datasheet [Emoteq Inc., 1998]. We only considered the actuator itself without motor/valve driver electronics, power source (electric means, batteries or fuel) nor power conversion system (i.e. electric power supply converter (220V to 24V) or hydraulic pump unit). However we included the valve, oil, connectors and hoses to the hydraulic actuator.

As expected, the comparison shows that hydraulic actuation has a significantly higher power-to-weight ratio compared to electric actuation.

6.3 Comments about Hydraulics for Mobile Robots

This chapter ends with some general comments and recommendations for the use of hydraulic actuation for mobile robots:

- It is very difficult to define reasonable robot specification at an initial phase in the design process. Some of them have to be adjusted several times during the design process, as for example the estimated robot weight: we had to correct an initial target weight of 50kg to 60-80kg and later to 90kg. Since the size and specifications of the actuation system depends on the robot weight and vice versa, there is the danger to enter a *vicious circle*: the heavier the robot the stronger the actuators have to be, etc. However, in the end the availability of compact hydraulic components dictates the overall size/weight of the robot. Compact hydraulic components for mobile robots are still difficult to find on the market or are very expensive.
- Most standard hydraulic connectors and hoses on the market are available in sizes above 1/4 or 3/16 (e.g. *Dunlop Hiflex*). The small 1/8inch connectors that we use for HyQ are less common.

6.3 Comments about Hydraulics for Mobile Robots

- The interpretation of the words *small* and *compact* are different for hydraulics people and roboticists. Traditionally, hydraulic actuation is used for machines where components' size and weight are not of great importance.
- Steel is commonly used to build valve manifolds. We use a steel manifold for the hopping leg experiments that can host a maximum of three valves. It weighs 9kg. An improved version built in aluminium alloy (three times lighter than steel) can host four valves and weighs only 1.6kg. The weight per valve dropped from 3kg to 0.4kg, which is almost an order of magnitude.
- Hydraulic connections are usually in imperial sizes, e.g. 1/8inch, 1/4inch etc. Newer components have metric ports (e.g. the Hoerbiger cylinder with M10x1 ports). This can lead to some confusion since the thread of the 1/8inch connectors is almost identical to the one of the M10x1 connectors.
- Hydraulic systems can be messy during changes in system configuration (connecting/disconnecting tubes etc.), but are quite clean once set up correctly. A proper design has almost no leakage.

6. DISCUSSION

7

Conclusion and Future Work

7.1 Conclusions

Legged robots are a popular field of research. While the main attention is given to biped and especially humanoid robots, quadruped machines promise to provide an even higher mobility in terms of moving over rough terrain, especially outside. Unfortunately, the actuators of most of today's robots lack the speed and torque to allow the robot to perform highly dynamic tasks such as running or jumping. The few exceptions, however, are specialized for a particular task and are tethered to an external power supply. To the author's best knowledge, only the quadruped robot BigDog is power-autonomous for an extended period, versatile and able to run and jump.

The lack of this family of robots and the abilities of BigDog have led to the start of the HyQ project, whose first milestone is the development of a highly dynamic and versatile robot platform with four legs. The robot should be able to cope with all sorts of rough terrain and work power-autonomously for several hours.

The objective of this dissertation was to make a significant contribution toward the development of a highly dynamic, versatile quadruped robot powered by a combination of electric and hydraulic actuators. Following goals have been reached to meet the final objective:

- Construction of a 90kg quadruped robot of the size between a large dog and a small horse with a hybrid actuation system with electrically and hydraulically

7. CONCLUSION AND FUTURE WORK

actuated joints. The actuation type has been selected according to the joint's specifications and requirements.

- Completion of several design studies for the development of a quadruped robot with a focus on hydraulic joint actuation design and kinematics.
- Experimental tests of hydraulic actuator units (with and without leg prototype). They demonstrated that hydraulic actuators are suitable to move the joints of highly dynamic legged robots, due to their ability to cope with high impact force peaks, high speed and force.
- Periodic hopping with leg prototype was achieved.

7.2 Future Work

The design and construction of the robot is only the first step of the HyQ project. Once the first version of the robot is tested, debugged and fully operational, a big variety of fields for future research is opened. The following list includes a selection of these future activities related to HyQ:

- Debugging and system testing of the first version of HyQ.
- Implementation and development of locomotion algorithms, gait patterns, gait transitions.
- Simulation of robot locomotion with SL simulator.
- Walking experiments with HyQ on the treadmill and on rough terrain.
- Running experiments with HyQ on the treadmill and on rough terrain.
- Balancing experiments with HyQ in various situations, e.g. disturbances due to uneven terrain, external forces on the robot torso or rapidly changing treadmill speeds.
- More experiments with the leg prototype on the slider. Experimental testing and comparison of *Leg V1* and *Leg V2*.

- Investigation and modelling of limit cycle hopping of the leg prototype on the slider.
- Experimental assessment if valve bandwidth is high enough for the required joint dynamics.
- Investigation of rotary hydraulic actuators as replacement for the hydraulic cylinders.
- Comparison studies and experiments between water and oil as hydraulic fluid.
- Design of various versions of the modular foot with compliance. Investigation if adjustable mechanical stiffness is beneficial for energy-efficient locomotion.
- Investigation if two active DOF in the leg-sagittal plane are sufficient for energy-efficient locomotion and rough terrain mobility (e.g. rock beds or on slopes) or if a third active DOF is required.
- Robot development stage 3 with a combustion engine or a similar onboard motor/engine to make the robot power-autonomous for several hours.
- Investigation of energy-efficient hydraulics with switching technology (e.g. buck converter ([Guglielmino et al., 2009])).
- Improvement and optimisation of leg and torso design, e.g. evaluating the option of using carbon composite tubes and sheets to replace some of the metal parts of the robot.
- Reducing the size and weight of the system components with a focus on the hydraulic system.

7. CONCLUSION AND FUTURE WORK

Appendix A

Publications and Patents

A.1 Publications

- **C. Semini**, N. G. Tsagarakis, B. Vanderborght, Y. S. Yang and D. G. Caldwell, “HyQ - Hydraulically Actuated Quadruped Robot: Hopping Leg Prototype,” IEEE/RAS Int. Conf. on Biomedical Robotics and Biomechatronics (BioRob), pp.593-599, 2008.
- Y. S. Yang, **C. Semini**, N. G. Tsagarakis, D. G. Caldwell, Y. Zhu, “Water hydraulics - A novel design of spool-type valves for enhanced dynamic performance,” IEEE/ASME Int. Conf. on Advanced Intelligent Mechatronics (AIM), pp. 1308-1314, 2008.
- B. Vanderborght, N. G. Tsagarakis, **C. Semini**, R. Van Ham, D. G. Caldwell, “MACCEPA 2.0: Adjustable Compliant Actuator with Stiffening Characteristic for Energy Efficient Hopping,” IEEE Int. Conf. on Robotics and Automation (ICRA), pp. 544-549, 2009.
- Y. S. Yang, **C. Semini**, E. Guglielmino, N. G. Tsagarakis, D. G. Caldwell, “Water vs. Oil Hydraulic Actuation for a Robot Leg,” IEEE Int. Conf. on Mechatronics and Automation (ICMA), pp. 1940-1946, 2009.
- Y. S. Yang, **C. Semini**, N. G. Tsagarakis, E. Guglielmino, D. G. Caldwell, “Leg Mechanisms for Hydraulically Actuated Robots,” IEEE/RSJ Int. Conf. on Intelligent Robots and Systems (IROS), pp. 4669-4675, 2009.

A. PUBLICATIONS AND PATENTS

- E. Guglielmino, **C. Semini**, Y. S. Yang, D. G. Caldwell, H. Kogler, R. Scheidl, “Energy Efficient Fluid Power in Autonomous Legged Robotics,” ASME Dynamic Systems and Control Conference (DSCC), 2009.
- T. B. Cunha, **C. Semini**, E. Guglielmino, V. J. De Negri, Y. S. Yang, D. G. Caldwell, “Gain Scheduling Control for the Hydraulic Actuation of the HyQ Robot Leg,” Int. Conf. of Mechanical Engineering (COBEM), 2009.
- M. Focchi, E. Guglielmino, **C. Semini**, T. B. Cunha, Y. S. Yang, D. G. Caldwell, “Control of a Hydraulically-Actuated Quadruped Robot Leg,” IEEE Int. Conf. on Robotics and Automation (ICRA), 2010.
- **C. Semini**, N. G. Tsagarakis, E. Guglielmino, and D. G. Caldwell, “Design of HyQ a Hydraulically and Electrically Actuated Quadruped Robot,” submitted to the Workshop on Human Adaptive Mechatronics (HAM), Loughborough University, United Kingdom, May 2010.
- **C. Semini**, N. G. Tsagarakis, E. Guglielmino, and D. G. Caldwell, “Design and Experimental Evaluation of a Hydraulically Actuated Robot Leg,” submitted to IEEE/RSJ Int. Conf. on Intelligent Robots and Systems (IROS), Taipei, Taiwan, October 2010.

A.2 Workshop Posters

- **C. Semini**, N. G. Tsagarakis, D. G. Caldwell, “Dynamic Tasks of a Hydraulically Actuated Quadruped Robot,” Poster at Dynamic Walking Conference, Delft (The Netherlands), May 2008.
- **C. Semini**, N. G. Tsagarakis, D. G. Caldwell, “Bio-Inspired Design of a Hydraulically Actuated Quadruped Robot [HyQ],” Poster at Robotics: Science and Systems (RSS) Conference, Zurich (Switzerland), June 2008.

A.3 Patents

- E. Guglielmino, Y. Yang, G. Pane, **C. Semini**, D. G. Caldwell, “Servovalvola rotativa, particolarmente di tipo idraulico”, in Italian, 2009.

Appendix B

Definition of Joint Angles and Cylinder Attachment Geometry

B. DEFINITION OF JOINT ANGLES AND CYLINDER ATTACHMENT GEOMETRY

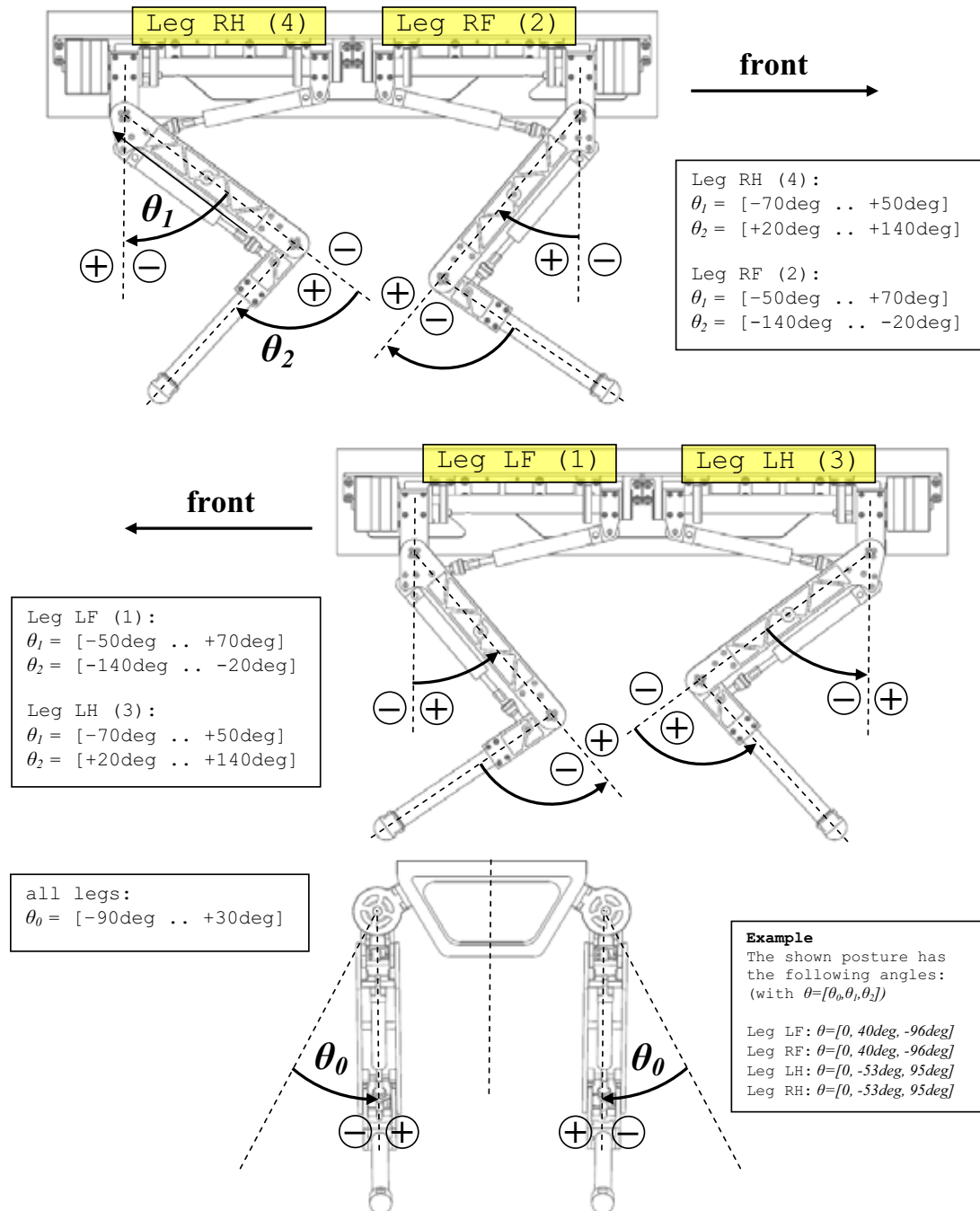


Figure B.1: Definition of joint angles of HyQ. The following abbreviations identify the four legs of the robot: Right Hind (RH), Right Front (RF), Left Front (LF) and Left Hind (LH).

**B. DEFINITION OF JOINT ANGLES AND CYLINDER
ATTACHMENT GEOMETRY**

Appendix C

Kinematic and Dynamic Model of 2-DOF Robot Leg

This appendix presents the kinematic and dynamic model of the 2-DOF robot leg with the *hip f/e* and the *knee f/e* joint, whose axes of rotation are parallel. Therefore the models (and consequently also all vectors) presented in this chapter are two-dimensional. For simplification the joint angles have been renamed as follows: $q_1 = \theta_1$, $q_2 = \theta_2$. Fig. C.1 shows a simplified model of the 2-DOF robot leg with the definition of the leg geometry (l_0, l_1, l_2, l_3), the leg base coordinate system (X-Z), joint angles (q_1, q_2) and torques (τ_1, τ_2), ground contact force F_G and location of the COM of the upper and lower leg (m_1, m_2).

Note that the variables ε_1 and ε_2 describe the location of the COM of the upper and lower leg segment in this chapter, which is different from the ε used for the geometry of the hydraulic actuator design presented in section 3.4.1.3.

C.1 Kinematic Model of 2-DOF Leg

The forward kinematic equations relate the position of the contact point between the foot and the horizontal ground plane \mathbf{r}_f with the joint angles q_1 and q_2 :

$$\mathbf{r}_f = \begin{bmatrix} x_f \\ z_f \end{bmatrix} = \begin{bmatrix} -l_1 \sin q_1 - l_2 \sin(q_1 + q_2) \\ -l_0 - l_1 \cos q_1 - l_2 \cos(q_1 + q_2) - l_3 \end{bmatrix} \quad (\text{C.1})$$

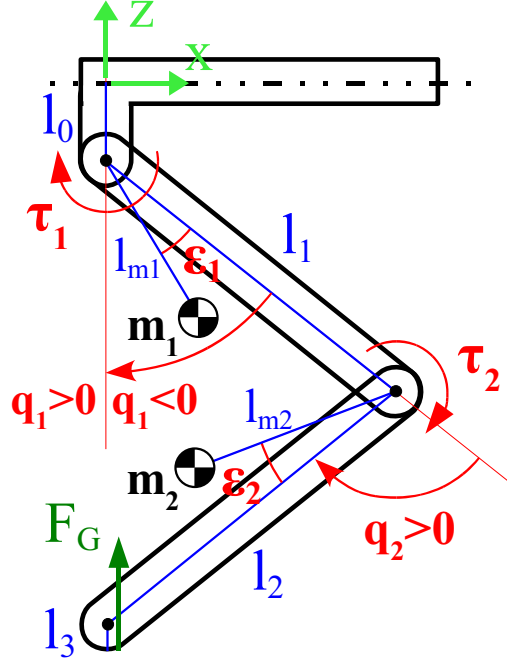


Figure C.1: Sketch of 2-DOF leg with definition of variables used for kinematic model and the derivation of the dynamic model, the COM of the upper and lower leg segments are shifted to the side due to mass of the hydraulic cylinders (not shown in the figure).

Directly differentiating, the forward kinematic equation yields the leg Jacobian \mathbf{J} , which relates the velocity of the foot tip $\dot{\mathbf{r}}_f$ as a function of velocities of the hip and knee joint angle $\dot{\mathbf{q}}$:

$$\dot{\mathbf{r}}_f = \mathbf{J} \cdot \dot{\mathbf{q}} \quad (\text{C.2})$$

with

$$\mathbf{J} = \begin{bmatrix} -l_1 \cos q_1 - l_2 \cos(q_1 + q_2) & -l_2 \cos(q_1 + q_2) \\ l_1 \sin q_1 + l_2 \sin(q_1 + q_2) & l_2 \sin(q_1 + q_2) \end{bmatrix} \quad (\text{C.3})$$

The transpose of the Jacobian matrix also relates the joint torque $\boldsymbol{\tau}$ with the ground contact force \mathbf{F}_G :

$$\boldsymbol{\tau} = \mathbf{J}^T \cdot \mathbf{F}_G \quad (\text{C.4})$$

C.2 Dynamic Model of 2-DOF Leg

This section presents the derivation of the Lagrange dynamic model of the 2-DOF leg. Note that for simplification, the mass of the hip cylinder has been neglected because it is fixed to the hip assembly and that the mass of the knee cylinder has been added to the mass of the upper leg segment. The relative angular motion of the cylinders around their mechanical connection at the cylinder bottom is small. Therefore this simplification is acceptable. The mass and inertia have been calculated in the CAD software with the cylinder in the central position of its angular excursion (see Table 4.5). This explains why the COM of the upper leg is shifted to the side. m_1 and m_2 are the centres of mass of the upper and lower leg segment in the x-z plane ($y_0 = 0$).

First of all, let us calculate the positions of m_1 and m_2 in the base coordinate system:

$$\begin{aligned} \mathbf{r}_{m1} &= \begin{bmatrix} x_{m1} \\ z_{m1} \end{bmatrix} = \begin{bmatrix} -l_{m1} \sin(q_1 + \varepsilon_1) \\ -l_0 - l_{m1} \cos(q_1 + \varepsilon_1) \end{bmatrix} \\ \mathbf{r}_{m2} &= \begin{bmatrix} x_{m2} \\ z_{m2} \end{bmatrix} = \begin{bmatrix} -l_1 \sin q_1 - l_{m2} \sin k \\ -l_0 - l_1 \cos q_1 - l_{m2} \cos k \end{bmatrix} \end{aligned} \quad (\text{C.5})$$

with

$$k = q_1 + q_2 + \varepsilon_2 \quad (\text{C.6})$$

Velocity of m_1 and m_2 in the base coordinate system:

$$\begin{aligned} \dot{\mathbf{r}}_{m1} &= \begin{bmatrix} \dot{x}_{m1} \\ \dot{z}_{m1} \end{bmatrix} = \begin{bmatrix} -l_{m1} \cos(q_1 + \varepsilon_1) & 0 \\ l_{m1} \sin(q_1 + \varepsilon_1) & 0 \end{bmatrix} \begin{bmatrix} \dot{q}_1 \\ \dot{q}_2 \end{bmatrix} \\ \dot{\mathbf{r}}_{m2} &= \begin{bmatrix} \dot{x}_{m2} \\ \dot{z}_{m2} \end{bmatrix} = \begin{bmatrix} -l_1 \cos q_1 - l_{m2} \cos k & -l_{m2} \cos k \\ l_1 \sin q_1 + l_{m2} \sin k & l_{m2} \sin k \end{bmatrix} \begin{bmatrix} \dot{q}_1 \\ \dot{q}_2 \end{bmatrix} \end{aligned} \quad (\text{C.7})$$

C. KINEMATIC AND DYNAMIC MODEL OF 2-DOF ROBOT LEG

$$\begin{aligned}
v_{m1}^2 &= \dot{x}_{m1}^2 + \dot{z}_{m1}^2 \\
&= \dot{q}_1^2 l_{m1}^2 \sin^2(q_1 + \varepsilon_1) + \dot{q}_1^2 l_{m1}^2 \cos^2(q_1 + \varepsilon_1) \\
\Rightarrow v_{m1}^2 &= \dot{q}_1^2 l_{m1}^2
\end{aligned} \tag{C.8}$$

$$\begin{aligned}
v_{m2}^2 &= \dot{x}_{m2}^2 + \dot{z}_{m2}^2 \\
&= (-\dot{q}_1 l_1 \cos q_1 - \dot{q}_1 l_{m2} \cos k - \dot{q}_2 l_{m2} \cos k)^2 \\
&\quad + (\dot{q}_1 l_1 \sin q_1 + \dot{q}_1 l_{m2} \sin k + \dot{q}_2 l_{m2} \sin k)^2 \\
&= (\dot{q}_1 l_1 \cos q_1 + (\dot{q}_1 + \dot{q}_2) l_{m2} \cos k)^2 \\
&\quad + (\dot{q}_1 l_1 \sin q_1 + (\dot{q}_1 + \dot{q}_2) l_{m2} \sin k)^2 \\
&= \dot{q}_1^2 l_1^2 \cos^2 q_1 + 2\dot{q}_1 l_1 \cos q_1 (\dot{q}_1 + \dot{q}_2) l_{m2} \cos k + (\dot{q}_1 + \dot{q}_2)^2 l_{m2}^2 \cos^2 k \\
&\quad + \dot{q}_1^2 l_1^2 \sin^2 q_1 + 2\dot{q}_1 l_1 \sin q_1 (\dot{q}_1 + \dot{q}_2) l_{m2} \sin k + (\dot{q}_1 + \dot{q}_2)^2 l_{m2}^2 \sin^2 k \\
&= \dot{q}_1^2 l_1^2 + (\dot{q}_1 + \dot{q}_2)^2 l_{m2}^2 + 2\dot{q}_1 l_1 l_{m2} (\cos q_1 \cos k + \sin q_1 \sin k) \\
&= \dot{q}_1^2 l_1^2 + (\dot{q}_1 + \dot{q}_2)^2 l_{m2}^2 + 2\dot{q}_1 l_1 l_{m2} \cos(q_1 - k) \\
\Rightarrow v_{m2}^2 &= \dot{q}_1^2 l_1^2 + (\dot{q}_1 + \dot{q}_2)^2 l_{m2}^2 + 2\dot{q}_1 l_1 l_{m2} \cos(q_2 + \varepsilon_2)
\end{aligned} \tag{C.9}$$

Potential energy U:

$$\begin{aligned}
U_1 &= -gm_1 l_{m1} \cos(q_1 + \varepsilon_1) \\
U_2 &= -gm_2 (l_1 \cos q_1 + l_{m2} \cos k)
\end{aligned} \tag{C.10}$$

$$\Rightarrow U = U_1 + U_2 \tag{C.11}$$

Kinetic energy T:

$$\begin{aligned}
T_1 &= \frac{1}{2} m_1 v_{m1}^2 + \frac{1}{2} I_{1ZZ} \dot{q}_1^2 \\
&= \frac{1}{2} m_1 \dot{q}_1^2 l_{m1}^2 + \frac{1}{2} \dot{q}_1^2 I_{1ZZ}
\end{aligned} \tag{C.12}$$

$$\begin{aligned}
T_2 &= \frac{1}{2} m_2 v_{m2}^2 + \frac{1}{2} I_{2ZZ} (\dot{q}_1 + \dot{q}_2)^2 \\
&= \frac{1}{2} m_2 (\dot{q}_1^2 l_1^2 + (\dot{q}_1 + \dot{q}_2)^2 l_{m2}^2 + 2\dot{q}_1 (\dot{q}_1 + \dot{q}_2) l_1 l_{m2} \cos(q_2 + \varepsilon_2)) \\
&\quad + \frac{1}{2} (\dot{q}_1 + \dot{q}_2)^2 I_{2ZZ}
\end{aligned} \tag{C.13}$$

$$\begin{aligned}
 \Rightarrow T &= T_1 + T_2 \\
 &= \frac{1}{2} \dot{q}_1^2 (m_1 l_{m1}^2 + m_2 l_1^2 + I_{1ZZ}) \\
 &\quad + \frac{1}{2} (\dot{q}_1 + \dot{q}_2)^2 (m_2 l_{m2}^2 + I_{2ZZ}) \\
 &\quad + \dot{q}_1 (\dot{q}_1 + \dot{q}_2) m_2 l_1 l_{m2} \cos(q_2 + \varepsilon_2)
 \end{aligned} \tag{C.14}$$

$$\begin{aligned}
 \Rightarrow L &= T - U \\
 &= \frac{1}{2} \dot{q}_1^2 (m_1 l_{m1}^2 + m_2 l_1^2 + I_{1ZZ}) \\
 &\quad + \frac{1}{2} (\dot{q}_1 + \dot{q}_2)^2 (m_2 l_{m2}^2 + I_{2ZZ}) \\
 &\quad + (\dot{q}_1^2 + \dot{q}_1 \dot{q}_2) m_2 l_1 l_{m2} \cos(q_2 + \varepsilon_2) \\
 &\quad + g m_1 l_{m1} \cos(q_1 + \varepsilon_1) \\
 &\quad + g m_2 l_1 \cos q_1 + g m_2 l_{m2} \cos k
 \end{aligned} \tag{C.15}$$

Lagrange equation

$$\frac{d}{dt} \frac{\partial L}{\partial \dot{q}_i} - \frac{\partial L}{\partial q_i} = \tau_i \quad i = 1, 2 \tag{C.16}$$

1st step: $\frac{\partial L}{\partial \dot{q}_i}$

$$\begin{aligned}
 \frac{\partial L}{\partial \dot{q}_1} &= \dot{q}_1 (m_1 l_{m1}^2 + m_2 l_1^2 + I_{1ZZ}) \\
 &\quad + (\dot{q}_1 + \dot{q}_2) (m_2 l_{m2}^2 + I_{2ZZ}) \\
 &\quad + (2\dot{q}_1 + \dot{q}_2) m_2 l_1 l_{m2} \cos(q_2 + \varepsilon_2)
 \end{aligned}$$

$$\begin{aligned}
 \frac{\partial L}{\partial \dot{q}_2} &= (\dot{q}_1 + \dot{q}_2) (m_2 l_{m2}^2 + I_{1ZZ}) \\
 &\quad + \dot{q}_1 m_2 l_1 l_{m2} \cos(q_2 + \varepsilon_2)
 \end{aligned} \tag{C.17}$$

C. KINEMATIC AND DYNAMIC MODEL OF 2-DOF ROBOT LEG

2nd step: $\frac{d}{dt} \frac{\partial L}{\partial \dot{q}_i}$

$$\begin{aligned}
\frac{d}{dt} \frac{\partial L}{\partial \dot{q}_1} &= \ddot{q}_1(m_1 l_{m1}^2 + m_2 l_1^2 + I_{1ZZ} + m_2 l_{m2}^2 + I_{2ZZ}) \\
&\quad + \ddot{q}_2(m_2 l_{m2}^2 + I_{2ZZ}) \\
&\quad + (2\ddot{q}_1 + \ddot{q}_2)m_2 l_1 l_{m2} \cos(q_2 + \varepsilon_2) \\
&\quad - (2\dot{q}_1 + \dot{q}_2)\dot{q}_2(m_2 l_1 l_{m2} \sin(q_2 + \varepsilon_2)) \\
&= \ddot{q}_1(m_1 l_{m1}^2 + m_2 l_1^2 + m_2 l_{m2}^2 + I_{1ZZ} + I_{2ZZ} + 2m_2 l_1 l_{m2} \cos(q_2 + \varepsilon_2)) \\
&\quad + \ddot{q}_2(m_2 l_{m2}^2 + I_{2ZZ} + m_2 l_1 l_{m2} \cos(q_2 + \varepsilon_2)) \\
&\quad - 2\dot{q}_1 \dot{q}_2 m_2 l_1 l_{m2} \sin(q_2 + \varepsilon_2) \\
&\quad - \dot{q}_2^2 m_2 l_1 l_{m2} \sin(q_2 + \varepsilon_2) \\
\\
\frac{d}{dt} \frac{\partial L}{\partial \dot{q}_2} &= (\ddot{q}_1 + \ddot{q}_2)(m_2 l_{m2}^2 + I_{2ZZ}) \\
&\quad + \ddot{q}_1(m_2 l_1 l_{m2} \cos(q_2 + \varepsilon_2)) \\
&\quad - \dot{q}_1 m_2 l_1 l_{m2} \sin(q_2 + \varepsilon_2) \dot{q}_2 \\
&= \ddot{q}_1(m_2 l_{m2}^2 + I_{2ZZ} + m_2 l_1 l_{m2} \cos(q_2 + \varepsilon_2)) \\
&\quad + \ddot{q}_2(m_2 l_{m2}^2 + I_{2ZZ}) \\
&\quad - \dot{q}_1 \dot{q}_2 m_2 l_1 l_{m2} \sin(q_2 + \varepsilon_2) \tag{C.18}
\end{aligned}$$

3rd step: $\frac{\partial L}{\partial q_i}$ for $i=1,2$

$$\begin{aligned}
\frac{\partial L}{\partial q_1} &= -gm_1 l_{m1} \sin(q_1 + \varepsilon_1) \\
&\quad - gm_2 l_1 \sin q_1 \\
&\quad - gm_2 l_{m2} \sin k \\
\\
\frac{\partial L}{\partial q_2} &= -(\dot{q}_1^2 + \dot{q}_1 \dot{q}_2)m_2 l_1 l_{m2} \sin(q_2 + \varepsilon_2) \\
&\quad - gm_2 l_{m2} \sin k \tag{C.19}
\end{aligned}$$

Lagrange equation

$$\frac{d}{dt} \frac{\partial L}{\partial \dot{q}_i} - \frac{\partial L}{\partial q_i} = \tau_i \quad i = 1, 2 \tag{C.20}$$

Now we can write down the equations for τ_i :

$$\begin{aligned}
 \Rightarrow \tau_1 &= \ddot{q}_1(m_1 l_{m1}^2 + m_2 l_1^2 + m_2 l_{m2}^2 + 2m_2 l_1 l_{m2} \cos(q_2 + \varepsilon_2) + I_{1ZZ} + I_{2ZZ}) \\
 &\quad + \ddot{q}_2(m_2 l_{m2}^2 + m_2 l_1 l_{m2} \cos(q_2 + \varepsilon_2) + I_{2ZZ}) \\
 &\quad - 2\dot{q}_1 \dot{q}_2 m_2 l_1 l_{m2} \sin(q_2 + \varepsilon_2) \\
 &\quad - \dot{q}_2^2 m_2 l_1 l_{m2} \sin(q_2 + \varepsilon_2) \\
 &\quad + g m_1 l_{m1} \sin(q_1 + \varepsilon_1) \\
 &\quad + g m_2 l_1 \sin q_1 \\
 &\quad + g m_2 l_{m2} \sin k
 \end{aligned} \tag{C.21}$$

$$\begin{aligned}
 \Rightarrow \tau_2 &= \ddot{q}_1(m_2 l_{m2}^2 + m_2 l_1 l_{m2} \cos(q_2 + \varepsilon_2) + I_{2ZZ}) \\
 &\quad + \ddot{q}_2(m_2 l_{m2}^2 + I_{2ZZ}) \\
 &\quad - \dot{q}_1 \dot{q}_2 (m_2 l_1 l_{m2} \sin(q_2 + \varepsilon_2)) \\
 &\quad + (\dot{q}_1^2 + \dot{q}_1 \dot{q}_2) m_2 l_1 l_{m2} \sin(q_2 + \varepsilon_2) \\
 &\quad + g m_2 l_{m2} \sin k \\
 \\
 &= \ddot{q}_1(m_2 l_{m2}^2 + m_2 l_1 l_{m2} \cos(q_2 + \varepsilon_2) + I_{2ZZ}) \\
 &\quad + \ddot{q}_2(m_2 l_{m2}^2 + I_{2ZZ}) \\
 &\quad + \dot{q}_1^2 m_2 l_1 l_{m2} \sin(q_2 + \varepsilon_2) \\
 &\quad + g m_2 l_{m2} \sin k
 \end{aligned} \tag{C.22}$$

This leads to the resulting equation of motion:

$$\begin{pmatrix} \tau_1(t) \\ \tau_2(t) \end{pmatrix} = \mathbf{B}(q) \begin{pmatrix} \ddot{q}_1(t) \\ \ddot{q}_2(t) \end{pmatrix} + \mathbf{C}(q, \dot{q}) \begin{pmatrix} \dot{q}_1(t) \\ \dot{q}_2(t) \end{pmatrix} + \mathbf{g}(q) \tag{C.23}$$

with

$$\mathbf{B} = \begin{pmatrix} B_{11} & B_{12} \\ B_{21} & B_{22} \end{pmatrix} \tag{C.24}$$

C. KINEMATIC AND DYNAMIC MODEL OF 2-DOF ROBOT LEG

$$\begin{aligned}
 B_{11} &= m_1 l_{m1}^2 + m_2 (l_1^2 + l_{m2}^2 + 2l_1 l_{m2} \cos(q_2 + \varepsilon_2)) + I_{1ZZ} + I_{2ZZ} \\
 B_{12} &= B_{21} = m_2 (l_{m2}^2 + l_1 l_{m2} \cos(q_2 + \varepsilon_2)) + I_{2ZZ} \\
 B_{22} &= m_2 l_{m2}^2 + I_{2ZZ}
 \end{aligned} \tag{C.25}$$

$$\mathbf{C} = \begin{pmatrix} -\dot{q}_2 m_2 l_1 l_{m2} \sin(q_2 + \varepsilon_2) & -(\dot{q}_1 + \dot{q}_2) m_2 l_1 l_{m2} \sin(q_2 + \varepsilon_2) \\ \dot{q}_1 m_2 l_1 l_{m2} \sin(q_2 + \varepsilon_2) & 0 \end{pmatrix} \tag{C.26}$$

$$\mathbf{g} = \begin{pmatrix} g m_1 l_{m1} \sin(q_1 + \varepsilon_1) + g m_2 l_1 \sin q_1 + g m_2 l_{m2} \sin(q_1 + q_2 + \varepsilon_2) \\ + g m_2 l_{m2} \sin(q_1 + q_2 + \varepsilon_2) \end{pmatrix} \tag{C.27}$$

The correctness of the above result can be check showing that $\dot{\mathbf{B}}(q_i) - 2\mathbf{C}(\dot{q}_i)$ is antisymmetric:

$$\begin{aligned}
 \dot{\mathbf{B}}(q_i) - 2\mathbf{C}(\dot{q}_i) &= \\
 &= \begin{pmatrix} 0 & -m_2 l_1 l_{m2} \sin(q_2 + \varepsilon_2) \dot{q}_2 + 2m_2 l_1 l_{m2} \sin(q_2 + \varepsilon_2) (\dot{q}_1 + \dot{q}_2) \\ -m_2 l_1 l_{m2} \sin(q_2 + \varepsilon_2) \dot{q}_2 - 2\dot{q}_1 m_2 l_1 l_{m2} \sin(q_2 + \varepsilon_2) & 0 \end{pmatrix} \\
 &= \begin{pmatrix} 0 & +\dot{q}_2 m_2 l_1 l_{m2} \sin(q_2 + \varepsilon_2) + 2\dot{q}_1 m_2 l_1 l_{m2} \sin(q_2 + \varepsilon_2) \\ -\dot{q}_2 m_2 l_1 l_{m2} \sin(q_2 + \varepsilon_2) - 2\dot{q}_1 m_2 l_1 l_{m2} \sin(q_2 + \varepsilon_2) & 0 \end{pmatrix} \tag{C.28}
 \end{aligned}$$

Appendix D

Finite Element Model (FEM) Analysis

Several simulation studies with Finite Element Model (FEM) of the robot torso, legs and motor-leg attachment have been performed by Ferdinando Cannella, a colleague of mine. They are reported in this Appendix.

D.1 FEM Analysis of Torso

A first FEM analysis was performed on the model of the robot torso. The goal was to determine the minimal thickness of the aluminium sheet and the effectiveness of the internal walls (see section 4.2.3 for more details on the torso). Both the vertical displacement and the Von Mises stress was simulated.

To simulate the robot in worst case situations, the simulation considered a fall of the robot from a height of 15cm landing on either four legs or a diagonal pair of legs (torsion). Furthermore, the contact between the feet and the ground was modelled in three different ways. The foot was considered without rubber and the ground property was changed: from landing on grass or rubber (soft case) to landing on plastic or wood (hard case) and landing on concrete or rock (hardest case). This three cases can also be thought of as having a spring in the ankle joint and a rubber coated foot (soft case), only rubber coated foot (hard) or directly the metal structure (hardest case). Several sheet thicknesses ranging from 1mm to 4mm have been simulated. The robot

D. FINITE ELEMENT MODEL (FEM) ANALYSIS

components inside the torso are modelled as additional masses located according to the component's position.

Fig. D.1 shows the result of the FEM analysis for the *hard case* with a sheet thickness of 4mm landing on four legs. Both the vertical displacement in [mm] and the Von Mises stress in [MPa] are shown.

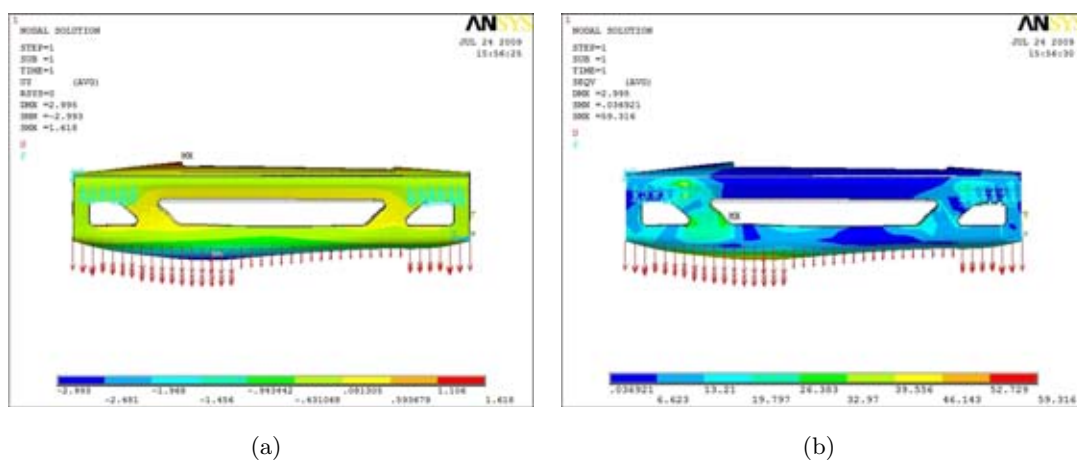


Figure D.1: Result plots of the FEM analysis of the robot torso, after a fall from 0.15m landing on four legs on a plastic or wood surface (hard case): (a) vertical displacement [mm] and (b) Von Mises Stress [MPa].

The study resulted that a sheet thickness of 2mm is strong enough. However, to be on the safe side for a first prototype, we decided for a thickness of 3mm. The weight difference between the 2mm and the 3mm version is approximately 1.7kg, which is acceptable.

D.2 FEM Analysis of Leg-Motor Connection

The second FEM study was about the connection between the motor unit and the leg. The proposal was to use 6 stainless steel pins with a diameter of 6mm, evenly aligned on a circle. The robustness of this design has been evaluated and a suitable diameter of the circle has been found. The input torque for the connection was 152Nm which is

D.3 FEM Analysis of Leg

the maximum permitted torque for the harmonic gear. Fig. D.2 shows the resulting Von Mises stress plots of the analyses of a too weak (pin circle diameter = 25mm) and an improved design (pin circle diameter = 32mm).

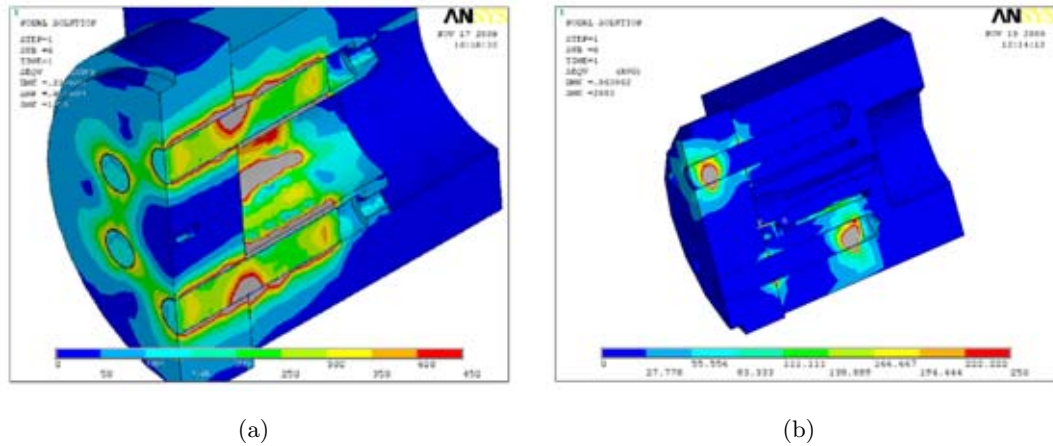


Figure D.2: Plots of the FEM analysis of the electric motor connection to the leg: (a) Von Mises stress [MPa] plot of an initial design that is too weak because the diameter of the pin circle is too small and (b) Von Mises stress [MPa] plot of robust design with larger pin circle diameter.

D.3 FEM Analysis of Leg

A third FEM study has been performed to evaluate the robustness of the leg in various configurations. One of the goals was to determine how much material can be removed from the leg plates while keeping the structure strong enough. Fig. D.3 shows the finite element mesh used for the analysis and the Von Mises stress plot with the knee joint set to an angle of 90° .

D. FINITE ELEMENT MODEL (FEM) ANALYSIS

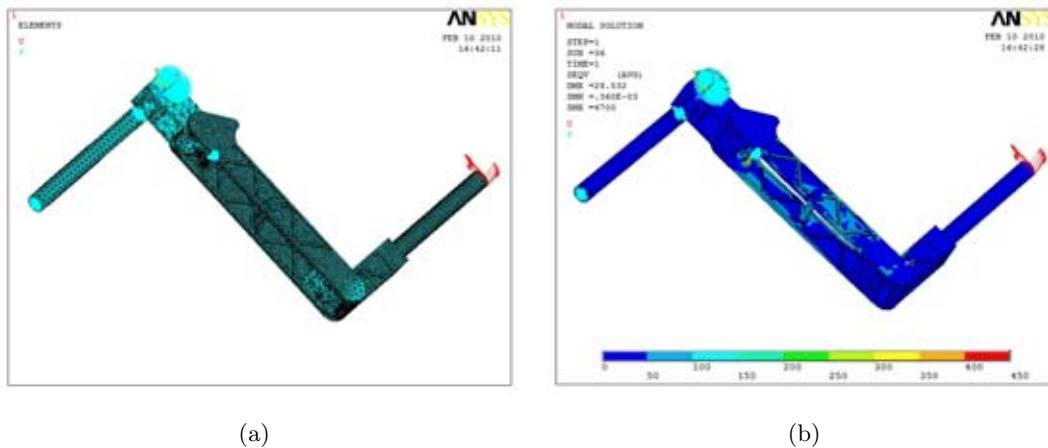


Figure D.3: Plots of the FEM analysis of the robot leg: (a) the mesh of the analysis and (b) Von Mises stress [MPa] plot of the leg with 90° knee angle.

Appendix E

Technical Details

E.1 Unit Conversions

Table E.1 shows the conversions of the different commonly used units of hydraulic flow and pressure.

Flow	$\frac{m^3}{s} = 60000 \frac{l}{min}$	$\frac{cm^3}{s} = 0.06 \frac{l}{min}$	$0.98 \frac{lpm}{cis}$	$3.78 \frac{lpm}{gpm}$
Pressure	$1bar = 0.1MPa$	$0.069 \frac{bar}{psi}$		

Table E.1: List of hydraulic flow and pressure unit conversions, with *lpm* (liter per minute), *cis* (cubic inch per second), *gpm* (gallon per minute), *psi* (pound per square inch).

E.2 Modular Foot Attachment Details

Fig. E.1 shows a simplified drawing with section view of the lower leg including the foot. The model is reduced to the six relevant mechanical parts to show how to design the attachment of new foot units with/without spring and/or damper.

E. TECHNICAL DETAILS

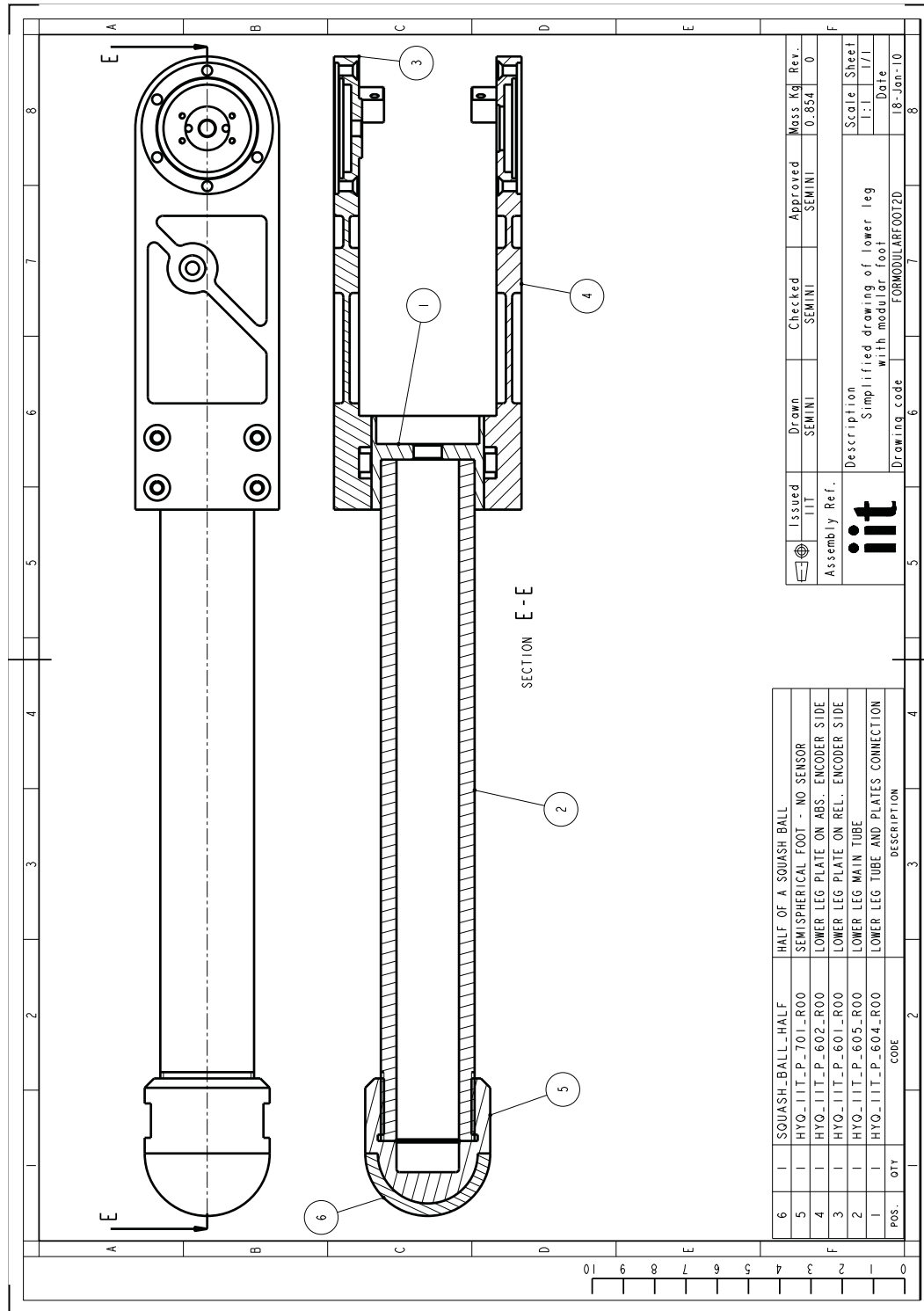


Figure E.1: Simplified drawing with section view of the lower leg including the foot. Note that the drawing has been scaled to fit the dissertation layout. The outside diameter of the tube is 30mm and can be used as a reference.

E.3 Hydraulic Cylinder Dimensions

Table E.2 lists the values of the most relevant geometric dimensions of the *Hoerbiger* hydraulic cylinder according to the drawing of Fig. E.2 [Hoerbiger, 2008].

Variable	Value [mm]
G	28
V1	8
ϕO	8
SW1	8
B1	M8
D1	14
D2	7
ϕA	26
R	M10x1
K1	15
L2	201
L3	237

Table E.2: List of *Hoerbiger* cylinder dimensions.

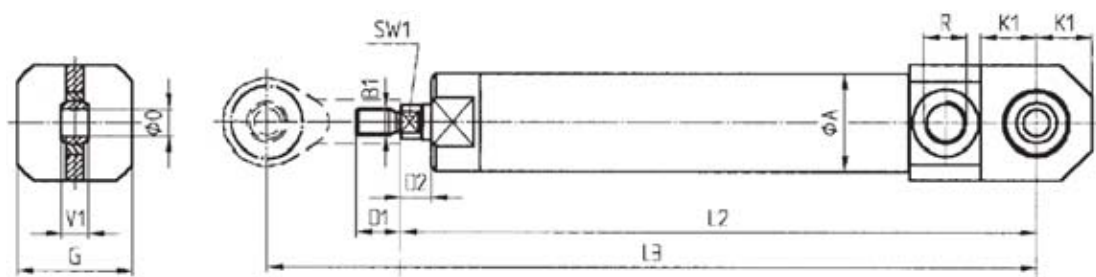


Figure E.2: Drawing of the *Hoerbiger* hydraulic cylinder LB6 with connection type 4 [Hoerbiger, 2008].

E. TECHNICAL DETAILS

Bibliography

- [ABB, 2008] ABB (2008). *Low voltage General performance motor Data Sheet*.
- [Alexander, 1988] Alexander, M. (1988). *Elastic mechanisms in animal movement*. Cambridge University Press.
- [Alexander, 1992] Alexander, R. M. (1992). *Exploring Biomechanics: Animals in Motion*. Scientific American Library.
- [Alexander, 2003] Alexander, R. M. (2003). *Principles of Animal Locomotion*. Princeton University Press.
- [Alfayad et al., 2009] Alfayad, S., Ouezdou, F. B., Namoun, F., Bruneau, O., and Hnaff, P. (2009). Three dof hybrid mechanism for humanoid robotic application: Modeling, design and realization. In *Proceedings of the 2009 IEEE/RSJ International Conference on Intelligent Robots and Systems (IROS)*.
- [Anybots Inc., 2010] Anybots Inc. (2010). Website. Accessed January 2010 at <http://www.anybots.com>.
- [Atkeson et al., 2000] Atkeson, C. G., Hale, J., Kawato, M., Kotosaka, S., Pollick, F., Riley, M., Schaal, S., Shibata, S., Tevatia, G., and Ude, A. (2000). Using humanoid robots to study human behaviour. *IEEE Intelligent Systems*, 15:46–56.
- [austriamicrosystems AG, 2006] austriamicrosystems AG (2006). *AS5045 12 Bit Programmable Magnetic Rotary Encoder Data Sheet*.
- [Avago, 2006] Avago (2006). *AEDA-3300 Series Ultra Miniature, High Resolution Incremental Kit Encoders Data Sheet*.

BIBLIOGRAPHY

- [Barai and Nonami, 2008] Barai, R. K. and Nonami, K. (2008). Locomotion control of a hydraulically actuated hexapod robot by robust adaptive fuzzy control with self-tuned adaptation gain and dead zone fuzzy pre-compensation. *Journal of Intelligent and Robotic Systems*, 53:35–56.
- [Berns, 2010] Berns, K. (2010). Walking machines catalogue (website). Accessed January 2010 at <http://www.walking-machines.org/>.
- [Blickhan, 1989] Blickhan, R. (1989). The spring-mass model for running and hopping. *Journal of Biomechanics*, 22:1217–1227.
- [Bose, 2006] Bose, B. K. (2006). *Power Electronics And Motor Drives: Advances and Trends*. Academic Press.
- [Boston Dynamics Corp., 2008] Boston Dynamics Corp. (2008). Bigdog overview. (Online) Accessed January 2010 at http://www.bostondynamics.com/img/BigDog_Overview.pdf.
- [Boston Dynamics Corp., 2010] Boston Dynamics Corp. (2010). Website. Accessed January 2010 at <http://www.bostondynamics.com>.
- [Brevini, 2009] Brevini (2009). *FP Hydraulic Power Pack Data Sheet*.
- [Buchli et al., 2009] Buchli, J., Kalakrishnan, M., Mistry, M., Pastor, P., and Schaal, S. (2009). Compliant quadruped locomotion over rough terrain. In *Proceedings of the 2009 IEEE/RSJ International Conference on Intelligent Robots and Systems (IROS)*, pages 814–820.
- [Buehler et al., 1999] Buehler, M., Cocosco, A., Yamazaki, K., and Battaglia, R. (1999). Stable open loop walking in quadruped robots with stick legs. In *Proceedings of the IEEE International Conference on Robotics and Automation (ICRA)*.
- [Buehler et al., 2006] Buehler, M., Grimminger, F., Campbell, D., and Raibert, M. (2006). Biologically inspired robots at boston dynamics. In *Bionic 2006 Industrie-Kongress*.
- [Buehler et al., 2005] Buehler, M., Playter, R., and Raibert, M. (2005). Robots step outside. In *Int. Symp. Adaptive Motion of Animals and Machines (AMAM)*.

BIBLIOGRAPHY

- [Burr Brown, 1999] Burr Brown (1999). *PWM solenoid/valve driver DRV102*.
- [Burster GmbH, 2009] Burster GmbH (2009). *Subminiature Load Cell Tension/Compression Model 8417 Data Sheet*.
- [Caldwell et al., 1993] Caldwell, D., Razak, A., and Goodwin, M. (1993). Braided pneumatic muscle actuators. In *Proceedings of the IFAC workshop on intelligent autonomous vehicles*.
- [Caldwell et al., 1995] Caldwell, D. G., Medrano-Cerda, G. A., and Goodwin, M. (1995). Control of pneumatic muscle actuators. *IEEE Control Systems*, pages 40–48.
- [Cavagna et al., 1964] Cavagna, G. A., Saibene, F. P., and Margaria, R. (1964). Mechanical work in running. *J. Appl. Physiol.*, 19(2):249–256.
- [Cheng et al., 2007] Cheng, G., Hyon, S., Morimoto, J., Ude, A., Hale, J. G., Colvin, G., W., S., and Jacobsen, S. C. (2007). Cb: a humanoid research platform for exploring neuroscience. *Journal of Advanced Robotics*, 21:1097–1114.
- [Cronin, 2005] Cronin, J. (2005). *Design, Construction and Control of an Industrial Scale biped Robot*. PhD thesis, University of New South Wales, Australia.
- [Cundiff, 2001] Cundiff, J. S. (2001). *Fluid Power Circuits and Controls: Fundamentals and Applications*. CRC Press.
- [Cunha et al., 2009] Cunha, T. B., Semini, C., Guglielmino, E., De Negri, V. J., Yang, Y., and Caldwell, D. G. (2009). Gain scheduling control for the hydraulic actuation of the hyq robot leg. In *Proceedings of 20th International Congress of Mechanical Engineering (COBEM)*.
- [ELMO Motion Control, 2009] ELMO Motion Control (2009). *Solo Whistle Digital Servo Drive Data Sheet*.
- [Emoteq Inc., 1998] Emoteq Inc. (1998). High torque series - brushless dc motors data sheet. Accessed March 2010 at http://www.alliedmotion.com/Data/Documents/HT_High_Torque_Selection_Guide.pdf.

BIBLIOGRAPHY

- [Estremera and Waldron, 2008] Estremera, J. and Waldron, K. J. (2008). Thrust control, stabilization and energetics of a quadruped running robot. *International Journal of Robotics Research*, 27:1135–1151.
- [Farley and Taylor, 1991] Farley, C. and Taylor, C. (1991). A mechanical trigger for the trot-gallop transition in horses. *Science*, 253:306–308.
- [Fischer et al., 2002] Fischer, M. S., Schilling, N., Schmidt, M., Haarhaus, D., and Witte, H. (2002). Basic limb kinematics of small therian mammals. *The Journal of Experimental Biology*, 205:1315–1338.
- [Focchi et al., 2010] Focchi, M., Guglielmino, E., Semini, C., Cunha, T. B., Yang, Y., and Caldwell, D. G. (2010). Control of a hydraulically-actuated quadruped robot leg. In *Proceedings of the IEEE International Conference on Robotics and Automation (ICRA)*.
- [Fujita and Kitano, 1998] Fujita, M. and Kitano, H. (1998). Development of an autonomous quadruped robot for robot entertainment. *Autonomous Robots*, 5:7–18.
- [Gomis-Bellmunt and Campanile, 2010] Gomis-Bellmunt, O. and Campanile, L. F. (2010). *Design Rules for Actuators in Active Mechanical Systems*. Springer.
- [González-de Santos et al., 2006] González-de Santos, P., Garcia, E., and Estremera, J. (2006). *Quadrupedal Locomotion: An Introduction to the Control of Four-legged Robots*. Springer, Secaucus, NJ, USA.
- [Gregorio et al., 1997] Gregorio, P., Ahmadi, M., and Buehler, M. (1997). Design, control, and energetics of an electrically actuated legged robot. *IEEE Transactions on Systems Man and Cybernetics, Part B: Cybernetics*, 27:626–634.
- [Guglielmino et al., 2009] Guglielmino, E., Semini, C., Yang, Y. S., Caldwell, D., Kogler, H., and Scheidl, R. (2009). Energy efficient fluid power in autonomous legged robotics. In *ASME Dynamic Systems and Control Conference (DSCC)*.
- [Harmonic Drive Inc., 2009] Harmonic Drive Inc. (2009). Harmonic gear csd & shd series data sheet. Accessed March 2010 at http://www.harmonicdrive.de/cms/upload/pdf/GK2007/english/1_Component_Sets/3_CSD/CSD_complete.en.pdf.

- [Heglund and Taylor, 1988] Heglund, N. and Taylor, C. (1988). Speed, stride frequency and energy cost per stride: how do they change with body size and gait? *J Exp Biol*, 138(1):301–318.
- [HiBot Corp., 2009] HiBot Corp. (2009). *Attitude Sensor Data Sheet*.
- [Hirose et al., 2009] Hirose, S., Fukuda, Y., Yoneda, K., Nagakubo, A., Tsukagoshi, H., Arikawa, K., Endo, G., Doi, T., and Hodoshima, R. (2009). Quadruped walking robots at tokyo institute of technology. *IEEE Robotics and Automation Magazine*, 16:104–114.
- [Hodoshima et al., 2007] Hodoshima, R., Doi, T., Fukuda, Y., Hirose, S., Okamoto, T., and Mori, J. (2007). Development of quadruped walking robot titan xi for steep slopes - slope map generation and map information application. *Journal of Robotics and Mechatronics*, 19:13–26.
- [Hoerbiger, 2008] Hoerbiger (2008). Hoerbiger micro hydraulic cylinder data sheet. (Online) Accessed January 2010 at http://www.hoerbiger.com/fileadmin/files/internet/AT/Anwendungssysteme/Micro_Fluid/PDF/zylinder.pdf.
- [Hollerbach et al., 1992] Hollerbach, J., Hunter, I., and Ballantyne, J. (1992). *The Robotics Review 2*, chapter A comparative analysis of actuator technologies for robotics, pages 299–342. MIT Press.
- [Honda, 2009] Honda (2009). *GX Series Engines Data Sheet*.
- [Howard, 2008] Howard, A. (2008). Real-time stereo visual odometry for autonomous ground vehicles. In *Proceedings of the 2008 IEEE/RSJ International Conference on Intelligent Robots and Systems (IROS)*, pages 3946–3952.
- [Hoyt and Taylor, 1981] Hoyt, D. and Taylor, R. (1981). Gait and the energetics of locomotion in horses. *Nature*, 292:239–240.
- [Huber et al., 1997] Huber, J. E., Fleck, N. A., and Ashby, M. F. (1997). The selection of mechanical actuators based on performance indices. *Proc. R. Soc. Lond. A*, 453:2185–2205.

BIBLIOGRAPHY

- [Hurst, 2008] Hurst, J. W. (2008). *The Role and Implementation of Compliance in Legged Locomotion*. PhD thesis, Carnegie Mellon University.
- [Hurst and Rizzi, 2008] Hurst, J. W. and Rizzi, A. A. (2008). Series compliance for an efficient running gait. *IEEE Robotics & Automation Magazine*, 15:42–51.
- [Hyon, 2009] Hyon, S. H. (2009). A motor control strategy with virtual musculoskeletal systems for compliant anthropomorphic robots. *IEEE/ASME Transactions on Mechatronics*, 14:677–688.
- [Hyon et al., 2003a] Hyon, S.-H., Abe, S., and Emura, T. (2003a). Development of a biologically-inspired biped robot kenkenii. In *Proceedings of 6th Japan-France Congress on Mechatronics & 4th Asia-Europe Congress on Mechatronics*, pages 404–409.
- [Hyon et al., 2003b] Hyon, S. H., Emura, T., and Mita, T. (2003b). Dynamics-based control of a one-legged hopping robot. *J. Syst. Control Eng.*, 217 (2):83–89.
- [Iida et al., 2005] Iida, F., Gomez, G., and Pfeifer, R. (2005). Exploiting body dynamics for controlling a running quadruped robot. In *Proceedings of the 12th Int. Conf. on Advanced Robotics (ICAR05)*, pages 229–235.
- [Ilg et al., 1998] Ilg, W., Berns, K., Jedele, H., Albiez, J., Dillmann, R., Fischer, M., Witte, H., Biltzinger, J., Lehmann, R., and Schilling, N. (1998). Bisam: From small mammals to a four legged walking machine. In Pfeifer, R., Blumberg, B., Meyer, J.-A., and Wilson, S., editors, *From Animals to Animats, Proceedings of the Fifth International Conference of The Society for Adaptive Behavior (SAB98)*. MIT Press.
- [Ingvast, 2006] Ingvast, J. (2006). *Quadruped robot control and variable leg transmissions*. PhD thesis, The Royal Inst. of Technology, Sweden.
- [Jaegger et al., 2002] Jaegger, G., Marcellin-Little, D., and Levine, D. (2002). Reliability of goniometry in labrador retrievers. In *AJVR*, volume 63, pages 979–986.
- [John Deere Corp., 2010] John Deere Corp. (2010). Website. Accessed March 2010 at http://www.deere.com/en_US/compinfo/media/pdf/publications/jd_journal/archives/fall_2001.pdf.

- [Kazerooni and Steger, 2006] Kazerooni, H. and Steger, R. (2006). The berkeley lower extremity exoskeleton. *ASME Journal of Dynamic Systems, Measurement and Control*, 128:14–25.
- [Kimura et al., 1999] Kimura, H., Akiyama, S., and Sakurama, K. (1999). Realization of dynamic walking and running of the quadruped using neural oscillators. *Autonomous Robots*, 7(3):247–258.
- [Kimura et al., 2007] Kimura, H., Fukuoka, Y., and Cohen, A. H. (2007). Adaptive dynamic walking of a quadruped robot on natural ground based on biological concepts. *International Journal of Robotics Research*, 26:475–490.
- [Kontron, 2008] Kontron (2008). *User’s Guide MOPSPM104*.
- [Koo et al., 2007] Koo, I. M., Trong, T. D., Kang, T. H., Vo, G., Song, Y. K., Lee, C. M., and Choi, H. R. (2007). Control of a quadruped walking robot based on biologically inspired approach. In *Proceedings of the 2007 IEEE/RSJ International Conference on Intelligent Robots and Systems (IROS)*.
- [Kurfess, 2004] Kurfess, T. R. (2004). *Robotics and Automation Handbook*. CRC Press.
- [Machado and Silva, 2006] Machado, J. A. T. and Silva, M. F. (2006). An overview of legged robots. In *Proceedings of the MME 2006 International Symposium on Mathematical Methods in Engineering*.
- [Mavroidis et al., 1999] Mavroidis, C., Pfeiffer, C., and Mosley, M. (1999). *Automation, Miniature Robotics and Sensors for Non-Destructive Testing and Evaluation*, chapter Conventional actuators, shape memory alloys and electrorheological fluids. The American Society of Nondestructive Testing.
- [McDowell, 1950] McDowell, L. (1950). *The Dog In Action*. Orange Judd Publishing Company, Inc.
- [McGeer, 1990] McGeer, T. (1990). Passive dynamic walking. *International Journal of Robotics Research*, 9(2):62–82.
- [McMahon and Cheng, 1990] McMahon, T. A. and Cheng, G. C. (1990). The mechanics of running: how does stiffness couple with speed? *Journal of Biomechanics*, 23:65–78.

BIBLIOGRAPHY

- [Meek et al., 2008] Meek, S., Kim, J., and Anderson, M. (2008). Stability of a trotting quadruped robot with passive, underactuated legs. In *Proceedings of the 2008 IEEE International Conference on Robotics and Automation (ICRA)*.
- [MIT Leg Lab, 2010] MIT Leg Lab (2010). Website. Accessed January 2010 at <http://www.ai.mit.edu/projects/leglab>.
- [MOOG Inc., 2003] MOOG Inc. (2003). *Data Sheet For E024 Series Microvalve*.
- [MOOG Inc., 2007] MOOG Inc. (2007). *Data Sheet of Type 30 Nozzle-flapper servo-valves*.
- [Nichol, 2005] Nichol, J. G. (2005). *Design for energy loss and energy control in a galloping artificial quadruped*. PhD thesis, Stanford University.
- [Niiyama et al., 2007] Niiyama, R., Nagakubo, A., and Kuniyoshi, Y. (2007). Mowgli: A bipedal jumping and landing robot with an artificial musculoskeletal system. In *Proceedings of the 2007 IEEE International Conference on Robotics and Automation (ICRA)*, pages 2546–2551.
- [Palmer and Orin, 2007] Palmer, L. and Orin, D. (2007). Quadrupedal running at high speed over uneven terrain. In *IROS 2007*, pages 303–308.
- [Palmer, 2007] Palmer, L. R. (2007). *Intelligent Control and Force Redistribution for a High-Speed Quadruped Trot*. PhD thesis, Ohio State University.
- [Peak, 2008] Peak (2008). *PC/104 to CAN Interface User Manual*.
- [Playter et al., 2006] Playter, R., Buehler, M., and M., R. (2006). Bigdog. *Proceedings of SPIE*, 6320.
- [Playter and Raibert, 1992] Playter, R. R. and Raibert, M. H. (1992). Control of a biped somersault in 3d. In *Proceedings of the 1992 IEEE/RSJ International Conference on Intelligent Robots and Systems (IROS)*.
- [Poulakakis et al., 2005] Poulakakis, I., Smith, J. A., and Buehler, M. (2005). Modeling and experiments of untethered quadrupedal running with a bounding gait: The scout II robot. *International Journal of Robotics Research*, 24:239–256.

- [Raibert, 1990] Raibert, M. (1990). Trotting, pacing and bounding by a quadruped robot. *Journal of Biomechanics*, 23:79–98.
- [Raibert et al., 2008] Raibert, M., Blankespoor, K., Nelson, G., Playter, R., and the BigDog Team (2008). Bigdog, the rough-terrain quadruped robot. In *Proceedings of the 17th World Congress The International Federation of Automatic Control (IFAC)*.
- [Raibert et al., 1986] Raibert, M., Chepponis, M., and Brown, B. (1986). Running on four legs as though they were one. *IEEE Journal of Robotics and automation*, RA-2:70–82.
- [Raibert, 1986] Raibert, M. H. (1986). *Legged Robots That Balance*. The MIT Press.
- [Raytheon Sarcos, 2010] Raytheon Sarcos (2010). Website. Accessed March 2010 at http://www.raytheon.com/newsroom/technology/rtn08_exoskeleton/.
- [Rummel and Seyfarth, 2008] Rummel, J. and Seyfarth, A. (2008). Stable running with segmented legs. *International Journal of Robotics Research*, 27:919–934.
- [Sakakibara et al., 1990] Sakakibara, Y., Kan, K., Hosoda, Y., Hattori, M., and Fujie, M. (1990). Foot trajectory for a quadruped walking machine. In *Proceedings of the 1999 IEEE International Conference on Intelligent Robots and Systems (IROS)*, pages 315–322.
- [Schaal, 2006] Schaal, S. (2006). The SL simulation and real-time control software package. Technical Report, (Online) Accessed February 2010 at <http://www-clmc.usc.edu/publications/S/schaal-TRSL.pdf>.
- [Schwind and Koditschek, 1997] Schwind, W. J. and Koditschek, D. E. (1997). Characterization of monopod equilibrium gaits. In *Proceedings of the IEEE International Conference on Robotics and Automation (ICRA)*, page 19861992.
- [Sciavicco and Siciliano, 2001] Sciavicco, L. and Siciliano, B. (2001). *Modelling And Control Of Robot Manipulators*. Springer.
- [Semini et al., 2008] Semini, C., Tsagarakis, N. G., Vanderborght, B., Yang, Y., and Caldwell, D. G. (2008). Hyq hydraulically actuated quadruped robot: Hopping leg prototype. In *Proceedings of the 2008 IEEE/RAS International Conference on Biomedical Robotics and Biomechatronics (BioRob)*, pages 593–599.

BIBLIOGRAPHY

- [Sensoray, 2002] Sensoray (2002). *Multifunctional I/O Board Model 526 Data Sheet*.
- [Slotine and Li, 1991] Slotine, J. J. and Li, W. (1991). *Applied Nonlinear Control*. Prentice Hall.
- [Song and Waldron, 1989] Song, S.-M. and Waldron, K. J. (1989). *Machines That Walk - The Adaptive Suspension Vehicle*. The MIT Press.
- [Stephens and Atkeson, 2009] Stephens, B. and Atkeson, C. (2009). Modeling and control of periodic humanoid balance using the linear biped model. In *Proceedings of the IEEE-RAS International Conference on Humanoid Robots (Humanoids)*.
- [Tanaka and Hirose, 2008] Tanaka, T. and Hirose, S. (2008). Development of leg-wheel hybrid quadruped airhopper - design of powerful light-weight leg with wheel. In *Proceedings of the 2008 IEEE/RSJ International Conference on Intelligent Robots and Systems (IROS)*, pages 3890–3895.
- [Trafag, 2008] Trafag (2008). *Industrial Pressure Transmitter 8251 Data Sheet*.
- [Tsagarakis et al., 2007] Tsagarakis, N., Becchi, F., Righetti, L., Ijspeert, A. J., and Caldwell, D. G. (2007). Lower body realization of the baby humanoid - icub. In *Proceedings of the 2007 IEEE/RSJ International Conference on Intelligent Robots and Systems (IROS)*, pages 3616–3622.
- [Wandfluh, 2007] Wandfluh (2007). Proportional spool valves - ng3-mini. (Online) Accessed March 2010 at http://www.wandfluh.com/fileadmin/user_upload/files/A_Dok/reg_1_10/1_10_65_d.pdf.
- [Wikipedia, 2010] Wikipedia (2010). Wikipedia, the free encyclopedia. Accessed January 2010 at <http://en.wikipedia.org>.
- [Witte et al., 2001] Witte, H., Hackert, R., Lilje, K. E., Schilling, N., Voges, D., Klauer, G., Ilg, W., Abliez, J., Seyfarth, A., Germann, D., Hiller, M., Dillmann, R., and Fischer, M. S. (2001). Transfer of biological principles into the construction of quadruped walking machines. In *Second workshop on Robot Motion and Control*.
- [Youtube, 2009] Youtube (2009). Youtube channel of boston dynamics. Accessed January 2010 at <http://www.youtube.com/BostonDynamics>.

BIBLIOGRAPHY

- [Zhang et al., 2005] Zhang, X., Zheng, H., Guan, X., Cheng, Z., and Zhao, L. (2005). A biological inspired quadruped robot: structure and control. In *IEEE International Conference on Robotics and Biomimetics*.
- [Zhang et al., 2006] Zhang, Z. G., Kimura, H., and Takase, K. (2006). Adaptive running of a quadruped robot using forced vibration and synchronization. *Journal of Vibration and Control*, 12:1361–1383.

Declaration

I herewith declare that I have produced this dissertation without the prohibited assistance of third parties and without making use of aids other than those specified; notions taken over directly or indirectly from other sources have been identified as such. This dissertation has not previously been presented in identical or similar form to any other Italian or foreign examination board.

The thesis work was conducted from January 2007 to March 2010 under the supervision of Prof. Darwin G. Caldwell and Nikos G. Tsagarakis at the Advanced Robotics Department of the Italian Institute of Technology.

Genoa,

Claudio Semini